Zeitschrift: IABSE reports of the working commissions = Rapports des commissions de travail AIPC = IVBH Berichte der Arbeitskommissionen

Band: 16 (1974)

Rubrik: Theme I: Physical-mathematical models and theoretical considerations

Nutzungsbedingungen

Die ETH-Bibliothek ist die Anbieterin der digitalisierten Zeitschriften auf E-Periodica. Sie besitzt keine Urheberrechte an den Zeitschriften und ist nicht verantwortlich für deren Inhalte. Die Rechte liegen in der Regel bei den Herausgebern beziehungsweise den externen Rechteinhabern. Das Veröffentlichen von Bildern in Print- und Online-Publikationen sowie auf Social Media-Kanälen oder Webseiten ist nur mit vorheriger Genehmigung der Rechteinhaber erlaubt. Mehr erfahren

Conditions d'utilisation

L'ETH Library est le fournisseur des revues numérisées. Elle ne détient aucun droit d'auteur sur les revues et n'est pas responsable de leur contenu. En règle générale, les droits sont détenus par les éditeurs ou les détenteurs de droits externes. La reproduction d'images dans des publications imprimées ou en ligne ainsi que sur des canaux de médias sociaux ou des sites web n'est autorisée qu'avec l'accord préalable des détenteurs des droits. En savoir plus

Terms of use

The ETH Library is the provider of the digitised journals. It does not own any copyrights to the journals and is not responsible for their content. The rights usually lie with the publishers or the external rights holders. Publishing images in print and online publications, as well as on social media channels or websites, is only permitted with the prior consent of the rights holders. Find out more

Download PDF: 26.01.2026

ETH-Bibliothek Zürich, E-Periodica, https://www.e-periodica.ch

On the Extreme Compressive Strain of Concrete for Calculating the Ultimate Strength of Reinforced Concrete Section

Raccourcissement ultime du béton et calcul de la sollicitation ultime d'une section en béton armé

Über den Grenzwert der Druckstauchung von Beton bei der Berechnung der Traglast von Stahlbetonquerschnitten

Hiroshi MUGURUMA — Prof., Doctor of Engineering
Shinzo TANAKA — Graduate Student
Kyoto University
Kyoto, Japan

1. Introduction

The failure of reinforced concrete section subjected to the flexural moment, axial load or combined flexural and axial loads is generally caused by crushing of concrete at the compression zone. For the calculation of ultimate strength it is necessary to assume the extreme compressive fiber strain of concrete, ε_{cu}, induced in the section at the ultimate strength. Usually, the values of ε_{cu} empirically or semi-empirically determined are adopted in the calculation. [1] For instance, ε_{cu} = 0.15 - 0.2% is assumed for pure axial loading failure and ε_{cu} = 0.25-0.35% for flexural failure under the action of pure flexural load or combined flexural and axial loads.

However, the extreme compressive fiber strain of concrete, ε_{cu}, at the ultimate strength is not always defined clearly from the theoretical view-point. The value of ε_{cu} seems to be affected by many factors such as the combination of applied axial and flexural forces, the characteristics of stress-strain curve of concrete, especially the falling branch of it after compressive strength, and the percentage of reinforcements etc. In this paper, numerical estimations are made on the value of ε_{cu} for ultimate strength calculation by using the typical stress-strain curves of concrete, and the effects of these factors upon the value of ε_{cu} are discussed.

2. Definition of concrete fiber strain, ε_{cu}, at ultimate strength

The ultimate loading capacity of reinforced concrete section subjected to combined axial and bending forces can be represented by the ultimate axial load-moment interaction curve. This can be calculated from the equilibrium of forces acting on the section under the consideration of stress and strain compatibility, where the compressive fiber strain of concrete, ε_{cu}, at ultimate strength should be assumed. While the collapse of reinforced concrete section is generally caused by crushing of concrete in compression zone, the applied load shows its' maximum value before the crushing of concrete. Fig. 1 shows such phenomenon by load-deflection curve of typical member. Thus, generally the maximum of applied

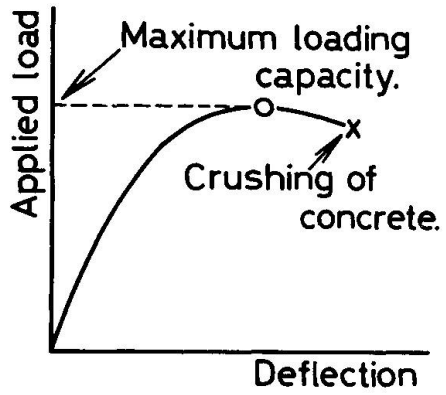

Fig. 1 Load-deflection curve of reinforced concrete member

load recorded until the collapse of section takes place by crushing of concrete is so defined as the ultimate loading capacity or the ultimate strength,[2),3)] And also the corresponding compressive fiber strain of concrete, ε_{cu}, is defined as the strain which should be used in the calculation of ultimate strength.

3. Method of numerical estimation of ε_{cu}

The purpose of this study is to obtain numerically the compressive fiber strain of concrete, ε_{cu}, at maximum loading capacity of reinforced concrete column section subjected to various combinations of applied axial load and flexural moment. To explain the procedure of numerical estimation, the rectangular column section shown in Fig. 2(a) is considered. The stress and strain distributions overall the section are shown in Fig. 2(b) and 2(c), respectively, in general form. The stress distribution shown in Fig. 2(c) is obtained in correspondence to the strain distribution in Fig. 2(b) by using the stress-strain relations of component materials. The compressive fiber strain of concrete, ε_c, and the distance of neutral axis, x, from compressive fiber of section are determined so as to satisfy the equilibrium equations for given combined loads, $P(\varepsilon_c)$ and $M(\varepsilon_c)$. That is, the applied combined loads, $P(\varepsilon_c)$ and $M(\varepsilon_c)$, are generally expressed as the function of ε_c and x. However, considering that loads, $P(\varepsilon_c)$ and $M(\varepsilon_c)$, are so applied as the eccentricity,

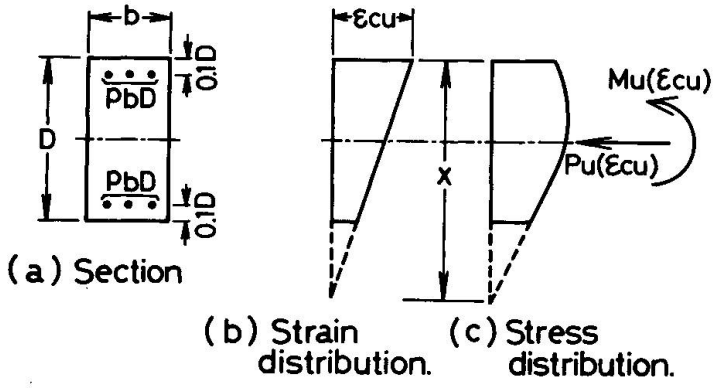

Fig. 2 Stress and strain distributions overall the rectangular column section.

$$e = M(\varepsilon_c)/P(\varepsilon_c) \qquad (1),$$

becomes constant without regard to their magnitude, the distance of neutral axis, x, can also be expressed as a function of ε_c. Thus, in other words, a set of combined loads, $P(\varepsilon_c)$ and $M(\varepsilon_c)$, can be obtained numerically for a given value of ε_c under the consideration of constant eccentricity, e.

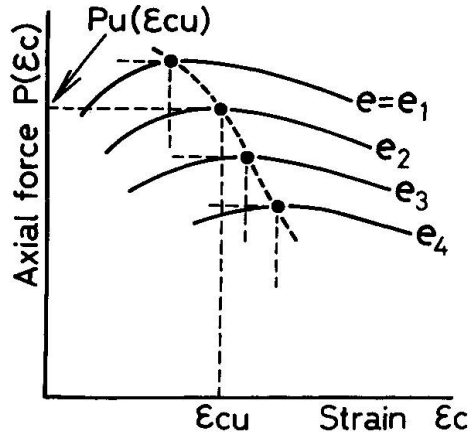

Fig.3 ε_c-$P(\varepsilon_c)$ or $M(\varepsilon_c)$relation

Fig. 3 shows ε_c - $P(\varepsilon_c)$ or $M(\varepsilon_c)$ relation for various values of eccentricity, $e = e_1, e_2, e_3, \cdots\cdots$, where the concrete fiber strain, ε_{cu}, corresponding to the peak value of $P(\varepsilon_c)$ coincides with that of $M(\varepsilon_c)$ because of the linear relation between $P(\varepsilon_c)$ and $M(\varepsilon_c)$. From the definition of ultimate strength described in 2 the peak values, $Pu(\varepsilon_{cu})$ and $Mu(\varepsilon_{cu})$, in ε_c - $P(\varepsilon_c)$ and ε_c - $M(\varepsilon_c)$ curves are defined as the maximum loading capacity for a given loading condition, $e = M(\varepsilon_c)/P(\varepsilon_c)$, and the corresponding compressive fiber strain, $\varepsilon_c = \varepsilon_{cu}$, is the strain to be used in the theoretical calculation of ultimate strength. In this paper using ε_c - $P(\varepsilon_c)$ or ε_c - $M(\varepsilon_c)$ relation as shown in Fig. 3, the ultimate strengths, $Pu(\varepsilon_{cu})$

and $Mu(\varepsilon_{cu})$, as well as corresponding compressive fiber strain of concrete, ε_{cu}, is estimated graphically for rectangular column section shown in Fig. 2(a).

Moreover, the ultimate strengths, $Pu(\varepsilon_{cu})$ and $Mu(\varepsilon_{cu})$, and corresponding concrete fiber strain, ε_{cu}, can be obtained as the values satisfying following mathematical conditions.[3]

$$\frac{dP(\varepsilon c)}{d\varepsilon_c} = 0 \quad \text{or} \quad \frac{dM(\varepsilon c)}{d\varepsilon_c} = 0 \qquad (2).$$

Of course, a set of values, ε_{cu}, $P_u(\varepsilon_{cu})$ and $M_u(\varepsilon_{cu})$, obtained from first equation in Eq. (2) satisfys the second condition in Eq. (2) simultaneously.

4. Stress-strain curves of component materials for numerical calculation

For numerical calculation of compressive fiber strain of concrete, ε_{cu}, at the ultimate strength of reinforced concrete column section, the stress-strain curves of component materials should be assumed. To simplifying the numerical calculation, the ideal elastic-plastic relation shown in Fig. 4 is assumed for reinforcement, where the elastic modulus of $E_s = 2{,}100{,}000$ kg/cm^2 is taken without respect to the yield strength of reinforcement.

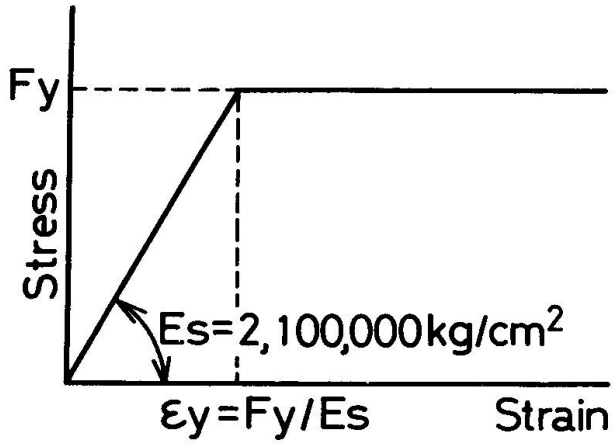

Fig. 4 Stress-strain curve of reinforcement

Fig. 5 shows three different types of typical stress-strain curve of plain concrete obtained from compressive tests on cylinder specimens of various kinds of concrete.[4),5)] The ordinate in Fig. 5 is expressed as the ratio of applied stress to the compressive strength. Curve I represents the stress-strain relation for ordinary aggregate concrete having 28-day compressive strength up to 350 kg/cm^2. Curve II is that of light-weight aggregate structural concrete. The strain at the peak stress (that is, at the compressive strength) as well as the negative inclination of strain softening region in Curve II is greater than that in Curve I. Curve III in Fig. 5 is identical one modified from Curve I for investigating the effect of the negative inclination of strain softening region upon the compressive fiber strain of concrete, ε_{cu}, at the ultimate strength. For convenience of the numerical calculation of ε_{cu}, the area surrounded by each stress-strain curve shown in Fig. 5 and its' center of gravity were calculated in correspondence to an arbitrary strain. The results are also shown in Fig. 5 in the coefficients, k_1k_3 and k_2, versus compressive strain, ε_c, relations, where k_1k_3 and k_2 denote the ratio of average stress of stress-strain curve until an arbitrary strain, ε_c, to the compressive strength, F_c, and the ratio of the location of center of gravity of corresponding area from an arbitrary strain, ε_c, to the strain ε_c, respectively. That is, coefficients, k_1k_3 and k_2, can be considered as the generalized stress block

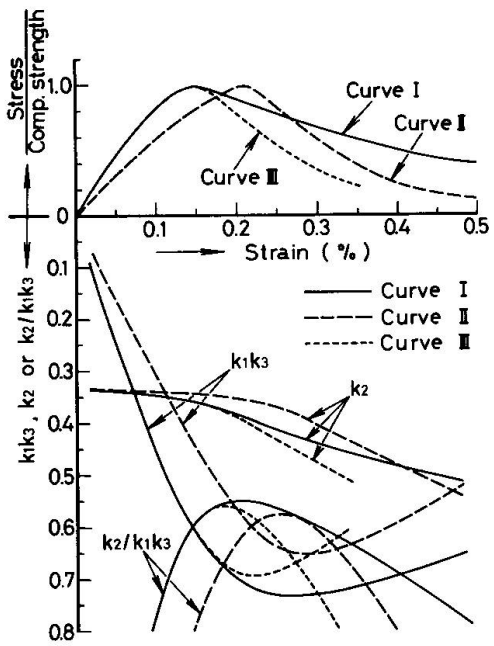

Fig. 5 Typical stress-strain curves of concrete and corresponding values of k_1k_3, k_2 and k_2/k_1k_3

coefficients of concrete in flexural compression zone of reinforced concrete section.

5. Effects of the eccentricity of applied axial load and the percentage of reinforcements upon ε_{cu}

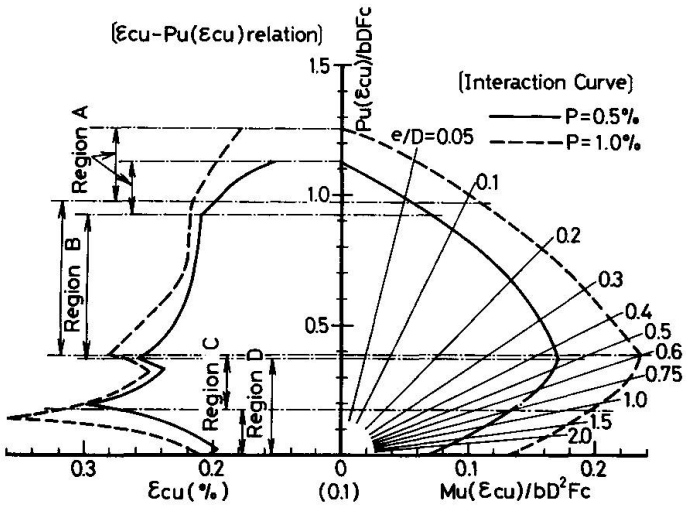

Fig. 6 ε_{cu} - $P_u(\varepsilon_{cu})$ - $M_u(\varepsilon_{cu})$ relations for rectangular column section (Curve I concrete stress-strain relation and F_y =4000 kg/cm^2 are used in calculation)

The numerical calculations of compressive fiber strain, ε_{cu}, at ultimate strength were performed on the percentage of reinforcements, p =0.5% and p = 1%, of rectangular column section shown in Fig. 2. The stress-strain relation of concrete as well as the yield strength of reinforcement adopted in calculation are Curve I in Fig. 5 and F_y=4000 kg/cm^2, respectively. The results are shown by ε_{cu}-$P_u(\varepsilon_{cu})$ relation with $P_u(\varepsilon_{cu})$ - $M_u(\varepsilon_{cu})$ interaction curve as in Fig. 6.

ε_{cu} - $P_u(\varepsilon_{cu})$ relations shown in Fig. 6 can be divided into following four regions.

Region A : Range that applied combined loads reach at their muximum without yielding of whole reinforcements.

Region B : Range that applied combined loads reach at their maximum after yielding of reinforcements in compression zone, where the stress in reinforcements in tensile zone still remains in elastic range.

Region C : Range that applied combined loads reach at their maximum after yielding of whole reinforcements.

Region D : Range that applied combined loads reach at their maximum after yielding of reinforcements in tensile zone, where the stress in reinforcements in compression zone still remains in elastic range.

In ε_{cu} - $P_u(\varepsilon_{cu})$ relation for the section of p = 0.5%, Region C disappears and is expressed border line between B and D.

It can be seen from Fig. 6 that the compressive fiber strain ε_{cu} is much influenced by the combination of applied axial and flexural loads. In Fig. 6 the pure axial loading column section shows the minimum value of ε_{cu}. These are listed in Table 1, which are a little larger than the strain, ε_{cu} = 0.15%, corresponding to the peak stress in concrete stress-strain curve. In Region A and B in Fig. 6, the compressive fiber strain ε_{cu} increases gradually with increase of the relative degree of applied moment $M(\varepsilon_c)$ to applied axial force $P(\varepsilon_c)$, that is, with increase of the eccentricity e = $M(\varepsilon_c)/P(\varepsilon_c)$. On the lower bound of Region B, the strain ε_{cu} reaches at a peak value, where the corresponding ultimate flexural moment $M_u(\varepsilon_{cu})$ becomes maximum in the interaction curve. In Table 1, the values of ε_{cu} on the lower bound of Region B are also listed. In Region C and D, considerable increase of ε_{cu} is recognized after a little decrease near the upper bound of Region C or D, and the maximum value of ε_{cu} is obtained at the middle portion of these range. After that, the value of ε_{cu} decreases rapidly to the value of about 0.21%, which corresponds to the value for pure flexure. The maximum values of ε_{cu} are also summarized in Table 1.

From such observation, it can be stated that for the exact calculation

Table 1 The values of ε_{cu} for critical point in ε_{cu} - $P_u(\varepsilon_{cu})$ relation (Curve I concrete stress-strain relation and $F_y = 4000$ kg/cm^2 are used in the calculation)

Percentage of reinforcement	P (%)	0.5	1
For pure axial loading	ε_{cu} (%)	0.152	0.180
	$P_u(\varepsilon_{cu})/bDF_c$	1.125	1.250
	$M_u(\ _{cu})/bD^2F_c$	0	0
On the lower bound of Region A	ε_{cu} (%)	0.211	0.217
	$P_u(\varepsilon_{cu})/bDF_c$	0.920	0.970
	$M_u(\varepsilon_{cu})/bD^2F_c$	0.070	0.107
On the lower bound of Region B	ε_{cu} (%)	0.267	0.281
	$P_u(\varepsilon_{cu})/bDF_c$	0.370	0.390
	$M_u(\varepsilon_{cu})/bD^2F_c$	0.171	0.233
At the peak value in ε_{cu} - $P_u(\varepsilon_{cu})$ relation	ε_{cu} (%)	0.300	0.360
	$P_u(\varepsilon_{cu})/bDF_c$	0.195	0.140
	$M_u(\varepsilon_{cu})/bD^2F_c$	0.139	0.185
For pure flexure	ε_{cu} (%)	0.204	0.210
	$P_u(\varepsilon_{cu})/bDF_c$	0	0
	$M_u(\varepsilon_{cu})/bD^2F_c$	0.068	0.132

* F_c denotes the compressive strength of concrete.

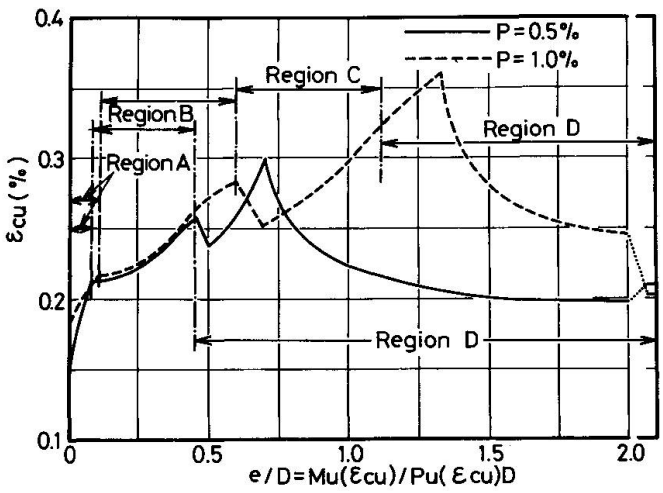

Fig. 7 e - ε_{cu} relations for rectangular column section of p = 0.5% and 1% (Curve I concrete stress-strain relation and F_y = 4000 kg/cm^2 are used in calculation)

of maximum loading capacity, especially that of corresponding deflection of reinforced concrete member the change of compressive fiber strain, ε_{cu}, as shown in Fig. 6 may be considered in correspondence to the combination of applied axial and flexural loads.

The effects of the percentage of reinforcement, p, upon the compressive fiber strain, ε_{cu}, can be observed from e - ε_{cu} relations shown in Fig. 7, which is rewritten from the results of Fig. 6. It seems from Fig. 7 that the effects of p is so small as negligible in Region A and B, while much difference of ε_{cu} between p = 0.5% and p = 1% is observed in Region C and D.

6. Effects of the shape of stress-strain curve of concrete upon the compressive fiber strain ε_{cu}

Using three different types of stress-strain curve of plain concrete shown in Fig. 5, the compressive fiber strain, ε_{cu}, at ultimate strength was calculated on the rectangular column section having p = 0.5%. The yield strength of reinforcement was assumed as 4000 kg/cm^2 in the calculation. The results are illustrated in Fig. 8. While three interaction curves are very closed with each other, much difference can be seen in three results on ε_{cu} - $P_u(\varepsilon_{cu})$ relation. Comparison between the results for concrete stress-strain Curve I and II shows that the larger compressive strain at the peak stress in stress-strain curve of

Table 2 Effects of the type of concrete stress-strain curve upon ε_{cu} for pure axial loading section of p = 5% (F_y = 4000 kg/cm2)

Type of stress-strain curve of concrete used in calculation	Ultimate axial load $P_u(\varepsilon_{cu})/bDF_c$	The value of ε_{cu} in %
Curve I	1.125	0.152
Curve II	1.160	0.208
Curve III	1.125	1.151

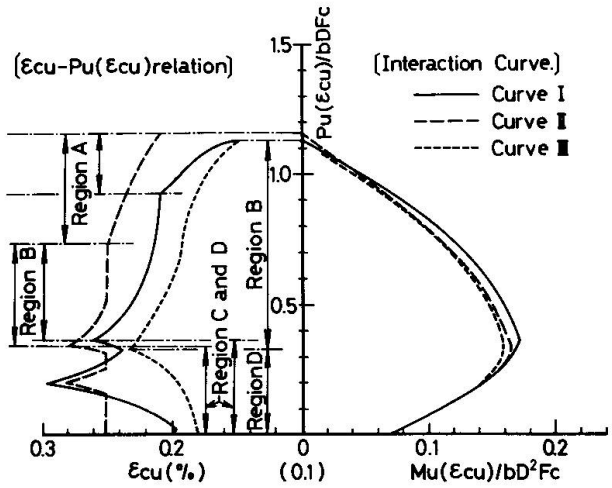

Fig. 8 Effects of the type of concrete stress-strain curve upon the compressive fiber strain, ε_{cu}, at ultimate strength (p = 0.5%, F_y = 4000 kg/cm2)

concrete results in the larger values of ε_{cu} within Region A and B in ε_{cu} - $P_u(\varepsilon_{cu})$ relation. The difference between the compressive fiber strains for Curve I and II becomes maximum in the case of pure axial loading. As a reference, the values of ε_{cu} obtained for pure axial loading are summarized in Table 2. On the contrary it appears from the comparison of the results for concrete stress-strain Curve III with that for Curve I that the increase of negative inclination in strain softening region of concrete stress-strain relation reduces the compressive fiber strain at ultimate strength of reinforced concrete section, while no obvious effect is recognized on the section subjected to pure axial force.

7. Effects of the yield strength of reinforcement, F_y, upon ε_{cu}

Fig. 9 shows the results of numerical calculation on the ultimate strengths, $P_u(\varepsilon_{cu})$ and $M_u(\varepsilon_{cu})$, and corresponding compressive fiber strain, ε_{cu}, for rectangular column section of p = 0.5% having various yield strengths of reinforcement. The stress-strain relation of concrete used in calculation is Curve I in Fig. 5.

Comparison between the results for F_y = 4000 kg/cm^2 and F_y = 5000 kg/cm^2 shows that Region A in ε_{cu} - $P_u(\varepsilon_{cu})$ relation becomes larger with increase of the yield strength of reinforcement, which results in the considerable increase of compressive fiber strain, ε_{cu}, in Region B. In Fig. 9, the strain ε_{cu} in Region B for F_y = 5000 kg/cm^2 is about 0.05% larger than that for F_y = 4000 kg/cm^2.

The use of reinforcement having smaller yield strength provides the decrease of Region A in ε_{cu} - $P_u(\varepsilon_{cu})$ curve. In Fig. 9, Region A disappears in ε_{cu} - $P_u(\varepsilon_{cu})$ relation for F_y = 2400 kg/cm^2 because the yield strain of reinforcement is smaller than the strain corresponding to the peak stress in stress-strain curve of concrete. In such case, the strain ε_{cu} for pure axial loading just coincides with the strain at peak stress in concrete stress-strain relation.

8. Conclusions

Based on the general concept that the ultimate loading capacity of reinforced concrete section is defined as the loads satisfying the equation $dP(\varepsilon_c)/d\varepsilon_c = 0$ or $dM(\varepsilon_c)/d\varepsilon_c = 0$, corresponding compressive fiber strain of concrete, ε_{cu}, was calculated numerically on the rectangular column section and the effects of the combination of applied axial and flexural loads, the percentage of reinforcement, the shape of stress-strain curve of concrete and the yield strength of reinforce-

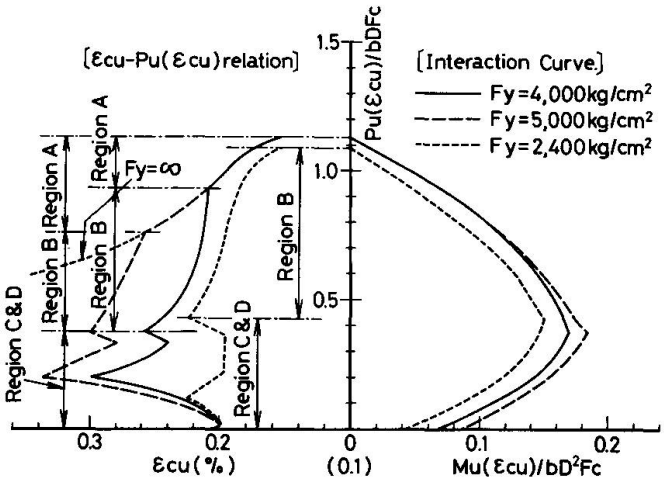

Fig. 9 Effects of the yield strength of reinforcement upon ε_{cu} - $P_u(\varepsilon_{cu})$ -$M_u(\varepsilon_{cu})$ relations of rectangular column section of p = 0.5% (Curve I concrete stress-strain relation is used in the calculation)

ment, etc. upon the compressive fiber strain were investigated. The following conclusions are obtained from the results.

(1) The compressive fiber strain ε_{cu} varies considerably with the relative intensity of applied flexural moment to axial load. ε_{cu} - $P_u(\varepsilon_{cu})$ relation obtained in this paper can be divided into four regions in corresponding to the yielding of reinforcement. The value of ε_{cu} becomes minimum in the case of pure axial loading and the increase of eccentricity results in the gradual increase of ε_{cu}. Also it decreases with increase of eccentricity after reaching the maximum value near pure flexure.

(2) No obvious effects of the percentage of reinforcement upon the value of ε_{cu} are recognized within Region A and B of ε_{cu} - P_u (ε_{cu}) curve, where relative intensity of applied axial load is larger in comparison with applied flexural moment.

(3) The larger strain at peak stress in concrete stress-strain curve increases the value of ε_{cu} within Region A and B of ε_{cu} - $P_u(\varepsilon_{cu})$ curve, especially the maximum increase of ε_{cu} is obtained in case of pure axial force. Also, the increase of negative slope of strain softening region in concrete stress-strain curve reduces the value of ε_{cu} considerably. These factors have no obvious effects on the ultimate axial load and flexural moment interaction curve of section.

(4) The use of reinforcements having larger yield strength results in considerable increase of ε_{cu} in region B of ε_{cu} - $P_u(\varepsilon_{cu})$ curve.

(5) The effects of the factors described in this paper upon the value of ε_{cu} may be necessary to consider for the exact estimation of ultimate strength as well as corresponding deformation of reinforced concrete member.

References

1) E. Hognestad, N. W. Hanson & D. McHenry: Concrete Stress Distribution in Ultimate Strength Design, J. of A.C.I., Vol. 52, No. 6, pp. 455~479, Dec. 1955.
2) S. Morita & N. Adachi: The Stress-Strain Behaviour of Concrete in the Compression Zone of Flexural Members, Proc. of the International Conference on Mechanical Behavior of Materials, Vol. IV, pp. 162~171, 1972.
3) R. F. Warner: Physical-Mathematical Models and Theoretical Considerations, Introductory Report on IABSE Symposium on Design and Safety of Reinforced Concrete Compression Members, pp. 1~21, April 1973.
4) F. Watanabe: Complete Stress-Strain Curve for Concrete in Concentral Compression, Proc. of the International Conference on Mechanical Behavior of Materials, Vol. IV, pp. 153~161, 1972.
5) H. Muguruma & S. Tanaka: Mechanical Properties of High Strength Concrete, Annual Report of Japan Cement Association, XXVII, 1973, (in Japanese).

I – EXTREME COMPRESSIVE STRAIN OF CONCRETE FOR CALCULATING THE ULTIMATE STRENGTH

SUMMARY

Numerical estimations were made on the value of extreme compressive fiber strain of concrete at ultimate strength of reinforced concrete column section subjected to various combinations of axial and flexural loads. The results showed that the extreme compressive fiber strain is much affected by many factors such as the combinations of axial and flexural loads, the caracteristics of stress-strain relation of concrete, the yiald strength of reinforcement and the percentage of reinforcements, etc.

RESUME

On a estimé la valeur de la tension de compression extrême dans le béton d'une colonne en béton armé soumise à diverses combinaisons de flexions et d'efforts axiaux. Les résultats montrent que l'allongement spécifique dans le béton varie considérablement en fonction de facteurs tels que les combinaisons de flexions et d'efforts axiaux, les caractéristiques de la courbe tension-déformation du béton, la limite d'élasticité des armatures, le pourcentage d'armature, etc.

ZUSAMMENFASSUNG

Zahlenmässige Schätzungen für den Wert der grössten Druckstauchung von Beton bei der Bruchbeanspruchung von Stahlbeton-Stützenquerschnitten unter Einwirkung verschiedener Kombinationen von Normalkraft und Biegemomenten wurden vorgenommen. Die Ergebnisse zeigten, dass die grösste Druckstauchung durch eine Reihe von Faktoren, wie die Kombination von Normalkraft und Biegemoment, den Verlauf des Spannungs-Dehnungs-Diagramms von Beton, die Streckgrenze der Bewehrung, den Bewehrungsgehalt usw. beeinflusst wird.

A Simplified Model for Nonlinearly Viscoelastic Columns

Un modèle simplifié pour le calcul visco-élastique non-linéaire des colonnes

Ein vereinfachtes Modell für nichtlineare viskoelastische Stützen

H. A. CERVERA
Assistant Professor

G. J. CREUS
Associate Professor

Institute of Applied Mechanics and Structures (I.M.A.E.)
Universidad Nacional de Rosario
Rosario, Argentina

1. INTRODUCTION

Adequate theories exist for the analysis of deformation and failure of linearly viscoelastic columns. J. N. Distéfano, /1/, has studied the problem in a series of papers of great generality, considering arbitrary end conditions, lateral loads and initial imperfections, and the most general expression for linear creep.

However, both instantaneous and time dependent deformations of concrete are nonlinear, specially at high stresses. In fact, the behaviour of concrete ranges from almost linear, bounded creep at low stresses to highly nonlinear, unbounded creep at stresses near the compressive strength.

The effect of nonlinear behaviour on creep buckling is analyzed in this paper. In Section 2 a nonlinear rheological model apt to describe the behaviour of concrete for the whole range of stresses is introduced.

In Section 3, the creep buckling problem is studied for the above mentioned rheological model, using a simplified model for the column.

In seccion 4, the model is refined by considering additional effects present in real situations, as the influence of axial thrust on the bending rigidity and the different behaviour of concrete in loading and unloading processes /2/.

For the simpler situations, analytical solutions to the differential equations are used. In the general case, a step by step numerical analysis is necessary. The effect of ageing of concrete may be easily taken into account by taking age dependent coefficients.

2. RHEOLOGICAL MODEL

The proposed model, shown in Fig.1 is similar to the well known standard solid. Its particular feature is the nonlinear stress-strain relation assumed for the spring elements 1 and 2. We denote with $\varepsilon_1(t)$ the strain due to the deformation of spring element 1 and with $\varepsilon_2(t)$ the strain corresponding to

spring 2 and dashpot. The total strain is $\varepsilon(t)=\varepsilon_1(t)+\varepsilon_2(t)$, where t denotes the time.

For spring 1 we assume the stress-strain relation

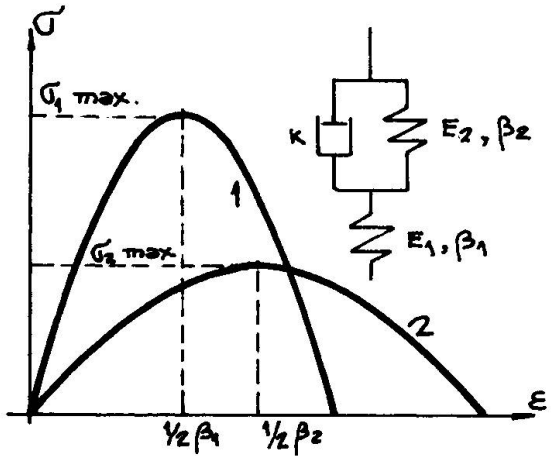

FIG. 1: RHEOLOGICAL MODEL

$$\sigma = E_1\varepsilon_1(1-\beta_1\varepsilon_1) \quad ; \quad 0 \leqslant \varepsilon_1 \leqslant \frac{1}{\beta_1} \tag{1}$$

Here $\sigma(t)$ is the stress and E_1, β_1 are material constants. This equation defines a maximum stress $\sigma_1^{max} = \frac{E_1}{4\beta_1}$ and a corresponding deformation $1/2\beta_1$. Increasing deformations from $1/2\beta_1$ to $1/\beta_1$ are possible for decreasing stresses. No physical meaning is attached to deformations larger than $\frac{1}{\beta_1}$.

The nonlinear Kelvin element constituted by the spring 2 and the dashpot is responsible for the time dependent behaviour. The spring 2 and the dashpot are defined by the relationships

$$\sigma' = E_2\varepsilon_2(1-\beta_2\varepsilon_2) \quad ; \quad 0 \leqslant \varepsilon_2 \leqslant \frac{1}{\beta_2}$$
$$\sigma'' = K\dot{\varepsilon}_2 \tag{2}$$

where E , β and K are material constants and the dot indicates differentiation with respect to time. Being $\sigma=\sigma'+\sigma''$ we obtain the equation for the nonlinear Kelvin element

$$\dot{\varepsilon}_2 - \frac{\beta_2 E_2}{K}\varepsilon_2^2 + \frac{E_2}{K}\varepsilon_2 = \frac{\sigma}{K} \tag{3}$$

which is a Riccati's first order nonlinear differential equation.

We shall consider now the case of a constant stress $\sigma(t)=\sigma_0$ applied at time t=0 and mantained thereafter. Inversion of Eq.(1) provides the expression

$$\varepsilon_1 = \frac{1}{2\beta_1}\left(1-\sqrt{1-\frac{\sigma_0}{\sigma_1^{max}}}\right) \quad ; \quad 0 \leqslant \varepsilon_1 \leqslant \frac{1}{2\beta_1} \tag{4}$$

for the instantaneous deformation. In order to determine the value of the delayed deformations, we must replace the value σ_0 into (3) and solve it (for more details see Ref./3/). Adding instantaneous and time dependent deformations, the final expressions are

$$\varepsilon(t) = \frac{1}{2\beta_1}\left(1-\sqrt{1-\frac{4\beta_1\sigma_0}{E_1}}\right) + \frac{1}{2\beta_2}\left(1-\sqrt{1-\gamma}\,\frac{-1-\sqrt{1-\gamma}+(-1+\sqrt{1-\gamma})\exp\left(-\frac{E_2}{K}\sqrt{1-\gamma}\;t\right)}{-1-\sqrt{1-\gamma}-(-1+\sqrt{1-\gamma})\exp\left(-\frac{E_2}{K}\sqrt{1-\gamma}\;t\right)}\right) \tag{5}$$

$$\varepsilon(t) = \frac{1}{2\beta_1}\left(1-\sqrt{1-\frac{4\beta_1\sigma_0}{E_1}}\right) + \frac{1}{2\beta_2}\left(\frac{t}{\frac{2K}{E_2}+t}\right) \tag{6}$$

$$\varepsilon(t) = \frac{1}{2\beta_1}\left(1-\sqrt{1-\frac{4\beta_1\sigma_0}{E_1}}\right) + \frac{1}{2\beta_2}\left(\gamma\,\frac{1+\sqrt{\gamma-1}\,\sin\frac{E_2}{K}\sqrt{\gamma-1}\;t-\cos\frac{E_2}{K}\sqrt{\gamma-1}\;t}{\gamma+2\sqrt{\gamma-1}\,\sin\frac{E_2}{K}\sqrt{\gamma-1}\;t+(\gamma-2)\cos\frac{E_2}{K}\sqrt{\gamma-1}\;t}\right) \tag{7}$$

for $\gamma<1$, $\gamma=1$ and $\gamma>1$ respectively, being $\gamma = 4\beta_2\sigma_0/E_2 = \sigma_0/\sigma_2^{max}$ (8)

The behaviour of the model under constant stress is indicated in Fig.2. We

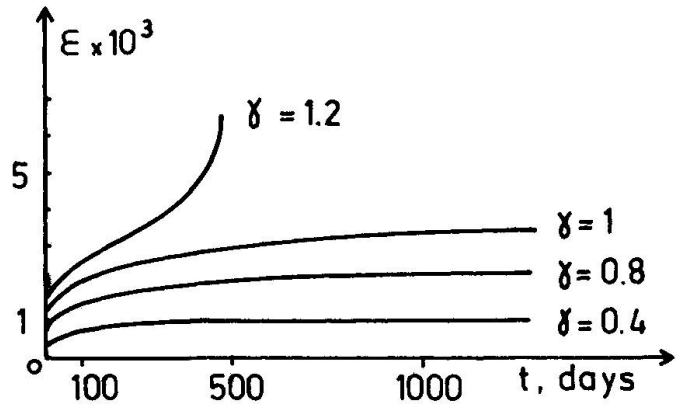

FIG.2:CREEP CURVES FOR THE RHEOLOGICAL MODEL

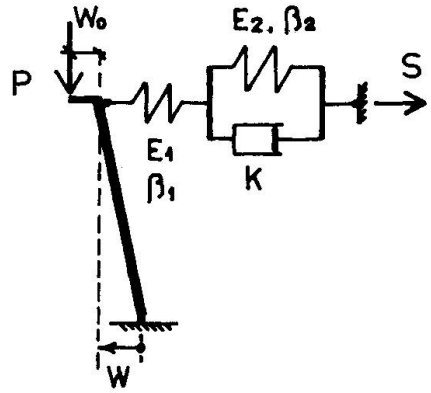

FIG.3:COLUMN MODEL

may see that for $\gamma > 1$,i.e. for $\sigma_0 > \sigma_2^{max}$ a condition similar to failure is reached after a finite time. As σ_1^{max} is the strength under instantaneous loading, σ_2^{max} may be interpreted as the strength under sustained load (static fatigue). In Ref./3/ a comparison of this model behaviour with the experimental results of Rüsch /4/ is given.

3. SIMPLIFIED COLUMN MODEL

Let us consider now the system in Fig.3. In this structure the deflexion of the hinged bar due to the action of the force P is prevented by a viscoelastic element which in turn reacts with a force S. This simple model contains many of the more interesting features of considerably more complex systems. For small, quasi-static deflexions, equilibrium provides the relation

$$S = P\,\frac{W + W_0}{L} \tag{9}$$

We are interested in the behaviour of this column model in the presence of nonlinear creep. For the sake of clarity, we shall study first some simpler situations.

<u>3.1. Linear spring</u> ($\beta_1 = 0$; $E_2 = \infty$): The force in the spring is $S = E_1 w$; from this and (9) we obtain

$$E_1 W = \frac{P(W + W_0)}{L} \qquad \text{or} \qquad W = \frac{W_0}{\frac{E_1 L}{P} - 1} \tag{10}$$

When $P \to LE_1$ we have $w \to \infty$;$P_E = LE_1$ may be considered the buckling load for this case.

<u>3.2. Linear Kelvin material</u> ($\beta_2 = 0$; $E_1 = \infty$): The force in the viscoelastic element is $S = E_2 w + K\dot{w}$; the differential equation for equilibrium is

$$\dot{W} + W\left(\frac{E_2}{K} - \frac{P}{LK}\right) - \frac{PW_0}{LK} = 0 \tag{11}$$

It may be seen that the solution of (11) shall be bounded for $t \to \infty$ whenever the the coefficient of w is possitive; thus, the creep buckling load in this case is $P_K = LE_2$, while the instantaneous load is infinite.

<u>3.3. Linear standard material</u> ($\beta_1 = \beta_2 = 0$): Proceeding in a similar way, we find

in this cae $P_E = LE_2$; $P_K = LE_1E_2/(E_1+E_2)$.

Both 3.2 and 3.3 are particular cases of the general linear viscoelastic problem as studied by Distéfano/1/. The creep buckling load is given (as it should) by the reduced modulus load. Physically, this may be interpreted saying that, in order to obtain the load stable for $t \to \infty$, only the spring constants are significant,as the action of the dashpot vanishes for $t \to \infty$ (*).

3.4. Nonlinear spring ($E_2 = \infty$): The force in the spring is now $S = E_1 w(1-\beta_1 w)$; from this and (9) we have

$$E_1 W (1-\beta_1 W) = \frac{P(W+W_0)}{L} \tag{12}$$

Solving for w we find that for each pair of values (P, w_0) there exist two equilibrium points, defined by

$$W = -\frac{1}{2\beta_1}\left(\frac{P}{LE_1}-1\right) \pm \frac{1}{2}\sqrt{\frac{1}{\beta_2^2}\left(\frac{P}{LE_1}-1\right)^2 - \frac{PW_0}{LE_1\beta_1}} \tag{13}$$

and represented by points A and B in Fig.4. It is easy to see that A corresponds to stable equilibrium and B to unstable equilibrium. The maximum load that allows stable equilibrium is obviously that corresponding to point C and may be obtained making the square root equal to zero. We obtain

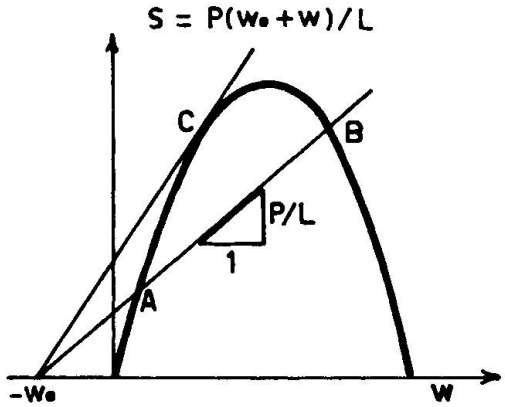

FIG.4: NONLINEAR SPRING

$$P_E = LE_1\left\{(2W_0\beta_1+1) - 2W_0\beta_1\sqrt{1+\frac{1}{W_0\beta_1}}\right\}$$

$$W_{cr} = W_0\left(\sqrt{1+\frac{1}{W_0\beta_1}} - 1\right) \tag{14}$$

Also from Fig.4 we may see that, in order to reach the critical condition, one may increase the load P to P_E or increase the initial excentricity w_0. Thus, a column whose material is characterized by a nonlinear stress-strain relation for instantaneous loading has a critical deflexion at which the applied load is the critical load. This fact is specially important in the treatment of creep buckling problems.

3.5. Nonlinear Kelvin material ($E_1 = \infty$):In this case we have $S = E_2 w(1-\beta_2 w) + K\dot{w}$; From this and (9) we obtain

$$\dot{W} - \frac{E_2\beta_2}{K}W^2 + \frac{E_2}{K}\left(1-\frac{P}{LE_2}\right)W - \frac{PW_0}{LK} = 0 \tag{15}$$

Eq.(15) is formally identical with (3). Following the same procedure we obtain the corresponding solution for w(t), namely

(*) This is of course only true for materials with bounded deformations, i.e. solids.

$$w(t)=\frac{1}{2\beta_2}\left(1-\frac{P}{LE_2}\right)\left\{1-\sqrt{1-\Gamma}\;\frac{1+\sqrt{1-\Gamma}+(1-\sqrt{1-\Gamma})\exp\left(-\frac{E_2}{K}\left(1-\frac{P}{LE_2}\right)\sqrt{1-\Gamma}\;t\right)}{1+\sqrt{1-\Gamma}-(1-\sqrt{1-\Gamma})\exp\left(-\frac{E_2}{K}\left(1-\frac{P}{LE_2}\right)\sqrt{1-\Gamma}\;t\right)}\right\} \tag{16}$$

$$w(t)=\frac{1}{2\beta_2}\left(1-\frac{P}{LE_2}\right)\left\{\frac{t}{\frac{2K}{E_2\left(1-\frac{P}{LE_2}\right)}+t}\right\} \tag{17}$$

$$w(t)=\frac{1}{2\beta_2}\left(1-\frac{P}{LE_2}\right)\left\{\Gamma\;\frac{1+\sqrt{\Gamma-1}\sin\frac{E_2}{K}\sqrt{\Gamma-1}\;t-\cos\frac{E_2}{K}\sqrt{\Gamma-1}\;t}{\Gamma+2\sqrt{\Gamma-1}\sin\frac{E_2}{K}\sqrt{\Gamma-1}\;t+(\Gamma-2)\cos\frac{E_2}{K}\sqrt{\Gamma-1}\;t}\right\} \tag{18}$$

for $\Gamma<1$, $\Gamma=1$ and $\Gamma>1$ respectively, being

$$\Gamma=\frac{\frac{4P}{LE_2}\,w_0\,\beta}{\left(1-\frac{P}{LE_2}\right)^2} \tag{19}$$

Thus, the critical load is given by

$$P_E=LE_2\left(1+2\beta w_0-\sqrt{4\beta w_0(\beta w_0+1)}\right) \tag{20}$$

Comparing this with $(14)_1$ we see that, as for the linear case, the load for infinite stability corresponds to the instantaneous critical load of a similar column where the Kelvin body has been replaced by the spring.

3.6. Nonlinear standard material: In this case, a closed solution has not been found. The problem has been solved numerically, using a step by step procedure.

The time interval of interest is divided into small (*) time intervals Δt. Then, at a time t, the force $S(t)$ satisfies the equation

$$S(t)=\frac{P}{L}(w_0+w)=\frac{P}{L}(w_0+w_D+w_E)=\frac{P}{L}\left(w_0+w_D(t)+\frac{1-\sqrt{1-\frac{4\beta_1 S(t)}{E_1}}}{2\beta_1}\right) \tag{21}$$

where w_D is the delayed deflexion for time t (of course, $w_D=0$ for $t=0$), and w_E is the elastic deflexion. In the following time interval $(t,t+\Delta t)$ we consider the spring 1 frozen, while the Kelvin element deforms under the action of force $S(t)$ assumed constant during the interval. The corresponding creep deformation is

$$\Delta w_D=\frac{S(t)-E_2 w_D(t)\left(1-\beta_2 w_D(t)\right)}{K}\Delta t \tag{22}$$

and the delayed deformation now amounts to $w_D(t+\Delta t)=w_D(t)+\Delta w_D$. Then, $w_D(t+\Delta t)$ is replaced into (21) and the process continues in the same fashion. The outlined procedure is very easily programmed for a digital computer.

The analysis of the results may be better understood looking at Fig.5. Line OA represents the $t=0$ isochronous curve for the material and corresponds to the $\sigma-\varepsilon$ relation for spring 1 in Fig.1. Line OFR corresponds to the $t=\infty$ isochronous curve and represents the behaviour of springs 1 and 2 in series.

(*) Small when compared with the characteristic retardation time of the model.

Different loads, applied with excentricity w_0 are represented by straight lines beggining at N. We observe that:

1)The instantaneous buckling load P_E (line NA) depends only on the characteristics of spring 1 and the initial excentricity w_0.

2)The creep buckling load P_K (line NF) depends on the characteristics of springs 1 and 2 and the initial excentricity w_0. More precisely, it may be evaluated as the instantaneous buckling load of an ideal elastic nonlinear column with a spring equivalent to springs 1 and 2 in series.

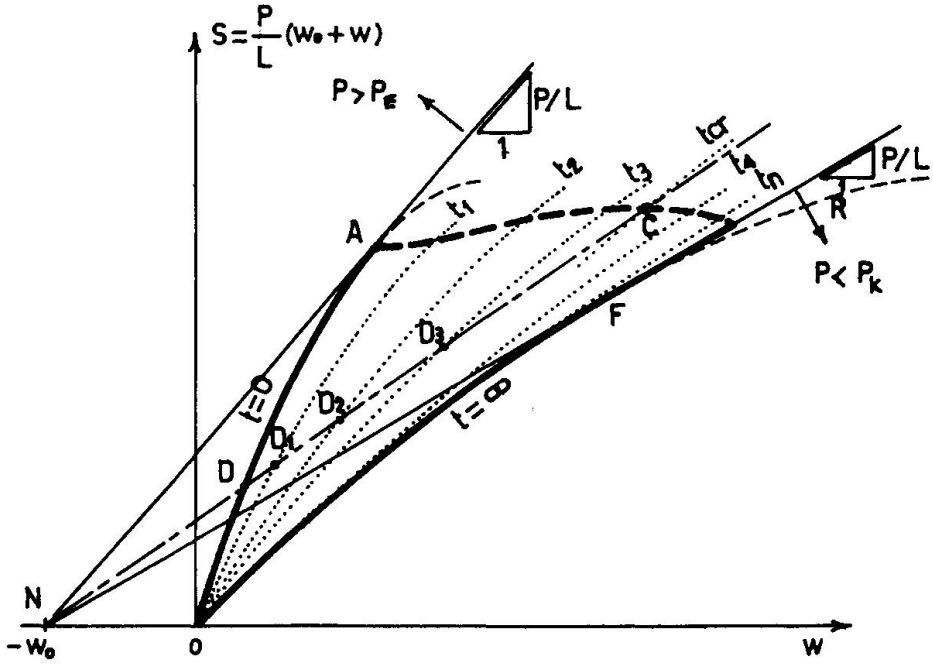

FIG.5: NONLINEAR STANDARD MATERIAL

This behaviour resembles in some ways the case of linear viscoelastic columns (see Section 3.3) where a reduced modulus exists. Of course, being the present problem nonlinear, a unique reduced modulus does not exists, and the load P_K depends on the initial excentricity.

3)A column loaded with $P_\phi < P_K$ reaches a limit deflexion with a velocity that depends on the value of K.

4)If a load $P_E > P_\phi > P_K$ (represented by NC) is applied, an instantaneous equilibrium position D is reached at t=0. As time goes on,successive equilibrium positions $D_1, D_2, \ldots$are reached.At some time t_{cr} (which depends on the value of K) the delayed deflexion w_D reaches a value for which P_ϕ is critical for spring 1. At this time, the column fails suddently. Failure points lay along a frontier indicated by AC.

The pattern of behaviour described closely resembles that observed experimentally /5,6/.

4. A REFINED MODEL

The model studied in Section 3 does not take into account:

a)the effect of axial thrust P on the bending rigidity

b) the different behaviour of concrete in loading and unloading processes. In order to take account of this influences, a refined model may be used, as indicated in Fig.6. Accordingly, the stress-strain relation for the springs in the rheological model has been generalized, as indicated in Fig.7

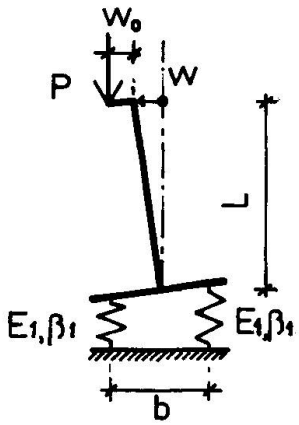

FIG.6: REFINED COLUMN MODEL

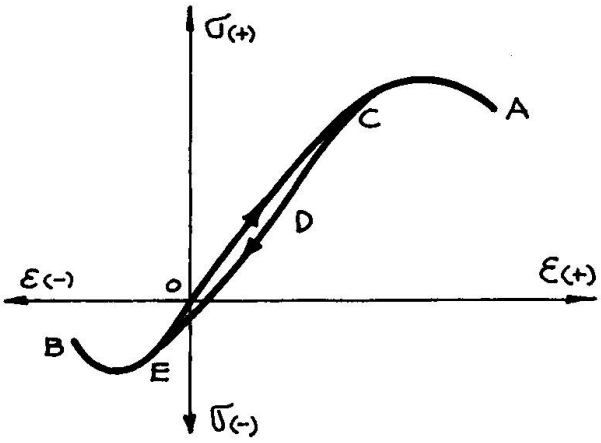

FIG.7:STRESS-STRAIN RELATION

Stresses and strains are now taken with their corresponding signs (compression:positive; tension:negative). Then, the base curve OA in compression is given by Eq.(1) with E_1 and $\beta_{1C} > 0$; the base curve OB in tension is given by the same Eq.(1) with E_1 and $\beta_{1T} < 0$. During unloading, the material behaves along line CDE with origin in C and E_1 , $\beta_1^* = \frac{\beta_{1C}\beta_{1T}}{\beta_{1C}-\beta_{1T}} < 0$. This curve contacts the base curve OB at point E smoothly (both curves have a common tangent at point).

By putting together the equilibrium and compatibility equations for the column model, and the constitutive relations of the springs, a system of equations is obtained that allows the study of the stability of the model. Comparing the critical loads obtained using this model (P_{cr2}) and the model in Section 3 (P_{cr1}), the effect of axial deformation may be evaluated.

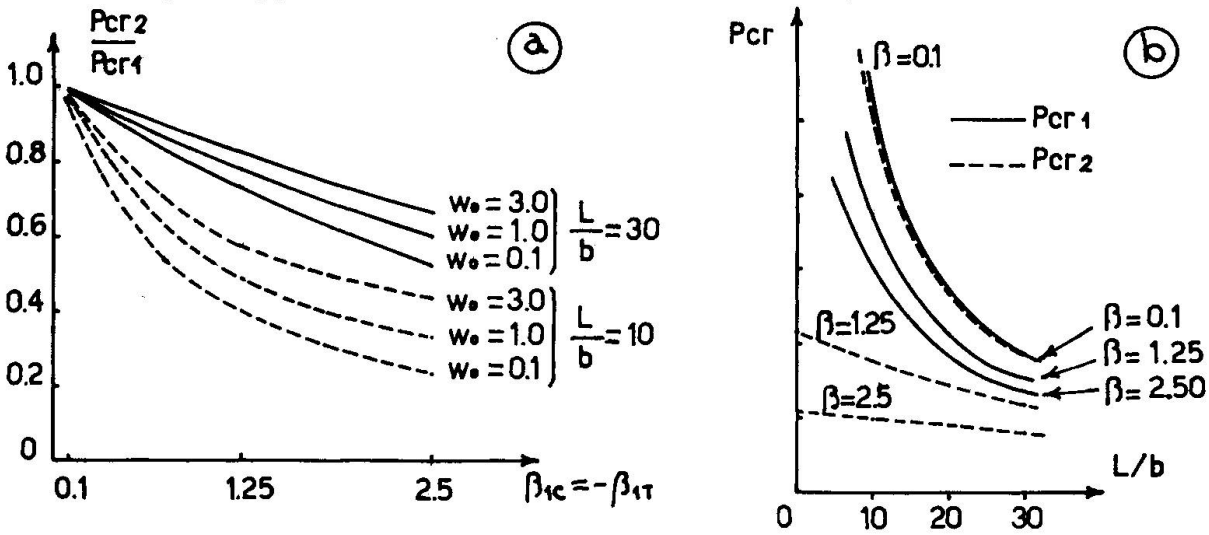

FIG.8: COMPARISON BETWEEN COLUMN MODELS

In Fig.8-a we observe that the influence of axial deformation increases with the nonlinearity coefficient β_{1C}. The influence of the initial excentricity w_0

and the slenderness ratio L/b is also shown. In Fig.8-b we may see how the critical loads for both models depend on β_{1c}, w_o and L/b.

ACKNOWLEDGEMENT

The work reported in this paper has been supported by the Research Council of the University of Rosario. The help received from the Computer Center staff is deeply acknowledged.

REFERENCES

1. Distéfano, J.N.:CREEP BUCKLING OF SLENDER COLUMNS, Journal, Struct. Div., ASCE, Vol. 91, No. ST3, June 1965.

2. Warner,R. F. :PHYSICAL MATHEMATICAL MODELS AND THEORETICAL CONSIDERATIONS, Introductory Report, Symposium IABSE, Québec, 1974.

3. Helman, H. and Creus, G.J.:A NONLINEAR RHEOLOGICAL MODEL DESCRIBING TIME DEPENDENT DEFORMATIONS AND FAILURE.Int.Report IMAE, 1973.

4. Rösch, H.:RESEARCHES TOWARD A GENERAL FLEXURAL THEORY FOR STRUCTURAL CONCRETE, ACI Journal, Proceedings, Vol.57, July 1960.

5. Distéfano, J.N. and Creus, G. J.:CREEP BUCKLING OF REINFORCED CONCRETE COLUMNS (Discussion), Journal, Struct. Div. ASCE, Vol.90, No.ST3 April 1964.

6. Creus, G. J.:CREEP BUCKLING OF CONCRETE COLUMNS. SOME THEORETICAL AND EXPERIMENTAL RESULTS, International Symposium RILEM,Argentina,1971.

SUMMARY

The effect of nonlinear behaviour on creep buckling is analized, using a nonlinear rheological element to express material properties and simplified models for the column.

RESUME

On analyse l'influence du comportement non-linéaire sur le flambement dû au fluage en utilisant un élément non-linéaire pour exprimer les caractéristiques du matériau, ainsi que des modèles simplifiés pur la colonne.

ZUSAMMENFASSUNG

Unter Verwendung eines nichtlinearen rheologischen Elementes für die Beschreibung der Materialeigenschaften und eines vereinfachten Modelles für die Stütze wird die Wirkung des nichtlinearen Verhaltens auf das Kriechknicken untersucht.

Zur wirklichkeitsnahen numerischen Bestimmung der zeitabhängigen Krümmung von Stahlbetonstützen

A Realistic Numerical Computation of the time dependent Curvature of Reinforced Concrete Columns

Contribution à l'analyse numérique réaliste de la courbure de colonnes en béton en fonction du temps

L. SPAROWITZ
Dipl. Ing.
Institut für Stahlbeton- und Massivbau
Technische Hochschule Graz
Graz, Oesterreich

1. EINFUEHRUNG

Als grundlegende Voraussetzung für eine wirklichkeitsnahe Traglastberechnung von Stahl- und Spannbetondruckstäben ist das zeitabhängige Verformungsverhalten des Verbundquerschnittes anzusehen. Die vorliegende Methode ist durch ihren sehr allgemeinen Aufbau vor allem für vergleichende theoretische Untersuchungen geeignet. Sie wird hier für beliebige einfach symmetrische Querschnittsform und gerade Biegung dargestellt, lässt sich jedoch auch auf unsymmetrische Querschnitte und zweiachsige Momentenbeanspruchung (schiefe Biegung) erweitern. Das Bild 1 zeigt die zeitabhängige Spannungsumlagerung und die dadurch bedingte Aufteilung der Gesamtbetondehnungen in Langzeit- und die schraffierten Kurzzeitanteile.

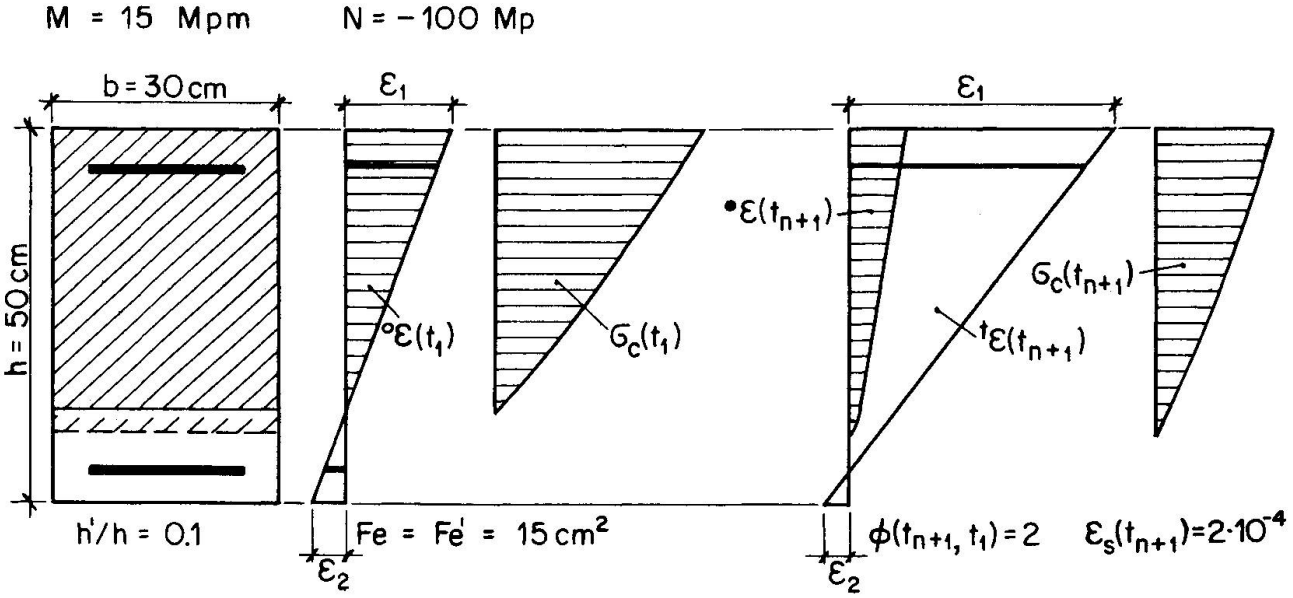

Bild 1: Zeitabhängige Spannungsumlagerung im Stahlbetonquerschnitt

2. GENERELLES VORGEHEN ZUR ERMITTLUNG DER KRUEMMUNG

Die iterative numerische Ermittlung der Krümmung K erfolgt mittels einer "räumlichen Regula Falsi" [1]. In den Achsrichtungen der Grundrissebene seien die beiden unbekannten Randdehnungen $-\varepsilon_1$ und ε_2, in der dritten Richtung die Differenz aus äusserem (aktivem) und innerem (reaktivem) Biegemoment aufgetragen (Bild 2). Dadurch entsteht eine räumliche Fläche, da jedem Wertepaar $-\varepsilon_1$ und ε_2 ein Wert $\Delta M = M_a - M_r$ zugeordnet ist. Trägt man weiters an Stelle von ΔM die Differenz aus äusserer und innerer Normalkraft auf, so entsteht eine zweite räumliche Fläche ΔN. Das Bild 4 zeigt eine Schichtenliniendarstellung derartiger Raumflächen ΔN und ΔM. Die Spuren dieser Flächen in der Grundrissebene $(\varepsilon_1, \varepsilon_2)$ schneiden sich in einem Punkt A, dessen Koordinaten ε_1 und ε_2 die gesuchten Randdehnungen darstellen, für die sowohl $\Delta M = M_a - M_r = 0$ als auch $\Delta N = N_a - N_r = 0$ ist, für die also Gleichgewicht zwischen inneren und äusseren Schnittlasten besteht.

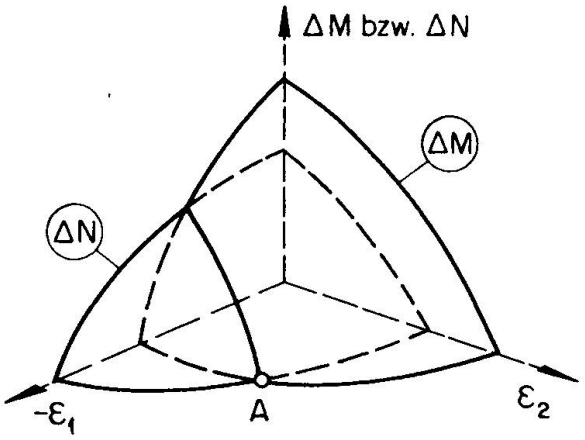

Bild 2

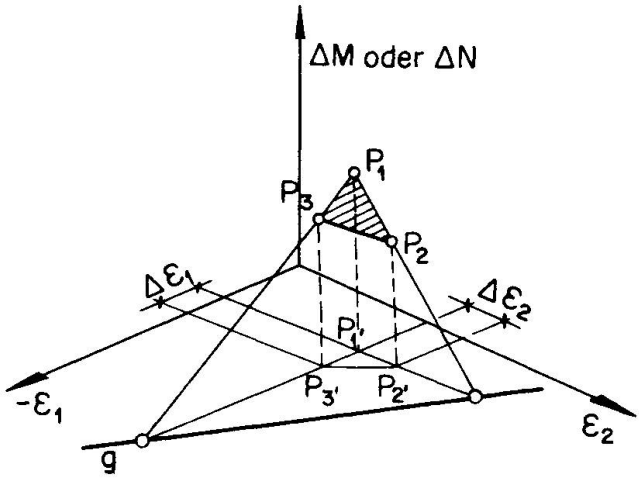

Bild 3

Ausgehend von Näherungswerten für ε_1 und ε_2, erhält man durch deren Variation je drei Punkte P_1, P_2, P_3 für ΔM bzw. ΔN, durch die je eine Ebene gelegt werden kann (Bild 3). Diese Ebenen ersetzen näherungsweise Tangentialebenen an die beiden Raumflächen ΔM und ΔN. Jede der beiden Tangentialebenen schneidet die Grundrissebene $(\varepsilon_1, \varepsilon_2)$ in einer Geraden g. Der Schnittpunkt der beiden Geraden liefert ein verbessertes Wertepaar ε_1 und ε_2. Dieses ersetzt die Grundrisskoordinaten jenes Punktes P, für den die relative Abweichung $\Delta M/M_a$ oder $\Delta N/N_a$ am grössten ist. Nun kann ein neues Tangentialebenenpaar aufgespannt werden, das einen verbesserten Schnittpunkt A in der $(\varepsilon_1, \varepsilon_2)$-Ebene liefert. Dieser Vorgang wird so lange wiederholt, bis die absoluten Werte ΔM und ΔN (innerhalb der Abbruchgenauigkeit) genügend gegen Null gehen. Damit sind zu den vorgegebenen Schnittlasten M_a und N_a jene beiden Randdehnungen ε_1 und ε_2 gefunden, für die sich innere und äussere Schnittkräfte im Gleichgewicht befinden. Die gesuchte Querschnittskrümmung ergibt sich zu $K = (\varepsilon_1 + \varepsilon_2)/h$.

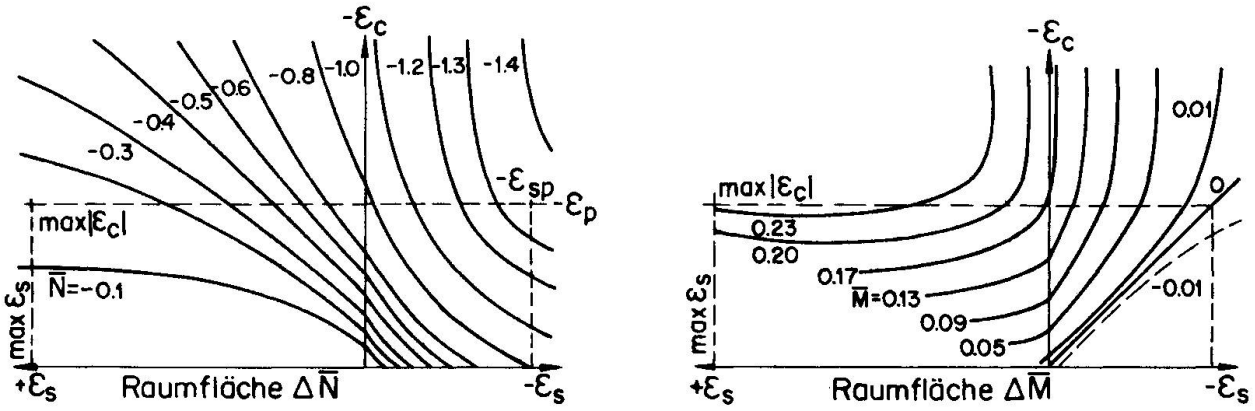

Bild 4

3. BERECHNUNG DER INNEREN SCHNITTLASTEN

Bei der Krümmungsberechnung nach Abschnitt 2 sind für ein bestimmtes Wertepaar ε_1 und ε_2 die inneren Schnittgrössen N_r und M_r erforderlich:

$$N_r = \int_{-h/2}^{+h/2} \sigma_c \cdot b \cdot dy + \Sigma A_s \cdot \sigma_s \ , \quad M_r = \int_{-h/2}^{+h/2} \sigma_c \cdot b \cdot y \cdot dy + \Sigma A_s \cdot \sigma_s \cdot y_s \qquad (1)$$

Zur numerischen Berechnung der Integrale in (1) nach Simpson wird der Betonquerschnitt diskretisiert (Bild 5a). Unter der Voraussetzung eben bleibender Querschnitte setzt sich das Gesamtdehnungsbild aus Kurz- und Langzeitdehnungen (Bild 1, Bild 5b) zusammen.

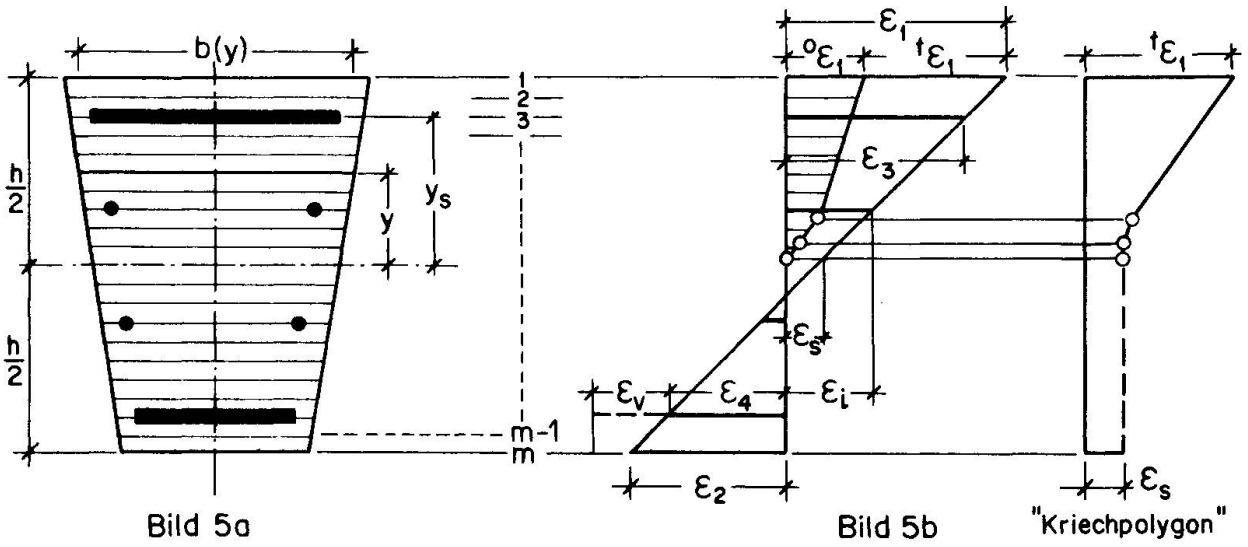

Bild 5a Bild 5b

Nur der elastische Anteil der Kurzzeitverformung liefert die Betonspannungen in (1), wogegen für den Stahl selbstverständlich die Gesamtdehnung massgebend ist. Die Berechnung der elastischen Kurzzeitdehnungen durch Abziehen der plastischen Kurzzeitverformung und der Langzeitverformungen vom Geamtdehnungsbild wird im Abschnitt 5 dargestellt.

4. DIE ZEITLICHE KRUEMMUNGSAENDERUNG

Das hier vorausgesetzte lineare Kriechen ist meist gegeben, wenn die ständige Last höchstens den mit dem vorgesehenen Sicherheitsfaktor reduzierten Kurzzeitlasten entspricht. Zur Ermittlung der zeitabhängigen Querschnittskrümmung wird der zeitliche Verformungsablauf diskretisiert. Innerhalb eines sog. "plastischen Intervalles" wird die kriecherzeugende Spannung konstant gehalten. Durch kriechbedingte Spannungsumlagerungen im Querschnitt vom Beton auf den Stahl würden die Betonspannungen innerhalb eines Intervalles abnehmen. Bei Stahlbetonstützen nehmen jedoch die Verformungsmomente infolge Kriechen zu, wodurch gegenläufig Betonspannungen aufgebaut werden. Dadurch liefert die Annahme konstanter Spannungen innerhalb eines Intervalles bereits für eine geringe Anzahl von Kriechintervallen gute Ergebnisse.

Nach jedem plastischen Intervall können die äusseren Schnittlasten verändert werden (Theorie 2. Ordnung und/oder Relaxation). Danach werden gemäss Abschnitt 2 die Randdehnungen ε_1 und ε_2 berechnet, für die Gleichgewicht zwischen inneren und äusseren Schnittlasten besteht. Aus den so erhaltenen elastischen Dehnungen kann nach Abschnitt 5 die plastische Verformung am Ende des nächsten Kriechintervalles bestimmt werden. Man berechnet also alternierend aus elastischen Verformungen plastische und danach entsprechend Theorie 2. Ordnung neue elastische Dehnungen.

Die Langzeitverformungen werden im sog. "Kriechvektor" gespeichert. Befindet sich der Querschnitt im Zustand II, so erhält das "Kriechpolygon" (Bild 5b) nach jedem plastischen Intervall einen weiteren Knick. Dadurch ist auch der Verlauf der Kurzzeitdehnungen im Bereich der zeitabhängigen Nullinienverschiebung nicht linear.

5. DIE BESTIMMUNG DER BETONSPANNUNGEN

5.1 Kurzzeitverformungen

Das Bild 6 stellt das σ-ε-Diagramm für eine mit σ_0 vorbelastete Querschnittsfaser dar. Der schraffierte Bereich entspricht den plastischen Kurzzeitstauchungen. Eine Erhöhung der Spannung (σ_1) bewirkt ein Anwachsen des plastischen Verformungsanteiles, wogegen dieser bei Abnahme der Spannung (σ_2) unverändert bleibt. Es muss daher stets in jeder betrachteten Querschnittsfaser der aus allen Vorbelastungen resultierende maximale Wert ${}^0\varepsilon_{pl0}$ bekannt sein. Er wird in der numerischen Berechnung auf den "plastischen Kurzzeitvektor" $\{EPO\}_m$ abgespeichert. Die plastische Kurzzeitverformung ist auch vom Belastungsalter (Festigkeitszunahme und "Versprödung") und der Belastungsgeschwindigkeit ("rasches Anfangskriechen") beeinflusst. Dieser Tatsache kann man durch zeitabhängiges Verändern des σ-ε-Diagrammes Rechnung tragen. Vereinfachend werden jedoch allgemein in den Normen mittlere σ-ε-Diagramme für Kurzzeitbelastungen angegeben.

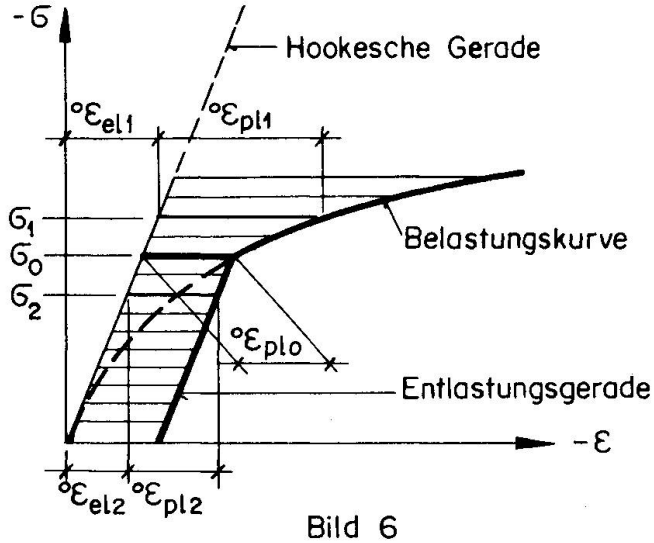

Bild 6

5.2 Langzeitverformungen

Aus der Integralgleichung für stetige Belastungsänderungen [3]

$$\varepsilon_{ges}(t_k) = {}^0\varepsilon_{el}(t_1)\cdot[1+\phi(t_k,t_1)] + \int_{t_i=t_2}^{t_i=t_k} \frac{\partial\,{}^0\varepsilon_{el}(t_i)}{\partial t_i}\cdot[1+\phi(t_k,t_i)]\cdot dt_i + \varepsilon_s(t_k)$$

erhält man durch Auswertung für mehrere konstante Belastungsstufen den plastischen Anteil der Langzeitverformung

$${}^t\varepsilon_{pl}(t_k) = {}^0\varepsilon_{el}(t_1)\cdot\phi(t_k,t_1) + \sum_{t_i=t_2}^{t_i=t_{k-1}} \Delta\,{}^0\varepsilon_{el}(t_i)\cdot\phi(t_k,t_i) + \varepsilon_s(t_k) \qquad (1)$$

Setzt man in (1) für $\Delta\,{}^0\varepsilon_{el}(t_i) = {}^0\varepsilon_{el}(t_i) - {}^0\varepsilon_{el}(t_{i-1})$ so ergibt sich

$${}^t\varepsilon_{pl}(t_k) = \sum_{t_i=t_1}^{t_i=t_{k-1}} {}^0\varepsilon_{el}(t_i)\cdot[\phi(t_k,t_i)-\phi(t_k,t_{i+1})] + \varepsilon_s(t_k) \qquad (2)$$

In [3] wird die verzögert elastische Verformung in den Kriechzahlen ϕ berücksichtigt. Erfasst man sie jedoch getrennt [2], so ändern sich die Kriechzahlen in (2).

$${}^t\varepsilon_{el}(t_k) = \sum_{t_i=t_1}^{t_i=t_{k-1}} {}^0\varepsilon_{el}(t_i)\cdot[0{,}4\cdot\Phi(t_{i+1}-t_i)]\cdot[1-\Phi(t_k-t_i)] \qquad (3)$$

Der jeweils erste Ausdruck in eckiger Klammer baut die verzögert elastische Verformung auf, der zweite bewirkt die elastische Rückverformung. Die Gleichungen (2) und (3) lassen sich zusammenfassen:

$${}^t\varepsilon(t_k) = {}^t\varepsilon_{el}(t_k) + {}^t\varepsilon_{pl}(t_k) = \sum_{t_i=t_1}^{t_i=t_{k-1}} {}^0\varepsilon_{el}(t_i)\cdot\Delta\phi(t_i,t_k) + \varepsilon_s(t_k) \qquad (4)$$

$$\Delta\phi(t_i,t_k)=[0{,}4\cdot\Phi(t_{i+1}-t_i)]\cdot[1-\Phi(t_k-t_i)]+[\phi(t_k,t_i)-\phi(t_k,t_{i+1})] \quad (5)$$

t_k durchläuft die Werte t_2 bis t_{n+1}, t_i die Werte t_1 bis t_n. Die in (4) erforderlichen elastischen Kurzzeitdehnungen werden, für die m-Querschnittsfasern (Bild 5a) angewendet, zur Matrix $[EEO]_{mxn}$ zusammengefasst, während die Vektoren $\{\Delta\phi(t_k)\}_{k-1}$ für $t_k=t_2$ bis t_{n+1} eine rechte Dreiecksmatrix belegen. Der Vektor der Langzeitdehnungen zur Zeit t_k ergibt sich zu:

$$\{EL\}_m = [EEO]_{mx(k-1)}\cdot\{\Delta\phi(t_k)\}_{k-1}$$

5.3 Die Betonspannung in einer Querschnittsfaser zur Zeit t_k

Durch Abziehen der Langzeitdehnungen ${}^t\varepsilon$ von der Gesamtdehnung ε_{ges} erhält man die Kurzzeitdehnung ${}^0\varepsilon$ (Bild 7). Das σ-ε-Diagramm für Kurzzeitbelastung stellt den nichtlinearen Zusammenhang

$$\sigma_c = f({}^0\varepsilon) \qquad [\text{z.B. } \sigma_c = \beta_c\cdot\frac{{}^0\varepsilon}{\varepsilon_\beta}\cdot(2-\frac{{}^0\varepsilon}{\varepsilon_\beta})] \quad (6)$$

dar, woraus sich die plastische Kurzzeitverformung ${}^0\varepsilon_{pl}$ errechnen lässt

$${}^0\varepsilon_{pl} = {}^0\varepsilon-\sigma_c/E_c \qquad [\text{z.B. } {}^0\varepsilon_{pl} = \frac{1}{2}\frac{{}^0\varepsilon^2}{\varepsilon_\beta}]$$

Durch Vergleich mit ${}^0\varepsilon_{plo}$ erhält man folgende Fallunterscheidungen:

a) $|{}^0\varepsilon_{pl}|>|{}^0\varepsilon_{plo}|$: Spannungszunahme (Bild 7). Wenn gemäss Abschnitt 2 Gleichgewicht gefunden ist, wird {EPO} korrigiert.

b) $|{}^0\varepsilon_{pl}|<|{}^0\varepsilon_{plo}|$: Spannungsrelaxation (Bild 8). Die Betonspannung ist neu zu berechnen: $\sigma_c = E_c({}^0\varepsilon-{}^0\varepsilon_{plo})$

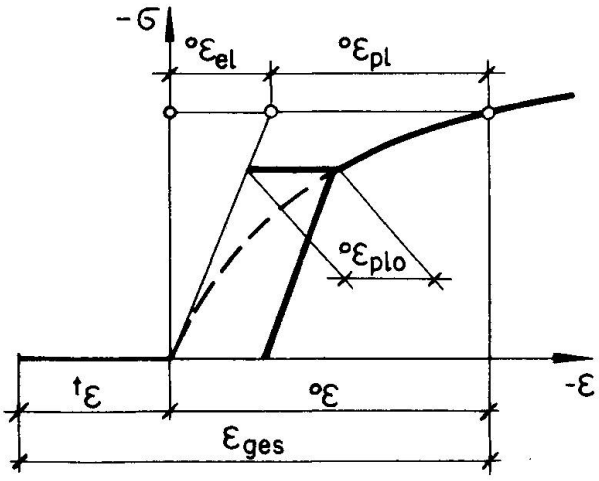

Bild 7

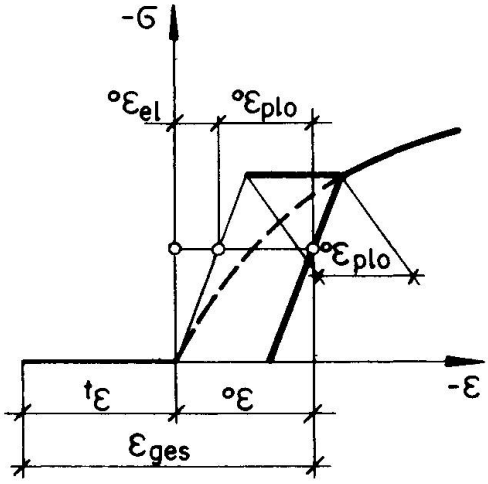

Bild 8

5.4 Vereinfachungen

Gelingt es, die Zeitintervalle $(t_{i+1}-t_i)$ für i=1,2,..n so zu wählen, dass alle Elemente $\Delta\phi(t_i,t_k)\neq 0$ gleich gross werden, so lässt sich die Gleichung (4) wie folgt schreiben:

$$^{t}\varepsilon(t_k) = \Delta\phi\cdot \sum_{t_i=t_1}^{t_i=t_{k-1}} {}^{0}\varepsilon_{el}(t_i) + \varepsilon_s(t_k)$$

In diesem Fall genügt zur Berechnung der Langzeitverformungen der Vektor $\{EL\}_m = \{\Delta\phi\cdot\Sigma^{0}\varepsilon_{el}(t_i)\}_m$. Die Matrizen $[EEO]_{mxn}$ und $[\Delta\phi]_{nxn}$ können entfallen.

Wird der Beton näherungsweise als nichtlinear elastisches Material angesehen, so erhält man die Betonspannungen stets aus Gleichung (6). Alle weiteren Ueberlegungen im Abschnitt 5.3 und der plastische Kurzzeitvektor {EPO} werden dann unnötig.

Bezeichnungen

M_a	äusseres (aktives) Moment
M_r	inneres (reaktives) Moment
N_a	äussere (aktive) Normalkraft
N_r	innere (reaktive) Normalkraft
K	Krümmung
$^{0}\varepsilon$	Kurzzeitverformung des Betons
$^{t}\varepsilon$	Langzeitverformung des Betons
$^{0}\varepsilon_{el}(t_i)$	elastische Kurzzeitdehnung zur Zeit t_i
$^{0}\varepsilon_{pl}(t_i)$	plastische Kurzzeitdehnung zur Zeit t_i
$^{t}\varepsilon_{el}(t_i)$	elastische Langzeitdehnung zur Zeit t_i
$^{t}\varepsilon_{pl}(t_i)$	plastische Langzeitdehnung zur Zeit t_i
$^{0}\varepsilon_{plo}$	maximale Dehnung einer Faser aus allen Vorbelastungen
t	wirksame Zeit
$\phi(t_k,t_i)$	Kriechzahl für das Zeitintervall t_i bis t_k
$\Phi(t_k-t_i)$	Beiwert, der den zeitlichen Verlauf der verzögert elastischen Verformung berücksichtigt ($o<\Phi<1$ ist nur von t_k-t_i abhängig)
$\varepsilon_s(t_k)$	Schwinddehnung bis zur Zeit t_k
ε_1	gesamte Dehnung am Druckrand
ε_2	gesamte Dehnung am Zugrand
ε_3	Dehnung der Druckbewehrung
ε_4	Dehnung der Zugbewehrung
ε_i	Dehnung der Stegbewehrung
ε_v	Vordehnung, falls es sich um Spannstahl handelt
σ_c	Betonspannung
σ_o	Betonspannung infolge der Vorbelastungen
β_c	Prismenfestigkeit des Betons
ε_β	absolut kleinste Betondehnung bei β_c
b	Breite eines Rechteckquerschnittes
h	Höhe eines Rechteckquerschnittes
$\bar{M}=M_r/\beta_c\cdot b\cdot h^2$	bezogenes Biegemoment (Rechteckquerschnitt)
$\bar{N}=N_r/\beta_c\cdot b\cdot h$	bezogene Normalkraft (Rechteckquerschnitt)
A_s	Querschnittsfläche eines Bewehrungsstabes
m	Anzahl der betrachteten Querschnittsfasern
n	Anzahl der "Kriechintervalle"
ε_{ges}	Gesamtdehnung zur Zeit t_k

Literaturverzeichnis

[1] Jänike, J.: Nichtlineare Berechnung von Stabwerken. Eine Algol-Studie, VEB Verlag für Bauwesen, 1968.

[2] Rüsch, H., Jungwirth, D., Hilsdorf, H.: Kritische Sichtung der Verfahren zur Berücksichtigung der Einflüsse von Kriechen und Schwinden des Betons auf das Verhalten der Tragwerke. Beton- und Stahlbetonbau 1973, Heft 3,4,6.

[3] Trost, H.: Auswirkungen des Superpositionsprinzips auf Kriech- und Relaxationsprobleme bei Beton- und Spannbeton. Beton- und Stahlbetonbau 1967, Heft 10.

ZUSAMMENFASSUNG

Es wird eine numerisch iterative Methode zur wirklichkeitsnahen Bestimmung des zeitabhängigen Verformungsverhaltens von Stahl- und Spannbetonquerschnitten dargestellt. Beliebige elastische und plastische zeitabhängige Betoneigenschaften, eine vorgegebene Belastungsgeschichte und verschiedene Stahltypen können berücksichtigt werden. Während des zeitabhängigen Verformungsvorganges kann der Querschnitt vom ungerissenen Zustand in den gerissenen übergehen und umgekehrt.

SUMMARY

A numerical method by trial and error to compute the time dependent deformation behavior of reinforced- and prestressed concrete cross-sections is described. Arbitrary elastic and plastic time dependent concrete properties, a given loading history and different types of reinforcing steel can be considered. During the time dependent deformation process the cross-section can change from an uncracked state to a cracked one and conversely.

RESUME

On présente une méthode numérique itérative qui approche le comportement réel à la déformation en fonction du temps de sections en béton armé ou précontraint. On peut introduire dans le calcul toutes les caractéristiques élastiques et plastiques du béton en fonction du temps, l'"historique" de la charge, ainsi que différents types d'acier. Au cours du processus de déformation, la section peut passer de l'état non fissuré à l'état fissuré et vice-versa.

An Experimental-Analytical Study of Complete Load-Deformation Characteristics of Concrete Compression Members Subjected to Biaxial Bending

Etude analytique et expérimentale de la relation charge-déformation de pièces comprimées en béton armé soumises à une flexion biaxiale

Eine rechnerische und versuchstechnische Untersuchung über die Beziehungen zwischen Last und Verformung von Druckgliedern unter schiefer Biegung

Cheng-Tzu HSU
Ph.D. Candidate
Department of Civil Engineering

M. Saeed MIRZA
Associate Professor of Civil Engineering
and Applied Mechanics and Dean of Students

McGill University
Canada

INTRODUCTION

This investigation was aimed at studying the "complete" behaviour of short reinforced concrete pin-ended columns subjected to biaxial bending moments as the applied compressive loads were increased from zero until failure which was defined as the stage at which spalling of concrete took place accompanied by buckling of the steel reinforcing bars. This paper discusses briefly the mathematical formulation leading to the computer program besides reviewing the experimental procedure. The experimental and computed load-deflection curves are compared for a symmetrically loaded column subjected to biaxial bending.

THEORETICAL ANALYSIS

A numerical analysis was developed by the writers (Ref.1,2) to determine strain and curvature distributions in any structural concrete section subjected to biaxial bending moment and axial compression. This analysis can account for any given section geometry and material properties. Member cross-section is divided into several small elements and the stress resultants P, M_x and M_y on this section can be expressed as function of ϕ_x, ϕ_y and ε_p given by the following equations (see Fig.1):

$$P = P(\phi_x,\phi_y,\varepsilon_p) \quad (1a), \qquad M_x = M_x(\phi_x,\phi_y,\varepsilon_p) \quad (1b),$$

$$\text{and} \qquad M_y = M_y(\phi_x,\phi_y,\varepsilon_p) \quad (1c)$$

where P = axial force
M_x = bending moment about the x-axis
M_y = bending moment about the y-axis
ε_p = uniform direct strain due to an axial load P
ϕ_x = the curvature produced by the bending moment component M_x and is considered positive when it causes compressive strains in the positive y-direction, and
ϕ_y = the curvature produced by the bending moment component M_y and is considered positive when it causes compression in the positive x-direction.

The strain ε_k across any element k can be assumed to be uniform and since plane sections remain plane during bending

$$\varepsilon_k = \varepsilon_p + \phi_x y_k + \phi_y x_k \tag{2}$$

where x_k and y_k are coordinates of the centroid of the element k.

Having established the strain distribution across the cross-section, the axial force P and the bending moment components M_x and M_y can be calculated using the following equations:

$$P_{(c)} = \sum_{k=1}^{n} f_k a_k \quad (3a), \quad M_{x(c)} = \sum_{k=1}^{n} f_k a_k y_k \quad (3b), \quad M_{y(c)} = \sum_{k=1}^{n} f_k a_k x_k \quad (3c)$$

Subscript (c) indicates values of P, M_x and M_y calculated in an iteration cycle, and a_k is the area of element k. The values of P, M_x and M_y can be estimated using the Taylor's theorem from the values of $P_{(c)}$, $M_{x(c)}$ and $M_{y(c)}$ from equations (3) as follows:

$$P = P_{(c)} + \frac{\partial P_{(c)}}{\partial \phi_x}\delta\phi_x + \frac{\partial P_{(c)}}{\partial \phi_y}\delta\phi_y + \frac{\partial P_{(c)}}{\partial \varepsilon_p}\delta\varepsilon_p \tag{4a}$$

$$M_x = M_{x(c)} + \frac{\partial M_{x(c)}}{\partial \phi_x}\delta\phi_x + \frac{\partial M_{x(c)}}{\partial \phi_y}\delta\phi_y + \frac{\partial M_{x(c)}}{\partial \varepsilon_p}\delta\varepsilon_p \tag{4b}$$

$$M_y = M_{y(c)} + \frac{\partial M_{y(c)}}{\partial \phi_x}\delta\phi_x + \frac{\partial M_{y(c)}}{\partial \phi_y}\delta\phi_y + \frac{\partial M_{y(c)}}{\partial \varepsilon_p}\delta\varepsilon_p \tag{4c}$$

The values $\delta\phi_x$, $\delta\phi_y$ and $\delta\varepsilon_p$ are increments in ϕ_x, ϕ_y and ε_p required to produce changes δP, δM_x and δM_y respectively. The partial derivatives $\frac{\partial P_{(c)}}{\partial \phi_x}$, ...etc. are the rates of change of P, M_x and M_y with ϕ_x, ϕ_y and ε_p.

These partial derivatives in equations (4) are replaced by the corresponding difference quotients; and by suitably incrementing

each deformation quantity at a time, the rates of change can be evaluated and substituted in equations (4). The resulting simultaneous equations (4) are solved for $\delta\phi_x$, $\delta\phi_y$ and $\delta\varepsilon_p$ and these increments are added to the initial deformations and the process is repeated using the new deformation values until convergence is obtained. For more details, the reader may refer to Reference 2 and 3.

The central deflections δ_{2x} and δ_{2y} along x and y-directions respectively (see Fig.2) were calculated using the following equation derived from a suitable modification of the moment-area theorems to account for behaviour non-linearities.

$$\delta_{2x} = \frac{\phi_y l^2}{8} \quad (5a) \qquad \delta_{2y} = \frac{\phi_x l^2}{8} \quad (5b)$$

The axial load P_3 for each loading step was calculated using the value of P computed and modified for the influence of mid-span deflections using the following equations:

(a) Loading Condition I (see Fig.3a)

$$P_3 = \frac{P(e_x^2 + e_y^2)^{1/2}}{[(e_x + \delta_{2y})^2 + (e_y + \delta_{2x})^2]^{1/2}} \quad (6a)$$

(b) Loading Condition II (see Fig.3b)

$$P_{3x} = \frac{Pe'_y}{2(e'_y + \delta_{2x})} \quad (6b) \qquad P_{3y} = \frac{Pe'_x}{2(e'_x + \delta_{2y})} \quad (6c)$$

and $P_3 = P_{3x} + P_{3y}$ (6d)

More details can be found in Reference 3.

EXPERIMENTAL PROCEDURE

The test specimens were designed as short, tied columns with a square under-reinforced section (see Fig.4). Eleven specimens were manufactured and tested to study the influence of the variation of eccentricities e_x and e_y and the total longitudinal steel percentage (p + p'). Details of the symmetrically loaded test specimen U-3 and the loading arrangement are shown in Fig.3(b) and 4. The stress-strain curves for the concrete and the reinforcing steel wire D5 are shown in Figs.5 and 6, respectively.

Hard rubber blocks were incorporated in the loading frame to dissipate some of the energy of the loading system. Beyond the ultimate load, this arrangement permitted the application of further deformations which were accompanied with a decrease in the applied loads measured using calibrated load cells.

The average curvatures along the mid-span section of the column were evaluated using two sets of experimental data - one from strain gauges installed on the concrete and the reinforcing steel wire and the other from the demec gauges suitably arranged near the section. Deflections along the x- and y-axes were measured using dial gauges with a least count of 0.001 in. Details of the test procedure, material properties, etc. along with the experimental data can be found in Reference 3.

CURVATURE EVALUATION

Experimental observation shows that the strain distributions across the mid-span section along the x and y-direction are very nearly linear, therefore curvature in either direction is given by

$$\phi = \frac{\varepsilon_c + \varepsilon_s}{d} \tag{7a}$$

where ε_c and ε_s are strains in the concrete and the reinforcing steel respectively and d is the distance between the points where ε_s (steel strain in tension reinforcement in x- or y- directions) and ε_c (the extreme concrete compressive strains in x- or y-directions) are measured. After significant cracking, it was observed from the strain gauges that the strain distribution in the compression block became non-linear. Similarly demec gauge results indicated a non-linear strain distribution across the entire section. Average curvature can be approximated by the equation

$$\phi = \frac{\varepsilon_c}{kd} \tag{7b}$$

where kd is the distance between the point where ε_c is measured and the point of zero strain and in x- or y-directions.

COMPARISONS OF EXPERIMENTAL AND ANALYTICAL RESULTS

The cross section was idealized as shown in Fig.7. The theoretical and experimental biaxial moment-curvature curves across the mid-span sections for the symmetrically loaded specimen U-3 (Fig.4) are shown in Fig.8. (e'_x = 17.78 cm. e'_y = 17.78 cm.) The experimental moment-curvature relationships were obtained until either strain gauges became damaged or demec points became dislodged while the theoretical values were computed until the maximum moment capacity. Fig.9 shows the axial load P_3 - central deflection relationship at mid-span of the column. The theoretical values were computed up to the stage when the maximum moment capacity was attained while the experimental values were measured up to the collapse or buckling of the reinforcement. More test data on symmetrically and unsymmetrically loaded specimens can be found in Reference 13.

CONCLUSIONS

The above theoretical analysis indicates that it is possible to predict biaxial moment-curvature and load-deflection curves up to the maximum moment capacity of the column specimen. Also the use of hard rubber blocks in column compression tests makes it possible to measure the complete biaxial moment-curvature and load-deflection curves up to the failure stage as defined earlier. The analysis in this paper has resulted in the evaluation of the flexural rigidity coefficients for members of three-dimensional structural concrete frames and can be incorporated without much difficulty into the existing computer programs for analysis of three-dimensional framed structures.

ACKNOWLEDGEMENTS

The writers gratefully acknowledge the financial support of the Department of Education, Government of Quebec, the National Research Council of Canada and the Canada Emergency Measures Organization to continuing studies of Structural Concrete Systems at McGill University. The results reported in this paper form a part of Mr. Hsu's Ph.D. thesis.

BIBLIOGRAPHY

1. Cheng-Tzu Hsu and M.S.Mirza, "A Numerical Analysis of Reinforced and Prestressed Concrete Sections under Combined Flexure and Axial Compression", Structural Concrete Series No.72-1, McGill University, Montreal, Canada, February 1972, pp.32.
2. Cheng-Tzu Hsu and M.S.Mirza, "Structural Concrete-Biaxial Bending and Compression", Journal of the Structural Division, ASCE, Vol.99, No.ST2, February 1973, pp.285-290.
3. Cheng-Tzu Hsu, "Behaviour of Structural Concrete Subjected to Biaxial Flexure and Axial Compression", Ph.D. Thesis, McGill University, June 1974.

SUMMARY

The above theoretical analysis indicates that it is possible to predict biaxial moment-curvature and load-deflection curves up to the maximum moment capacity of the column specimen. Also the use of hard rubber blocks in column compression tests makes it possible to measure the complete biaxial moment-curvature and load-deflection curves up to the failure stage as defined earlier. The analysis in this paper has resulted in the evaluation of the flexural rigidity coefficients for members of three-dimensional structural concrete frames and can be incorporated without much difficulty into to existing computer programs for analysis of three-dimensional framed structures.

RESUME

L'étude théorique rend possible la détermination des courbes moment-courbure et charge-déformation jusqu'à la charge ultime de la colonne considérée. L'utilisation d'éléments en caoutchouc durci lors d'essais de colonnes comprimées rend possible la mesure

intégrale des courbes moment biaxial-courbure et charge-déformation jusqu'à l'état de rupture mentionné plus haut. L'étude présentée ici a permis l'évaluation des coefficients de rigidité à la flexion d'éléments de cadres tridimensionnels en béton armé; elle peut être incorporée sans grandes difficultés aux programmes existants d'ordinateur pour l'étude des structures tridimensionnelles.

ZUSAMMENFASSUNG

Die vorliegende Untersuchung zeigt, dass es möglich ist, die Beziehungen zwischen Biegemoment und Krümmung sowie zwischen Last und Verformungen bis zur Biegetragfähigkeit der Versuchsstützen auch für schiefe Biegung theoretisch vorauszusagen. Die Verwendung von Gummiblöcken für die Lagerung der Versuchsstützen gestattet die vollständige Beobachtung dieser Beziehungen bis zum Bruch. Das vorgelegte Berechnungsverfahren führt zu Koeffizienten für die Ermittlung der Biegefestigkeit von Bauteilen in räumlichen Tragwerken und kann leicht in bestehende Computer-Programme eingebaut werden.

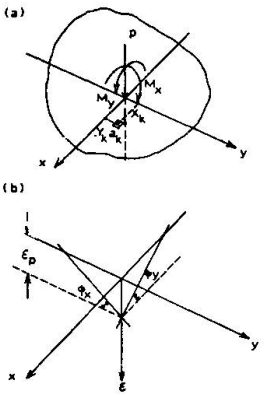

FIG.1 IDEALIZATION OF A CROSS-SECTION SUBJECTED TO BIAXIAL BENDING AND AXIAL COMPRESSION

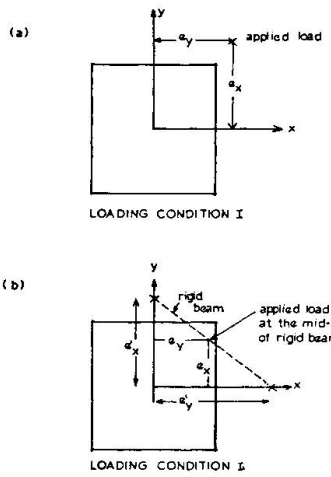

FIG.3 LOADING CONDITIONS FOR BIAXIALLY LOADED SHORT COLUMN

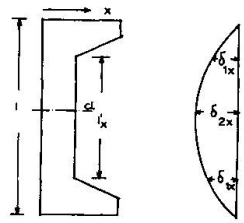

FIG.2 BIAXIALLY LOADED COLUMN

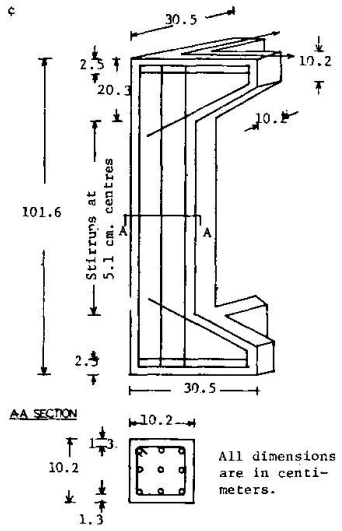

FIG.4 DETAILS OF SPECIMEN U-3

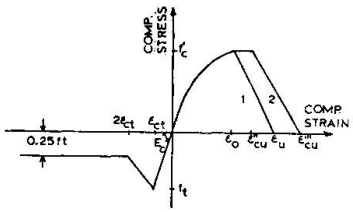

1: Unconfined concrete
2: Confined concrete

FIG.5 IDEALIZED STRESS-STRAIN CURVE

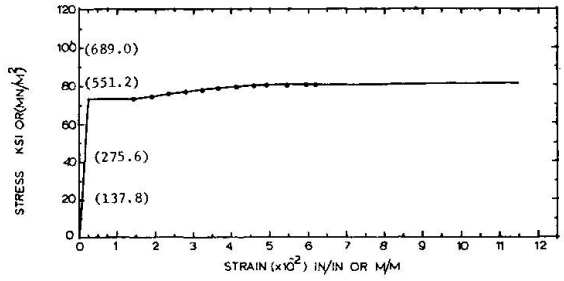

FIG.6 STEEL STRESS-STRAIN CURVE FOR D-5 DEFORMED BAR

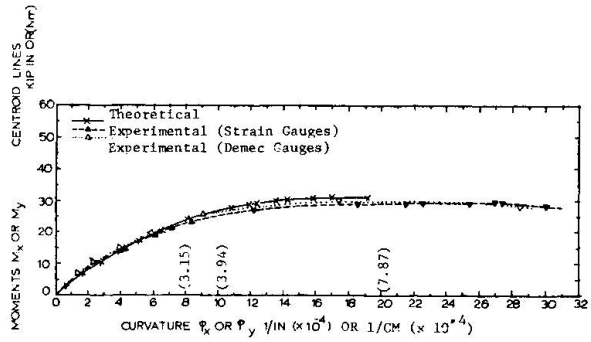

FIG.8 BIAXIAL MOMENT-CURVATURE CURVES FOR SPECIMENT U-3

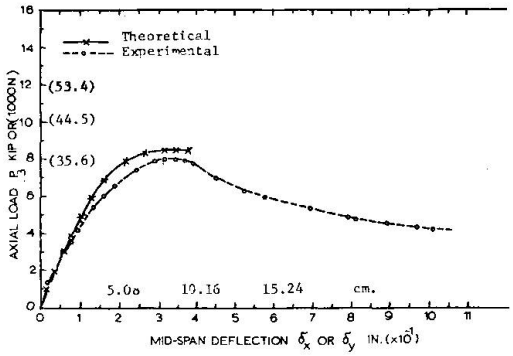

FIG.9 LOAD-DEFLECTION CURVES FOR SPECIMEN U-3

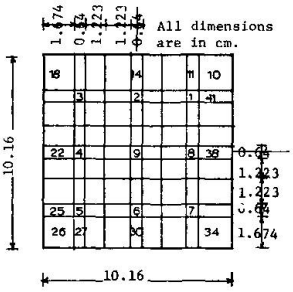

FIG.7 BIAXIALLY LOADED COLUMNS: SPECIMEN U-3

A Study on the Behaviour of Steel Reinforced Concrete Columns and Frames

Une étude sur le comportement des colonnes et des cadres en béton armé

Eine Untersuchung über das Verhalten von Stahlbeton-Stützen und -Rahmen

Minoru WAKABAYASHI
Professor
Disaster Prevention Research Institute
Kyoto University
Kyoto, Japan

Michio SHIBATA
Lecturer
Osaka Institute of Technology
Osaka, Japan

Chiaki MATSUI
Associate Professor
Kyushu University
Fukuoka, Japan

Koichi MINAMI
Lecturer
Osaka Institute of Technology
Osaka, Japan

1. INTRODUCTION

For ascertaining the safety of a column or a frame under severe earthquake loading it is important to know the load-deflection relation of a column or a frame in the unloading range as well as the loading range under constant vertical and monotonically increasing or alternately repeated horizontal loading(1). Although several experimental investigations have been reported, the theoretical approach to the problem has not been well developed in the field of steel reinforced concrete (SRC).

The behavior of a SRC column under axial force and bending moment is almost the same as that of an ordinary reinforced concrete column in loading range if it is not subjected to severe shear force. However, a SRC column shows some-what different behavior from that of an ordinary reinforced concrete column in the unloading range in the following sence; the covering concrete falls off during the unloading, and the steel flange is not apt to buckle.

As pointed out in the introductory report the computation may become formidable if we start from accurate stress-strain relation. In this paper, starting from idealized hysteretic stress-strain relations and using discrete element approach, moment-curvature relations of a column under constant axial force are calculated. Since, as quoted in the introductory report, consideration of a finite length of the member is unavoidable when the negative slope range of the stress-strain curve of material is to be analyzed, the analysis of a member or a frame is carried assuming the flexural portions with a finite length near the member ends in which the curvature is uniformly distributed.

2. THEORETICAL INVESTIGATION

a. Moment-Curvature Relation: Let us consider a steel-reinforced concrete column section subjected to constant axial force and varying bending moment,

in which stress and strain distributions are uniquely determined at a certain loading stage, and suppose that the state of stress at this stage is given by a piecewise-linear function of the state of strain, $\sigma_z = f_z(\varepsilon_z)$, where σ_z and ε_z are the stress and the strain in the fiber in the distance of z from the central axis. The shear force effect is neglected. The increments of axial force, dN, and the bending moment, dM, developed in the subsequent loading are given by

$$0 = dN = \int d\sigma_z \cdot dA = \int f_z' \cdot dA \cdot d\varepsilon_z \tag{1}$$

$$dM = \int d\sigma_z \cdot z \cdot dA = \int f_z' \cdot z \cdot dA \cdot d\varepsilon_z \tag{2}$$

where $d\sigma_z$ and $d\varepsilon_z$ are the stress and the strain increments, respectively, the prime denotes the derivative with respect to ε_z and the integration is carried over the cross sectional area.

If we assume that the plane section normal to the central axis remains plane, $d\varepsilon_z$ is explained by the strain increment on the central axis, $d\varepsilon$, and the curvature increment, $d\kappa$. Employing the definitions,

$$\bar{A} \equiv \int f_z' \cdot dA, \quad \bar{S} \equiv \int f_z' \cdot z \cdot dA, \quad \bar{I} \equiv \int f_z' \cdot z^2 \cdot dA \tag{3}$$

Eqs. (1) and (2) become

$$\bar{A} \cdot d\varepsilon + \bar{S} \cdot d\kappa = 0 \tag{4}$$

$$\bar{S} \cdot d\varepsilon + \bar{I} \cdot d\kappa = dM \tag{5}$$

Eliminating $d\varepsilon$ from Eqs. (4) and (5), the incremental moment-curvature relation is determined as

$$dM = (\bar{I} - \bar{S}^2/\bar{A}) \cdot d\kappa \tag{6}$$

This procedure does not always demand the linearity of the stress-strain relationship, but the nonlinear relationship requires the iterative procedure and the application to the deflection analysis of frames may become difficult. $\bar{A}$, $\bar{S}$ and $\bar{I}$ can be evaluated from Eq. (3) by deviding the cross section into a finite number of strip elements perpendicular to z axis, and by assuming the uniform distrubution of f'_z in a strip.

The hysteretic stress-strain relationship of steel is assumed to be the one shown in Fig. 1(a), taking Bauschinger effect into account. In the figure, σ_y, ε_y, and E_s are the yield stress, yield strain and Young's modulus of steel, respectively. The compressive strength of the covering concrete deteriorates due to the crash at an early stage of the compressive strain. On the other hand, the crashing strain of the confined concrete may be quite large due to the restraining action of steel flanges. From this point of view, two different kinds of the hysteretic stress-strain relations, shown in Figs. 1(b) and (c), are assumed for the confined and covering concrete, respectively. For both of them, the maximum strength σ_B is taken as 75% of the cylinder strength of concrete and the tensile strength is neglected.

b. Deflection Analysis of a Single Column and a Framed Structure: When the shear force effect is neglected, the deflection of a member subjected to bending can be determined by integrating the curvature, if the material is "stable" according to Drucker's postulate, and thus the moment is uniquely related to the curvature. However, as pointed in the introductory report, we must consider that finite lengths of section are governed by the same relationship between moment and curvature, when to deal with the unstable material like concrete.

In this paper, the following mathematical model is considered for

simplicity to conduct the deflection analysis of a column or a frame. Let us consider a cantilever subjected to a lateral load P at its tip. When it is assumed that a curvature κ, which corresponds to the bending moment at the end ($=P\cdot\ell$), is uniformly distributed along the length s, and that the remaining portion of the cantilever with length of (ℓ-s) is rigid, the deflection at the tip, δ, can be obtained as

$$\delta = \kappa\cdot s\cdot(\ \ell - s/2\ ) \tag{7}$$

In the actual computation, the length s is so determined that the deflection, δ, of this model coincides the exact tip deflection of the entirely elastic cantilever, and it is given as

$$s = (\ 1 - 1/\sqrt{3}\ )\cdot\ell \tag{8}$$

The incremental load-displacement relation for the cantilever is directly obtained by rewriting Eq.(7) in the incremental form, and using Eq.(6), as follows:

$$dP = \frac{\ell\cdot(\ \bar{I} - \bar{S}^2/\bar{A}\ )}{s\cdot(\ \ell - s/2\ )}\cdot d\delta \tag{9}$$

This method of approach can be applicable to the deflection analysis of a portal frame subjected to the constant vertical load, N, on columns and monotonic or alternately repeated horizontal load, Q. As conducted in the deflection analysis of a column, the flexural portions are imposed at both ends of the beam and columns, in which uniform curvatures are assumed to be distributed, and all other portions are assumed to show the rigid body motion. A simple computation based on the equilibrium condition at the joints and the geometrical relation gives the linear relation between the load increment and displacement increment.

3. EXPERIMENTS

To ascertain the accuracy of the theoretical treatment, the theoretical results are compared with the experimental ones which have been obtained by the authors(2, 3, 4). A brief explanation on the tests is given here.

The experimental works are composed of six series as shown in Table 1. Shapes and dimensions of specimens and the loading system are given in Fig. 2. In all series, the axial loads, N, are kept constant, and the horizontal or lateral loads, Q, are applied in the monotonic or alternately repeated manner, as identified by the second alphabet of each specimen, M or R, respectively. Numerals appearing in the specimen numbers denote the axial load ratio N/N_o, where N_o is the ultimate compressive strength of a SRC cross section obtained by the method of superposition.

In SM and SR series, the specimen is subjected to uniform bending, and moment-curvature relations are derived from the deflection data detected at three points along the member axis. The column specimens in CR series are subjected to double curvature bending, and the chord rotation angle, R, is computed from the deflection data detected at the top and bottom of the column. On the other hand, the drift angle, R, of the frame is given by the horizontal displacement, δ, divided by the column height, h, as shown in Fig. 3.

In SM, SR and CR series, the bending cracks are first observed during the tests, the ultimate strength of each specimen is attained due to the yielding of steel and the development of the ultimate compressive strain of the concrete. And finally the covering concrete falls off causing the decrease of resistance.

Damaged portion is located at the center in SM and SR series, and at member ends in CR series. In the frame tests, the bending cracks are observed at beam and column ends, and the final failure occurs at both ends of columns. In all frame specimens, the concrete crash is not observed at the beam ends.

4. DISCUSSION ON THE RESULTS

The theoretical results(solid lines) are compared with the experimental ones(dashed lines) in Figs. 4 to 8. The moment-curvature relations are drawn for SM and SR series in Figs. 4 and 5. For monotonic loading cases, it is observed that the theory well predicts the strength deterioration after the attainment of the maximum strength. The negative slope of the moment-curvature curve becomes steeper with the increase of the axial load. In the large curvature range, the strength seems to converge to the sum of the strengths contributed from the confined concrete and the steel. Since the theory assumes entirely ductile stress-strain relation for the confined concrete, the strengths given by the theory are larger than that by the tests, and the positive slope appears again on the curve in the large curvature range due to the strain-hardening of the steel, except for the case of zero axial load. For repeated loading cases, the theoretical results of SRO shows a very good agreement with the experimental one. Particularly the stiffning effect due to the closing of cracks are well predicted by the theory, although the stiffness change appears rather sudden in the theory. On the other hand, the large discrepancy is seen between the experimental and theoretical maximum strengths of SR3. However, it is clearly shown in case of SR3, that the strength converges to the sum of the strengths of the confined concrete and the steel.

The hysteresis loops of column specimens subjected to double curvature bending repeatedly are shown in Fig. 6. In general, the theory well predicts the experimental results. As clearly shown in the case of CRO, the discrepancy is seen on the shapes of hysteresis loops; stable spindle type in the test and rather parallelogrammic type in the theory. Since this discrepancy is not obvious in the moment-curvature relation, this is because the theory does not take into consideration the cracks due to bending distributed entire length of the column and the shear deformation. The test result of CR3 shows that the confined concrete already crashed at the final stage of the test.

Shown in Figs. 7 and 8 are the results of the frame analysis. One point that cannot be properly explained yet is the large discrepancy between the theoretical and experimental maximum strengths of FM series. This discrepancy is more or less observed in the results of FR series. It may be said that the accuracy of the theoretical results becomes poorer as the objective structure becomes more complicated. From this point of view, the development of the more refined mathematical model for the deflection analysis is needed. Since the members in CR, FM and FR series are subjected to double curvature bending, the moment curvature relation for such a member may have to be checked by the theory to give an explanation to the discrepancy. The difference in the shapes of the hysteresis loops of the frame is very similar to that observed in case of the columns. The large strength reduction observed in the final experimental loop of FRO may be caused by the fracture of the steel.

5. CONCLUSIVE REMARKS

The moment-curvature relation of a steel reinforced concrete cross section under the constant axial force and monotonic or alternately repeated bending is computed by separating the cross section into a finite number of strip

elements based on the assumption that the plane remains the plane. It can be concluded that it is needed to employ the accurate stress-strain relation of the concrete when to carry out the deflection analysis of the reinforced or steel reinforced concrete members, and its accuracy shows the critical effect on the result of the analysis. When the axial load is zero, the maximum bending moment of the cross section, and thus the maximum strength of the member, depends only on the strength of the bare steel portion including reinforcing bars, and the concrete strength hardly affects on the numerical results. However, when the axial load is present, the estimation of σ_B plays a key role to determine the maximum strength of the member. In the present analysis, σ_B is assumed to be 75% of the cylinder strength, and different types of stress-strain relations are assumed for the covering and confined concrete. The theoretical result shows a good agreement with the experimental one under the loading condition where the mean strain in the confined concrete is small.

The main advantage of the present method of analysis may lie on the point that the hysteretic load-deflection relation of the member of the frame can be directly derived from the moment-curvature relation of the member cross section, by considering the flexural portions with a finite lengths concentrated at the member ends. In general, the deflection analysis of the frames shows the discrepancy between the maximum strength obtained by the present method and that from the test. It seems adequate to impose the rigid portion with a finite length at the member ends, in order to obtain a good agreement with the test result.

REFERENCES

1. Wakabayashi, M.:STUDIES ON DAMPING AND ENERGY ABSORPTION OF STRUCTURES, Introductory Report, IABSE Symposium, Lisbon, 1973, pp. 27-46.

2. Wakabayashi, M., Minami, K. and Komura, K.:AN EXPERIMENTAL STUDY ON ELASTO-PLASTIC CHARACTERISTICS OF COMPOSITE MEMBERS USING AN ENCASED H-SECTION SUBJECTED TO COMBINED BENDING AND AXIAL FORCE, Annuals, Disaster Prevention Research Institute, Kyoto University, No. 14-A, April 1971, pp. 417-437(In Japanese).

3. Wakabayashi, M., Minami, K. and Nakamura, T.:EXPERIMENTAL STUDIES ON STEEL REINFORCED CONCRETE COLUMNS UNDER CONSTANT AXIAL FORCE AND ALTERNATE REPEATED BENDING AND SHEAR, Annuals, Disaster Prevention Research Institute, Kyoto University, No. 15-B, April 1972, pp. 69-97(In Japanese).

4. Wakabayashi, M., et al.:EXPERIMENTAL STUDIES ON STEEL-REINFORCED CONCRETE COLUMNS UNDER CONSTANT AXIAL FORCE AND ALTERNATE REPEATED BENDING MOMENT AND SHEARING FORCE, PARTS 1-4, Abstracts, Annual Meeting of Architectural Institute of Japan, Oct. 1972, pp. 1103-1110(In Japanese).

TABLE AND FIGURES

Table 1. Test Specimens and Material Properties

Series	SM				SR		CR		FM		FR	
Loading Type	Monotonic				Repeated		Repeated		Monotonic		Repeated	
Specimen No.	SM0	SM2	SM4	SM6	SR0	SR3	CR0	CR3	FM0	FM4	FR0	FR3
N (ton)	0	30	60	90	0	25	0	35	0	40	0	34.4
N/N_o	0	0.2	0.4	0.6	0	0.3	0	0.3	0	0.4	0	0.3
F_c(ton/cm^2)	.215	.269	.295	.275	.233	.216	.364	.326	.228	.242	.349	.328
$_s\sigma_y$(ton/cm^2)	3.05	3.12	3.12	3.12	3.42	3.42	3.48	3.48	2.95	2.83	3.46	3.09
$_r\sigma_y$(ton/cm^2)	3.68	3.68	3.68	3.68	4.18	4.18	3.38	3.91	2.61	2.61	3.87	3.87

N:Axial Load, N_o:Ultimate Compressive Strength, F_c:Cylinder Strength of Concrete, $_s\sigma_y$:Yield Stress of Steel, $_r\sigma_y$:Yield Stress of Main Reinforcing Bars.

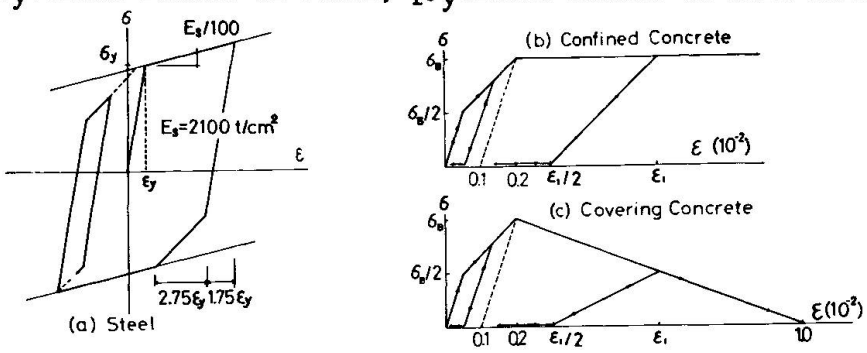

Fig. 1 Stress-Strain Relations

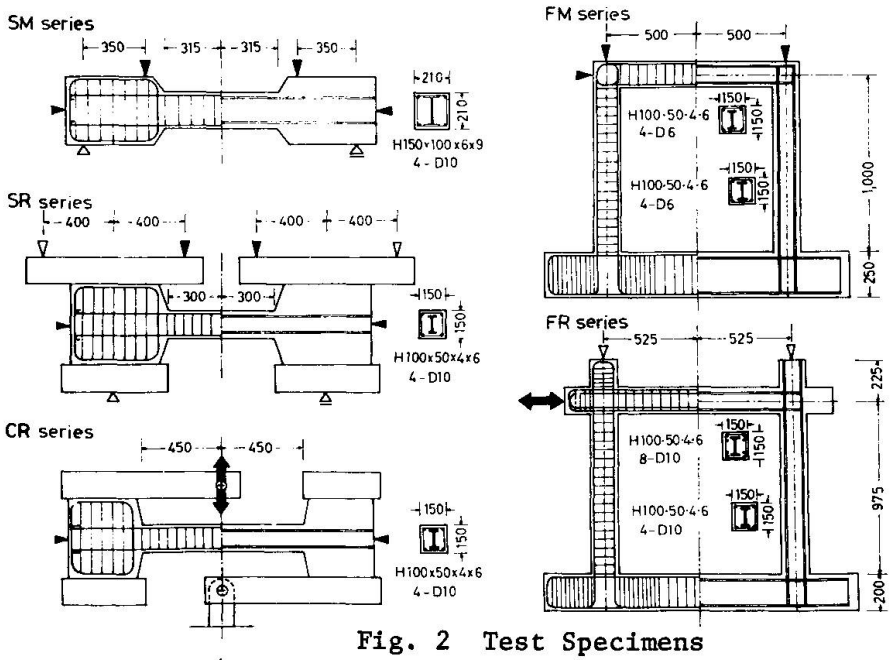

Fig. 2 Test Specimens

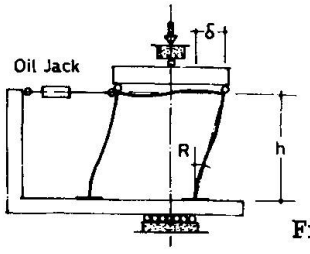

Fig. 3 Loading System of Frame Tests

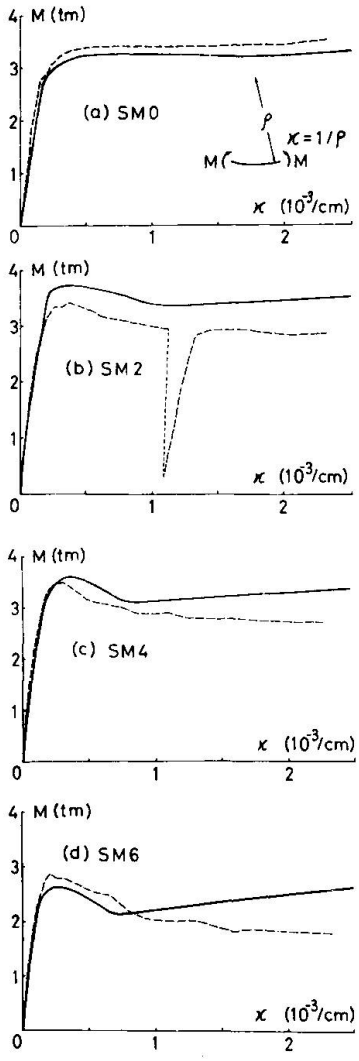

Fig. 4 Moment-Curvature Curves of SM Series

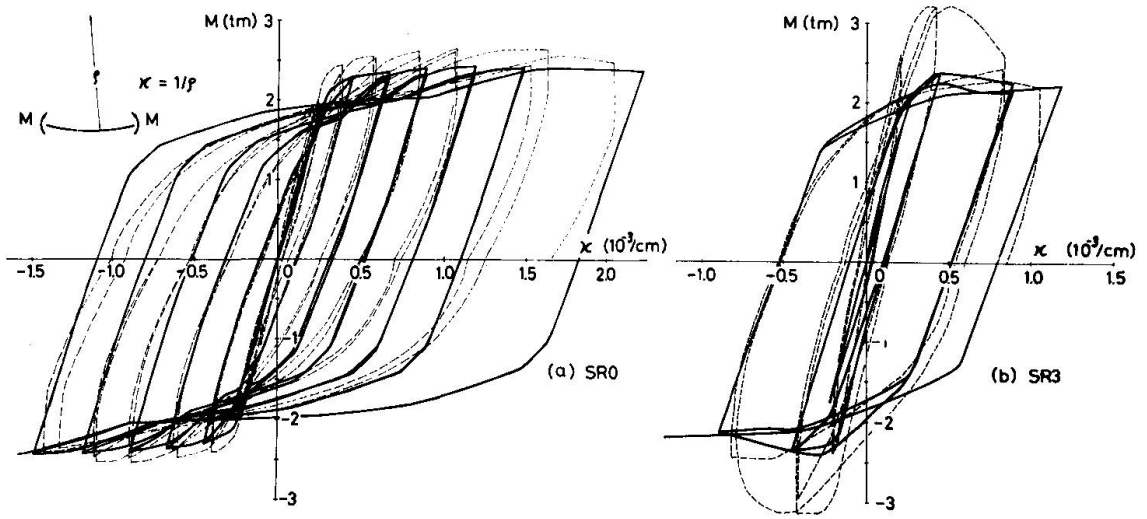

Fig. 5 Moment-Curvature Curves of SR Series

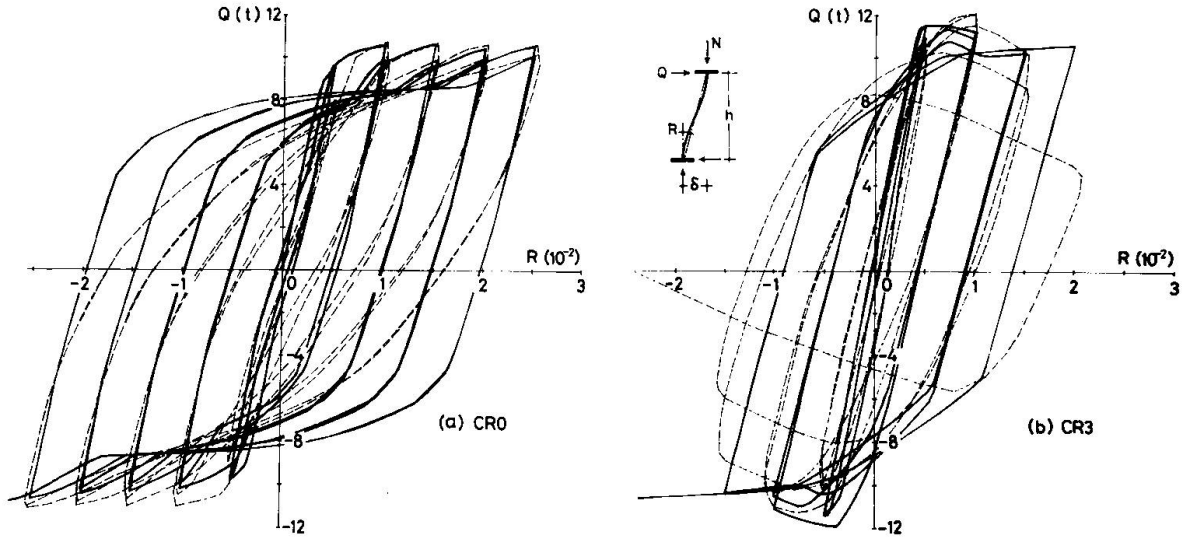

Fig. 6 Load-Deflection Curves of CR Series

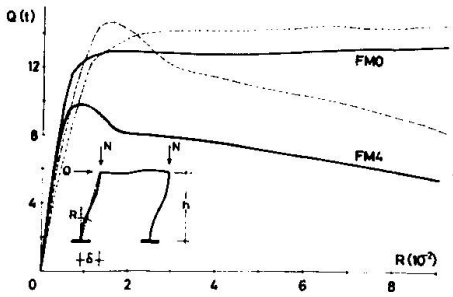

Fig. 7 Load-Deflection Curves of FM Series

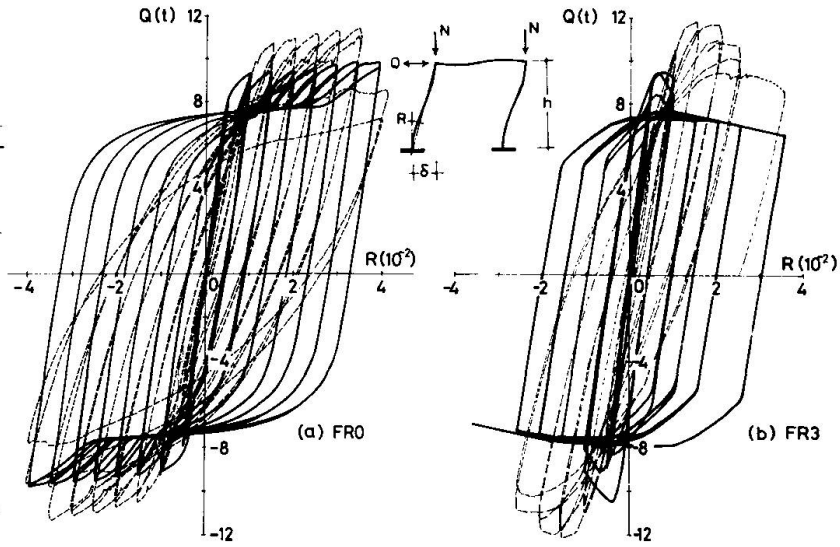

Fig. 8 Load-Deflection Curves of FR Series

I – A STUDY ON THE BEHAVIOUR OF STEEL REINFORCED CONCRETE COLUMNS AND FRAMES

SUMMARY

A numerical analysis is carried out to obtain the moment-curvature relationship of the steel reinforced concrete cross section under constant axial force and monotonic or alternately repeated bending moment, based on the idealized stress-strain relations for steel and concrete. A method of the deflection analysis of steel reinforced concrete columns and frames is proposed, introducing a mathematical model. The numerical results are compared with the experimental ones that have been obtained by the authors.

RESUME

On procède à un calcul numérique pour obtenir la relation moment-courbure d'une section en béton armé soumise à une force axiale constante et à un moment de flexion constant ou alterné; on se base sur des diagrammes tension-déformation idéalisés pour l'acier et le béton. On propose une méthode pour le calcul des déformations des cadres et colonnes en béton armé, qui utilise un modèle mathématique. On compare les résultats numériques avec des resultats expérimentaux des auteurs.

ZUSAMMENFASSUNG

Eine numerische Berechnung wird durchgeführt, um die Moment-Krümmungs-Beziehung von Stahlbetonquerschnitten unter konstanter Axiallast und gleichförmig ansteigendem oder wechselndem Biegemoment zu bestimmen. Hierbei werden idealisierte Spannungs/Dehnungs-Beziehungen für Stahl und Beton eingeführt. Eine Methode für die Berechnung der Verformungen von Stahlbetonstützen und -Rahmen wird vorgeschlagen, welche auf einem mathematischen Modell beruht. Die numerischen Resultate werden mit den Ergebnissen von Versuchen der Autoren verglichen.

Large Deformation and Stability Analysis of Reinforced Concrete Frames Considering Material Nonlinearities

Calcul des grandes déformations et de la stabilité des cadres en béton armé, tenant compte des comportements non-linéaires du matériau

Berechnung grosser Deformationen und der Stabilität von Stahlbetonrahmen unter Berücksichtigung der Nichtlinearitäten des Materials

E. ALDSTEDT
Research Fellow

P.G. BERGAN
Associate Professor of Civil Engineering

The Norwegian Institute of Technology
The University of Trondheim
Trondheim-NTH, Norway

Introduction

It is widely recognized that the true behavior of reinforced concrete is extremely complicated. Among the various physical phenomena that occur on a macro-scopic level in reinforced concrete, the following will be mentioned: nonlinear compressive stress-strain relationship of concrete; cracking of concrete; yielding of steel reinforcement bars; bond slip between reinforcement bars and concrete. Geometric imperfections and second-order geometric effects are also of considerable importance for beam, plate and shell structures. The picture is further complicated by various time dependent phenomena. In spite all of this, the analyses of most concrete structures today are based on greatly simplified models for the materials.

The finite element method has proved to be a very efficient tool for analysis of a great variety of nonlinear problems [1], [2]. A review of applications of the method to nonlinear analysis of concrete structures has been given by Scordelis [3]. Studies considering both material nonlinearities and large deformations have previously been reported by Berg et.al. [4] who analyzed concrete plates and by Blaauwendraad [5] and Aas-Jakobsen and Grenacher [6] who dealt with concrete frames.

In theory, the finite element method can be formulated so that almost an unlimited number of complex physical and geometrical effects may be incorporated in the numerical algorithms. A prerequisite for this is of course that the various effects can be defined mathematically. But at least as important as to include various physical phenomena in the analytical model is to ensure that the method becomes economical and practical in use.

In the present paper an attempt is made to achieve a method of analysis that is capable of accurately predicting the inplane behavior of plane, slender, reinforced concrete frames and arches that are subjected to loads up to the ultimate carrying capacity. Major efforts have been made to make the analytical model economical and efficient. The approach is based on the finite element method utilizing a beam displacement model. The material properties of concrete and steel reinforcement may be relatively general. The loading , geometry, support conditions and distribution of reinforcement may also be arbitrary. The cross-sections are assumed to be rectangular. Large deflections of the frame are also accounted for. The present method is demonstrated by two numerical examples, eccentric buckling of a column and stability analysis of an arch.

Governing equations

In the proceeding, a simple but powerful approach for large displacement analysis of frames will be followed. The structure is assumed to be divided into finite elements. To every element is "attached" a local Cartesian coordinate system going through the end nodal points, see Fig. 1.

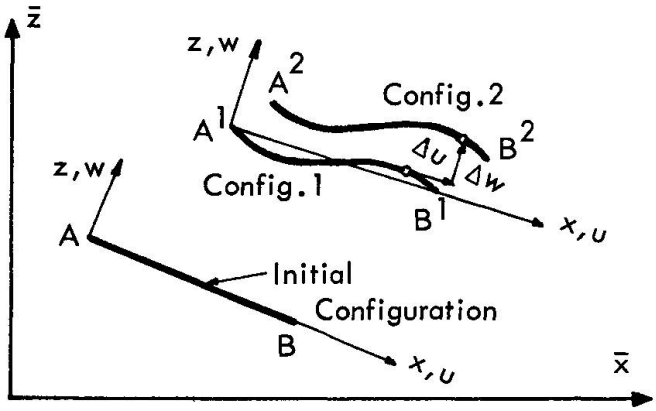

Fig.1. Description of motion of an element during deformation.

This coordinate system follows the element during the deformation. On the local element level the deformations are assumed to be small (small strains). However, forces and displacements for each element are transformed to a global coordinate frame in which the equilibrium equations for the entire system are assembled. In effect, this approach is a matter of updating the nodal point geometry of the structure in accordance with the current deformations. The geometric nonlinearities entering this procedure are entailed in the continuously changing transformation matrices between local and global systems (rotational effect of elements).

Two equations are of great importance for a nonlinear analysis: the equilibrium equations and the incremental form of the equilibrium equations. The condition of equilibrium for an element can be stated in terms of the virtual work principle

$$\int_V \sigma\delta\varepsilon dV - \int_{S_1} T_i \delta u_i dS = 0 \qquad (1)$$

For a beam element σ is the axial stress, V the element volume, T_i the surface traction which is prescribed on surface S_1, δu_i are the virtual displacements and $\delta\varepsilon$ the corresponding virtual strain. Using the approach just described, Eq. (1) yields the small displacement (secant) stiffness relation, i.e. the equilibrium equation, referred to the local coordinate system in the current deformed configuration. Eq. (1) may very well account for nonlinear material effects.

By considering equilibrium of two configurations 1 and 2 of the element that are close to each other, an incremental form of the virtual work principle may be obtained

$$\int_V \Delta\sigma\delta\varepsilon dV + \int_V \sigma\delta\Delta\varepsilon dV - \int_{S_1} \Delta T_i \delta u_i dS = 0 \qquad (2)$$

where Δ denotes increment of quantities between the two configurations. In accordance with the previous description Eq. (2) has been linearized by neglecting the term $\int_V \Delta\sigma\delta\Delta\varepsilon dV$.

The reference frame for Eq. (2) is the local coordinate system in configuration 1, see Fig. 1. For a beam element the term $\delta\Delta\varepsilon$ may be obtained from the nonlinear strain term which includes the rotational effect $\frac{1}{2}(\frac{\partial w}{\partial x})^2$, so that

$$\delta\Delta\varepsilon = \delta[\tfrac{1}{2}(\frac{\partial w}{\partial x} + \frac{\partial \Delta w}{\partial x})^2 - \tfrac{1}{2}(\frac{\partial w}{\partial x})^2] = \delta(\frac{\partial w}{\partial x}) \frac{\partial \Delta w}{\partial x} \tag{3}$$

Equation (2) yields the socalled incremental or tangent stiffness relation which accounts for both nonlinear material properties and geometric effects (geometric stiffness on linearized form).

Finite Element Model

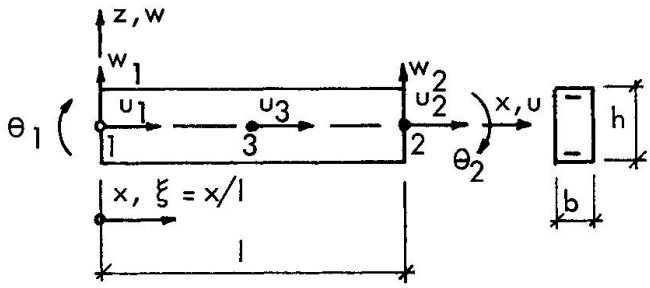

Fig.2. The beam element.

The finite element idealization of the beams is here based on a pure displacement model [1]. The axial displacement along the x-axis of a beam element is defined by

$$u_o = \mathbf{N}_u \mathbf{u} \tag{4}$$

where

$$\mathbf{N}_u = [\xi,\ 1-\xi,\ 4\xi(1-\xi)] \tag{5}$$

$$\mathbf{u} = [u_1,\ u_2,\ u_3]^T \tag{6}$$

The internal degree of freedom at the midplane, see Fig. 2, is introduced in order that the strain due to axial deformation be of the same degree as the strain due to flexure. The lateral displacement w is defined by

$$w = \mathbf{N}_w \mathbf{w} \tag{7}$$

where

$$\mathbf{N}_w = [1-3\xi^2+2\xi^3, -\ell\xi(1-\xi)^2,\ 1-3(1-\xi)^2+2(1-\xi)^3, \ell\xi^2(1-\xi)] \tag{8}$$

$$\mathbf{w} = [w_1, \theta_1, w_2, \theta_2]^T \tag{9}$$

Adopting Kirchhoff's hypothesis, the strain at an arbitrary point within the beam element is given by

$$\varepsilon = \frac{du}{dx} = \mathbf{N}_{u,x}\mathbf{u} - z\mathbf{N}_{w,xx}\mathbf{w} \tag{10}$$

The comma denotes differentiation. The above model does not account for shear deformations.

Assuming that forces act only at the nodal points of an element, the element equilibrium equation is obtained by substitution of Eq. (10) into Eq. (1).

$$\int_V \sigma \begin{bmatrix} \mathbf{N}^T_{u,x} \\ -z\mathbf{N}^T_{w,xx} \end{bmatrix} dV = \begin{bmatrix} \mathbf{S}_u \\ \mathbf{S}_w \end{bmatrix} = \mathbf{S} \tag{11}$$

$\mathbf{S}$ is the nodal point force vector corresponding to the state of stress σ. The stress σ is given by the current strain, see the next section.

The increment of the axial stress is related to the strain increment through the equation

$$\Delta\sigma = E_T \Delta\varepsilon \tag{12}$$

where E_T is the current tangent modulus. By substitution of Eqs. (10) and (12) into Eq. (2), the incremental force-displacement relationship for the element is obtained

$$\left[\int_V E_T \begin{bmatrix} N_{u,x}^T N_{u,x}, & -zN_{u,x}^T N_{w,xx} \\ \text{symm.}, & z^2 N_{w,xx}^T N_{w,xx} \end{bmatrix} dV + N\int_\ell \begin{bmatrix} 0 & 0 \\ 0 & N_{w,x}^T N_{w,x} \end{bmatrix} dx\right] \begin{bmatrix} \Delta u \\ \Delta w \end{bmatrix} = \begin{bmatrix} \Delta S_u \\ \Delta S_w \end{bmatrix} = \Delta S \quad (13)$$

Here, N is the resulting axial force over the element cross section. The second term of Eq. (13) is the geometric contribution to the incremental force-displacement relationship. A similar incremental relationship for the total structure is obtained by transformation from the current local to the global coordinate system and using a standard assemblage process.

Material properties

The method described herein allows for a general, nonlinear stress-strain relationship for both concrete and reinforcement. The concrete and the steel are assumed to be perfectly bonded.

In the computational procedure, it is assumed that there is a unique relationship between stresses and strains (total deformation formulation). The stress-strain curve for the concrete is identified by a set of discrete points, see Fig. 3. Linear interpolation between these points are used for intermediate values. The tangent modulus needed in Eq. (13) is given in a similar way by utilizing discrete tangent values from the experimental stress-strain curve. The tangent modulus may be negative. In tension the concrete is assumed to behave linearly up to a cracking strain ε_{cr} beyond which the concrete has no strength. The computer program which was developed can also automatically generate the standard CEB-FIP design curve for concrete [7] (also used in the Norwegian building code NS 3473).

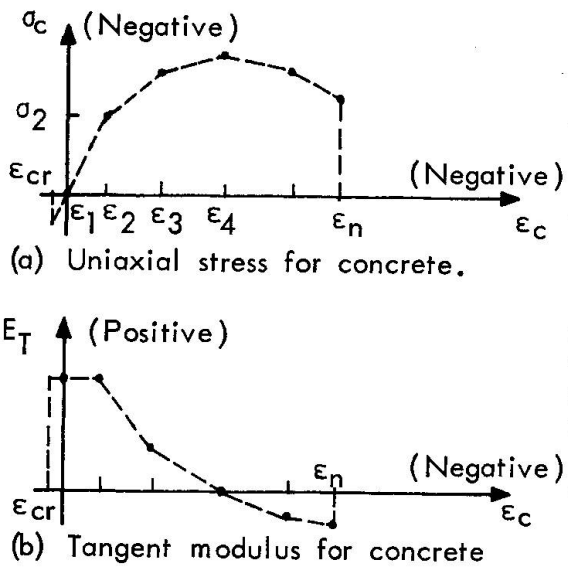

Fig.3. Material properties for concrete.

The material properties for the steel are obtained in a similar way as for the concrete by identifying discrete values from experimental curves.

Numerical solution

The major constituents in the solution process are the equilibrium equation (11) and its incremental form Eq. (13). These equations require integration to be carried out over the volume of the beam elements. A Gaussian quadrature scheme is adopted for this purpose. This integration is performed by utilization of 2 to 4 cross sections located at Gaussian points along the longitudinal axis of the beam element. Integration is also carried out over the height of each section employing Gaussian integration for stress

points in the compression zone. The material properties at these points are obtained from diagrams like that of Fig. 3. The part of the tension zone where the strain exceeds the cracking limit is excluded from the integration. Several layers of reinforcement can also be accounted for.

The response of the structure during increasing external loading is basically determined by applying the external load in increments and by performing equilibrium iterations at each new level of loading. It may well happen that equilibrium of the structure is not satisfied after a new displacement vector has been obtained. The difference between the external forces acting on the structure and the assemblage of element force vectors from Eq. (11) give rise to a set of unbalanced forces. This residual force vector is utilized in a Newton-Raphson iteration in which the gradient matrix is supplied by Eq. (13). The iteration is terminated when the displacements have converged or material rupture has occured. The material properties at the integration points and the extension of the cracked zones are constantly updated during solution according to the current state of deformations. Also the local coordinate systems for the elements are steadily updated to account for the change in geometry of the frame.

The solution process is capable of proceeding beyond points of maximum carrying capacity of the structure. The load-steps automatically change sign after maximum point has been passed (reduction of external loading). This capability can be of great importance for determining the safety of a design. Further details on the solution procedure that is used may be found in Ref. [8].

Numerical Examples

The present method will be illustrated by two numerical examples.

The first example is a hinged column subjected to eccentric axial loading, see Fig. 4. The steel reinforcement is symmetric and it is assumed to behave elastic-ideally plastic. Its modulus of elasticity is $E_s = 2.055 \cdot 10^5$ N/mm^2 ($29.2 \cdot 10^6$ psi) and its yield strength is $f_y = 461$ N/mm^2 (65500 psi). The compressive stress-strain relationship of concrete is described by the standard CEB-FIP curve [7] with an ultimate strain of $\varepsilon_c = -0.0035$. The maximum compressive strength is taken as $f_c = 25.7$ N/mm^2 (3660 psi) corresponding to 80 per cent of the cube strength. The tensile strenght of concrete is neglected. Half the total length of the column is divided into six beam elements. The axial loading is applied in 18 increments and an equilibrium iteration is carried out at each level of loading. Fig. 4 shows the load-deflection curve for the present analysis compared with test and analytical results from Ref. [6]. The results obtained agree closely with the two other curves. For all the curves the maximum point corresponds to an axial force of N = 242 kN (53.4 kips). To some extent, the discrepancy between the test curve and the analytical curves may be due to that the tensile strength has been set equal to zero. Fig. 5 shows a graph of the relationship between moment (M) and axial force (N) at the critical section of the column during deformation. The interaction diagram which represents material failure is also plotted in the figure. It is clearly demonstrated

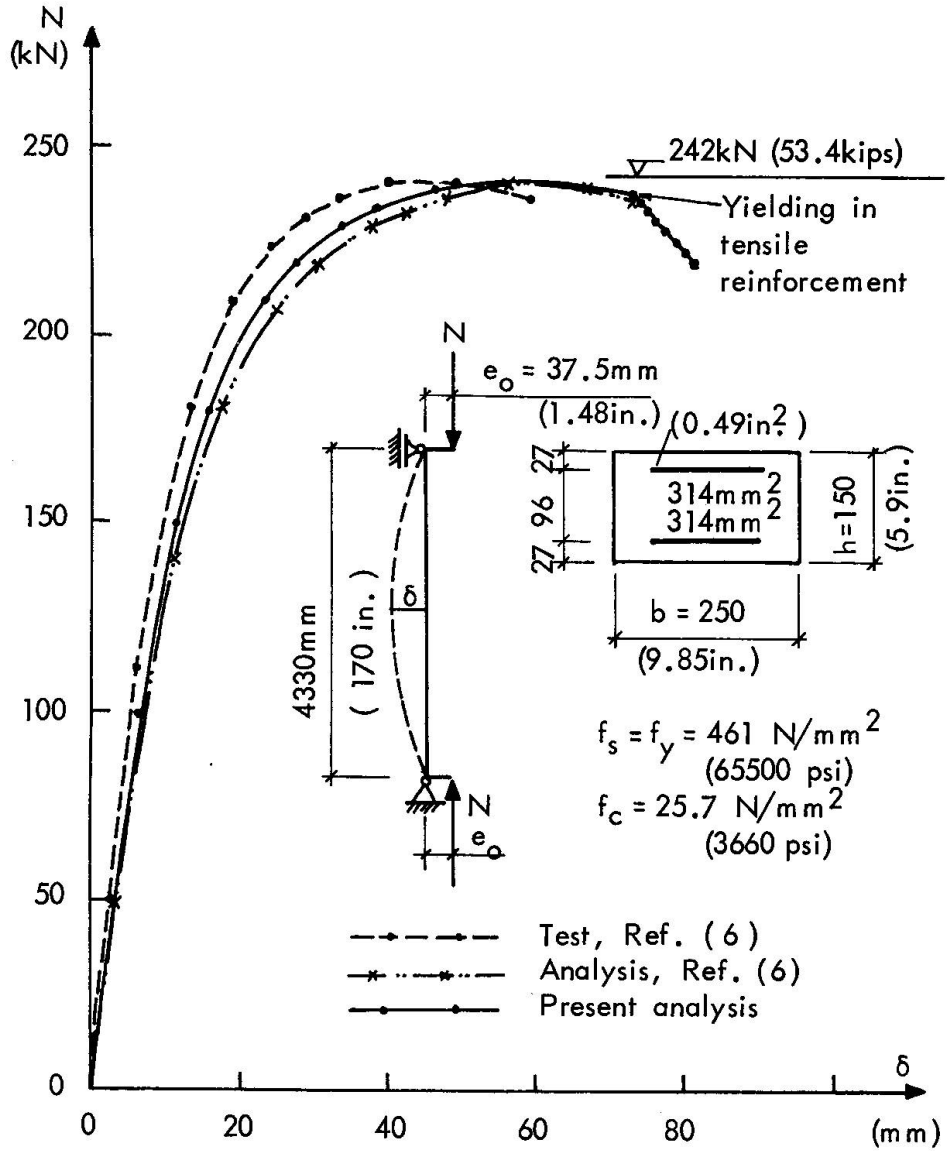

Fig.4. Load - deflection curves for column.

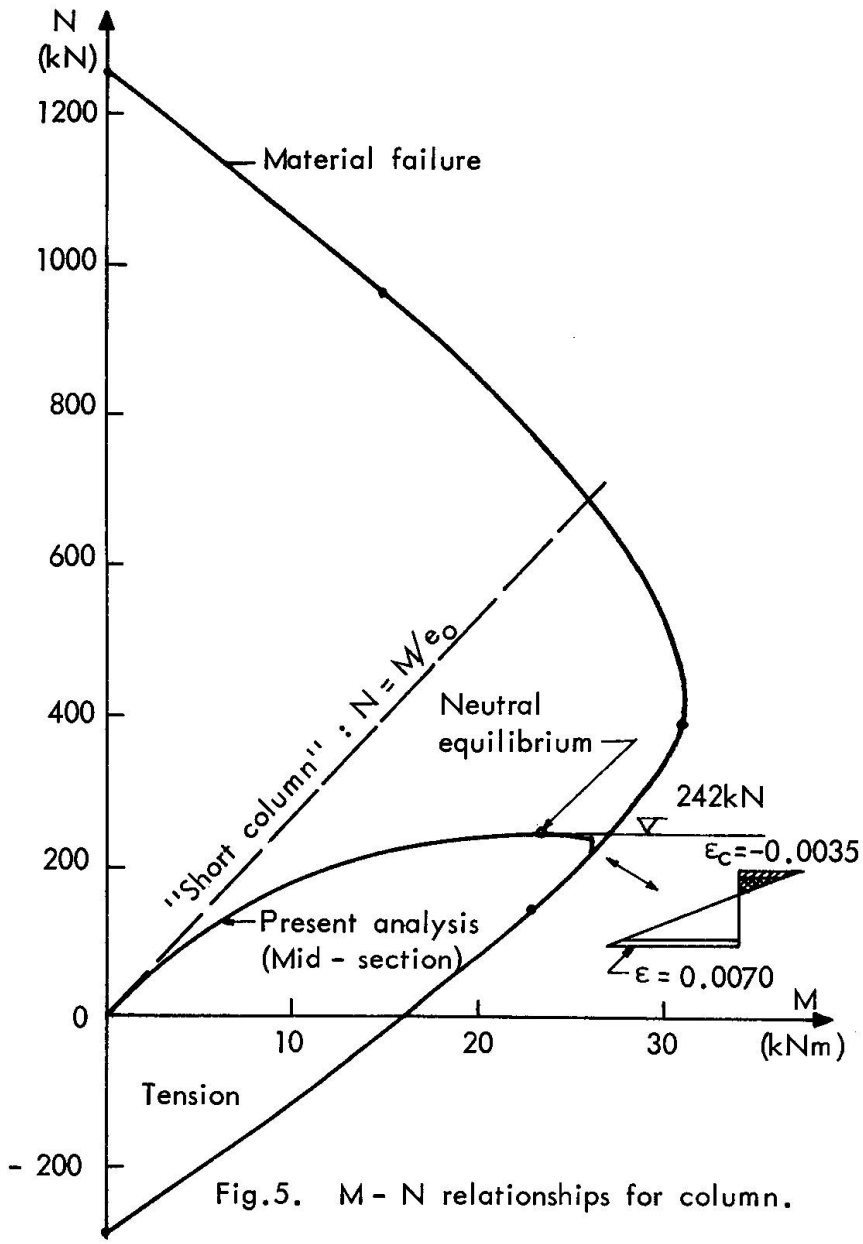

Fig.5. M - N relationships for column.

that the final collapse of the column occurs when the M-N curve of the column reaches the interaction diagram (failure envelope). The total solution time for this example was 18 CPU-seconds on a UNIVAC 1108 computer.

The second example is a 180° hinged arch subjected to uniform hydrostatic pressure. Since no test data or alternative analytical results are available, the main purpose of this example is to demonstrate various capabilities of the present approach. The dimensions of the arch are given in Fig. 7. It is assumed to have a geometric imperfection defined by $e = e_o \sin 2\alpha$. The ultimate strain of the steel is taken as $\varepsilon_{su} = \varepsilon_y + 0.005 = 0.0069$. The arch is analyzed both as an unreinforced concrete structure with perfectly linear elastic material properties and as a reinforced concrete structure with nonlinear material properties. The shape of the nonlinear stress-strain relationship is assumed to be the same as for the previous example, and the numerical values are given in Fig. 6. The hydrostatic pressure is applied both as a conservative loading for which the original direction of the force is kept during deformation and as a nonconservative loading for which the water pressure always is acting perpendicular to the deformed configuration. The arch is divided into 12 equal elements.

The results obtained are shown in Figs. 6 and 7. In Fig. 6, the horizontal displacement of node 4, u_{x4}, is plotted against the load intensity p. Curve ② shows the load-displacement relationship for an elastic structure subjected to a nonconservative load. The curve approaches the critical load level for linearized buckling $p_{cr} = 3EI/R_o^3 = 418$ N/mm. A similar curve for conservative loading is marked ①. Curve ③ and ④ represent a reinforced concrete arch with conservative and nonconservative load, respectively. Curve ③ reaches its peak value at a load level of $p_{s3} \approx 250$ N/mm. Material failure is reached at $p_{m3} \approx 140$ N/mm $= 0.56\ p_{s3}$. The corresponding values for curve ④ are $p_{s4} \approx 230$ N/mm and $p_{m4} \approx 125$ N/mm $= 0.54\ p_{s4}$. The curves representing nonconservative load are located approximately 10 per cent lower than the corresponding curves representing conservative load. This demonstrates that practical design procedures ought to account for changes in the direction of loads. From Fig. 6 it may also be seen that the asymptotes of the elastic curves are located about 80 per cent higher than the maximum points of the corresponding reinforced concrete curves. Fig. 7 shows the relationship between moment (M) and axial force (N) at the critical section (node 4) for the reinforced concrete arch with conservative and nonconservative loading, respectively. Also the corresponding interaction diagram (failure envelope) is shown. The loading was applied in 11 to 22 load increments corresponding to a total solution time of 30 to 76 CPU-seconds on a UNIVAC 1108 computer.

References

[1] ZIENKIEWICZ, O.C., *The Finite Element Method in Engineering Science*, McGraw-Hill, London (1971)

[2] ODEN, J.T., *Finite Elements of Nonlinear Continua*, McGraw-Hill, New York (1971)

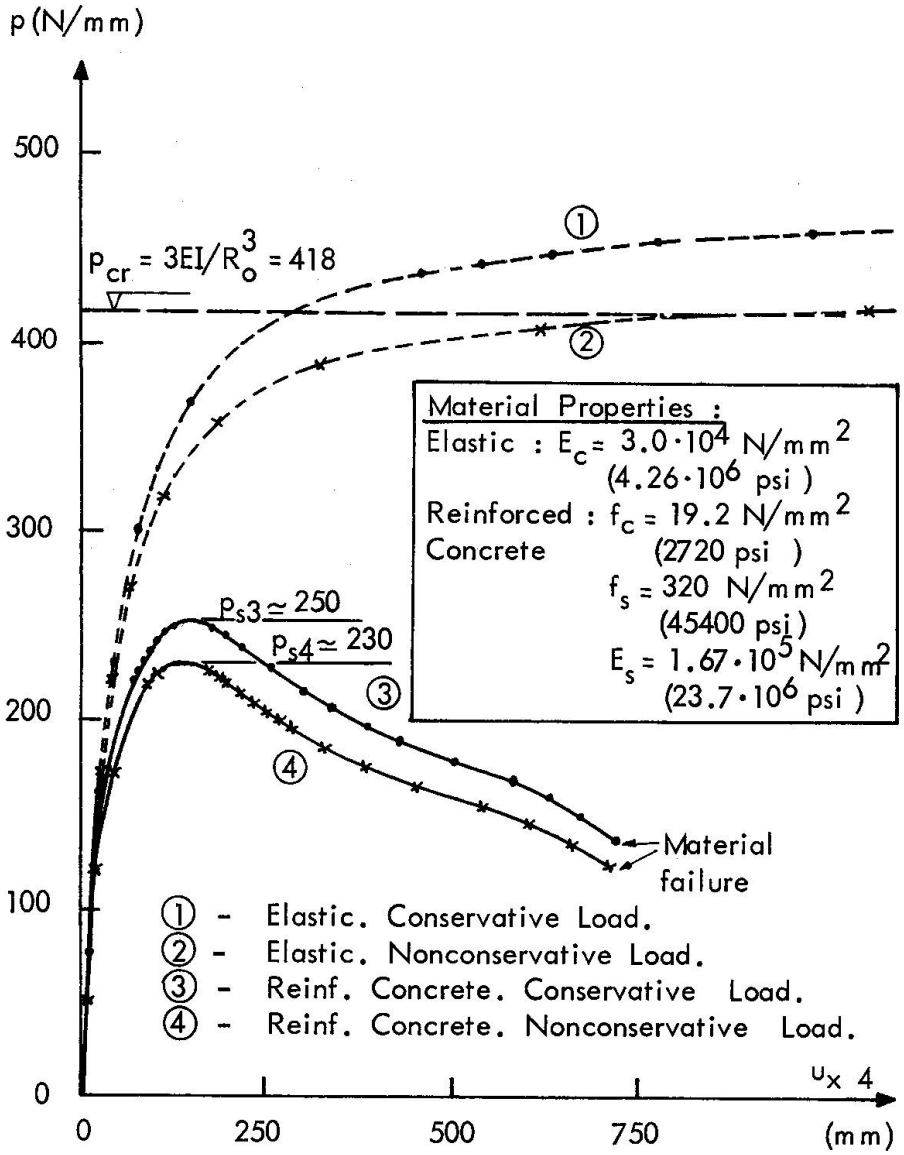

Fig.6. Load - deflection curves for arch. (Horizontal displacement of node 4)

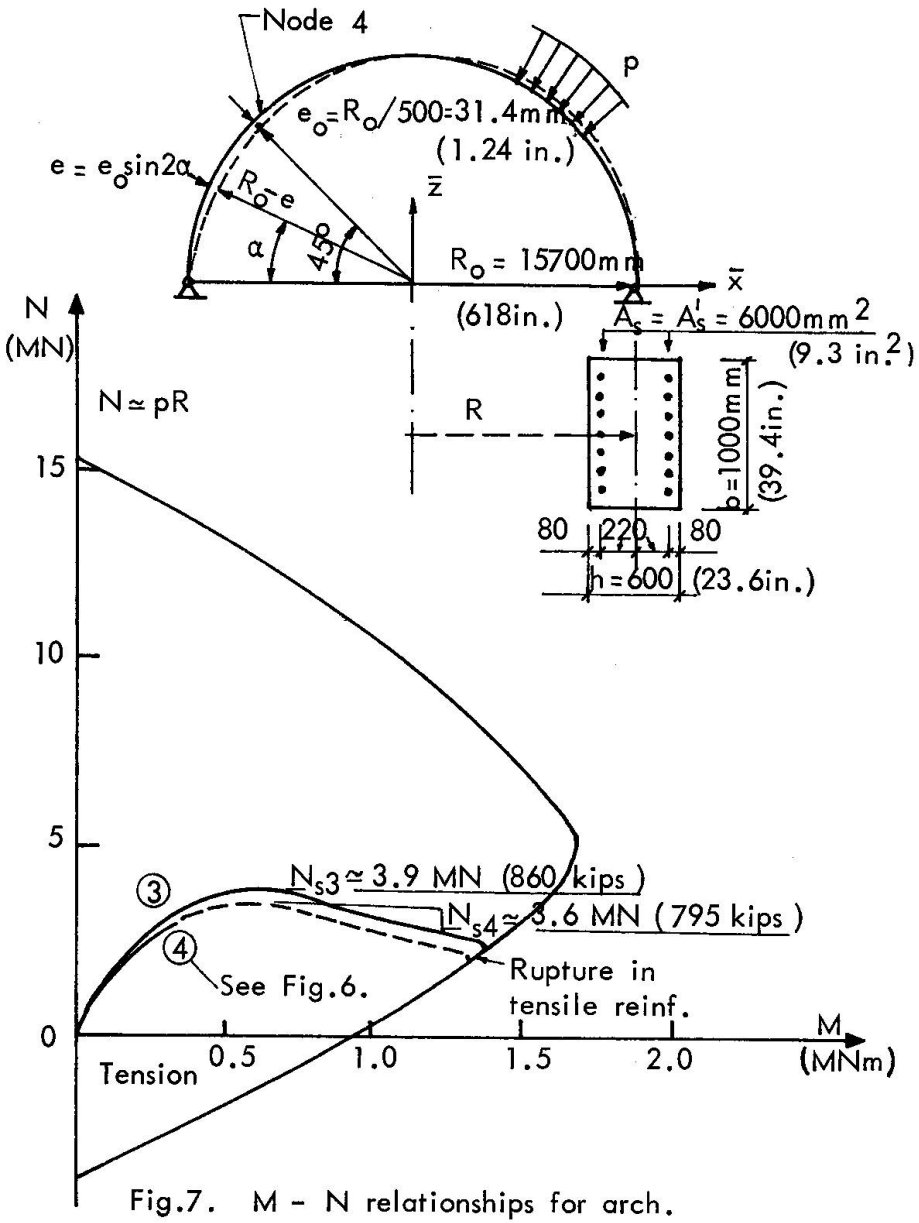

Fig.7. M - N relationships for arch.

[3] SCORDELIS, A.C., "Finite Element Analysis of Reinforced Concrete Structures", presented at the *June 1-2. 1972, Speciality Conference on the Finite Element Method in Civil Engineering*, Montreal, Canada.
[4] BERG, S., BERGAN, P.G., HOLAND, I., "Nonlinear Finite Element Analysis of Reinforced Concrete Plates", *Proceedings of the 2nd International Conference on Structural Mechanics in Reactor Technology*, Vol. M, Berlin, Sept. 1973.
[5] BLAAUWENDRAAD, Ir.J., "Realistic Analysis of Reinforced Concrete Framed Structures", *HERON*, Vol. 18, No. 4, 1972.
[6] AAS-JAKOBSEN, K.A., GRENACHER, M., *Berechnung unelastischer Rahmen nach der Theorie 2. Ordnung*, Bericht Nr. 45, Institut für Baustatik, ETH, Zürich, Januar 1973.
[7] CEB-FIP, *International Recommendations for the Design and Construction of Concrete Structures*, English Edition, June 1970.
[8] BERGAN, P.G., SØREIDE, T., "A Comparative Study of Different Numerical Solution Techniques as applied to a Nonlinear Structural Problem", *Computer Methods in Applied Mechanics and Engineering* 2 (1973) 185 - 201.

SUMMARY

The paper presents a method of nonlinear analysis for plane, reinforced concrete frames. Both geometric and material nonlinearities are accounted for. The method allows for incremental application of the external loads and the structural behaviour may be followed even beyond the point of maximum carrying capacity. The analysis is based on a finite element formulation in which the frames are modelled by small beam elements. The present method has proved to be very efficient and accurate.

RESUME

Ce rapport présente une méthode de calcul non-linéaire pour les cadres plans en béton armé. On tient compte des comportements non-linéaires et de la géométrie et du matériau. Cette méthode permet d'étudier le comportement d'une structure sous l'accroissement de la charge extérieure, même au-delà du point où la charge maximum est atteinte. Le calcul se base sur la méthode des éléments finis: les cadres sont considérés comme un assemblage de petits éléments de poutre. On a démontré que la méthode ci-dessus était efficace et exacte.

ZUSAMMENFASSUNG

Der Beitrag stellt eine Methode vor, mit welcher eine nichtlineare Berechnung ebener Stahlbetonrahmen möglich ist. Sowohl die geometrischen Nichtlinearitären als auch diejenigen der Baustoffe werden berücksichtigt. Die Methode gestattet stufenweises Aufbringen der äusseren Belastung, und das Verhalten lässt sich selbst über den Punkt der maximalen Tragfähigkeit hinaus verfolgen. Die Berechnung benützt die Methode der Finiten Elemente, wobei der Rahmen aus kleinen Balkenelementen zusammengesetzt wird. Die vorliegende Methode hat sich als sehr leistungsfähig und genau erwiesen.

Leere Seite
Blank page
Page vide

Inelastic Analysis of Reinforced Concrete Beam Columns

Calcul non-élastique de poutres-colonnes en béton armé

Unelastische Berechnung von Balken-Stützen-Systemen aus Stahlbeton

John M. KULICKI — Visiting Assistant Professor
Celal N. KOSTEM — Associate Professor
Fritz Engineering Laboratory
Lehigh University Bethlehem
Bethlehem, Pennsylvania, USA

INTRODUCTION

This paper presents the results of a pilot study on the application of an incremental, tangent stiffness finite element analysis technique to the solution of beam-column problems. Results of numerical investigations on reinforced concrete and steel beam-columns subjected to concentrated midspan lateral loads were compared to results obtained using the Column-Curvature-Curve (CCC) method (Ref.1) and, in some cases, the Column-Deflection-Curve (CDC) method (Ref.5) via interaction diagrams. The results have been presented in Ref.4. Only those examples dealing with reinforced concrete beam-columns will be presented here. In each case it will be assumed that the complete axial load is applied first, then the lateral load is applied.

BASIC MODEL

Consistent with the finite element method, the beam-column will be assumed to be divided into elements along its length as shown in Fig.1. A frame or beam type finite element will be used and bending will be assumed to occur about only one axis. Inelastic biaxial bending could also be analyzed by an extended version of the same element. There will be three degrees of freedom at each node point used to define the elements. They are the axial displacement, U, the lateral displacement, V, and the bending rotation, θ. These displacements will occur along an arbitrary reference axis shown as the X axis in Fig.1.

The elements are subdivided into layers which are also indicated in Fig.1. Each layer is assumed to be in uniaxial tension or compression with the strain in each layer analytically related to the strain at the reference axis by the assumption that the cross-section is a plane before and after bending. Each layer may have its own stress-strain relation. Ascending portions of stress-strain curves are idealized using a Ramberg-Osgood formulation for either steel or concrete (Ref.3). Unloading legs of stress-strain curves are modeled as straight line segments.

The displacements within the elements are described by the polynomials below.

$$U = \alpha_1 + \alpha_2 X \tag{1}$$

$$V = \alpha_3 + \alpha_4 X + \alpha_5 X^2 + \alpha_6 X^3 \tag{2}$$

$$\theta = - dV/dX \tag{3}$$

The generalized stresses are chosen as the normal force and moment at the reference axis. The corresponding strains are the axial strain and curvature. Utilizing the assumption of plane sections it is possible to define the elasticity matrix as:

$$\begin{Bmatrix} N \\ M \end{Bmatrix} = \begin{bmatrix} \bar{A} & \bar{S} \\ \bar{S} & \bar{I} \end{bmatrix} \begin{Bmatrix} dU/dX \\ -d^2V/dX^2 \end{Bmatrix} \tag{4}$$

in which:

$$\bar{A} = \sum_{i=1}^{J} E_i A_i \ , \quad \bar{S} = \sum_{i=1}^{J} E_i A_i Z_i \ , \quad \bar{I} = \sum_{i=1}^{J} E_i A_i Z_i^2 \tag{5}$$

The tangent stiffness matrix given below was developed following the well established procedures of the finite element method, e.g. Ref. 7.

$$\left[K_E\right] = \frac{1}{\ell^3} \begin{bmatrix} \bar{A}\ell^2 & & & & & \\ 0 & 12\bar{I} & & \text{symm} & & \\ \bar{S}\ell^2 & -6\bar{I}\ell & 4\bar{I}\ell^2 & & & \\ -\bar{A}\ell^2 & 0 & -\bar{S}\ell^2 & \bar{A}\ell^2 & & \\ 0 & -12\bar{I} & 6\bar{I}\ell & 0 & 12\bar{I} & \\ -\bar{S}\ell^2 & -6\bar{I}\ell & 2\bar{I}\ell^2 & \bar{S}\ell^2 & 6\bar{I}\ell & 4\bar{I}\ell^2 \end{bmatrix} \tag{6}$$

The arbitrary reference axis mentioned earlier has been used in the development of the stiffness matrix above. This facilitates consideration of the change in the position of the neutral axis as nonlinear action proceeds. The equilibrium equations are applied in incremental form so as to treat a nonlinear problem as a series of piecewise linear problems.

The P-Δ effect caused by the deflection of the beam-column can be included by using the geometric stiffness matrix. The particular form used here was found in Ref.6. The bending displacements are related to the axial force by Eq.7 in which the axial force P is positive if it causes tension.

$$\left[K_G\right] = \frac{P}{30\ell} \begin{bmatrix} 0 & & & & & \\ 0 & 36 & & \text{symm} & & \\ 0 & -3\ell & 4\ell^2 & & & \\ 0 & 0 & 0 & 0 & & \\ 0 & -36 & 3\ell & 0 & 36 & \\ 0 & -3\ell & -\ell^2 & 0 & 3\ell & 4\ell^2 \end{bmatrix} \tag{7}$$

Combining Eqs.6 and 7 results in the equilibrium equations for the displaced beam-column element.

$$\{F\} = \left[\left[K_G\right] + \left[K_G\right]\right] \{\delta\} \tag{8}$$

The total stiffness matrix of each element can then be assembled to form the global equilibrium equations. After application of the boundary conditions these equations can be solved for each increment of load.

A more complete discussion of the basic model is contained in Ref. 3. Comparisons of analytic and experimental load-deflection curves for reinforced and prestressed concrete beams are also presented as verification of the model.

ITERATION SCHEME

The iteration procedure for a given lateral load increment is started by solving the global equilibrium equations for the increments of displacement. Strain increments are computed from the displacement increments. Using the

latest level of stress available new tangent moduli are computed for each layer, the tangent stiffness matrix, Eq.6, is regenerated and added to the geometric stiffness matrix. The equilibrium equations are solved again. If the new increments of displacement are within a relative tolerance of the previous set, convergence is said to have occurred. If convergence is not attained in several trials the load increment is reduced and the process is repeated. If no convergence is attained after a number of reductions in load the process is stopped. If convergence is attained in relatively few trials the load increment to be applied for the next load step is increased.

Once convergence has been attained for the load step, consideration is given to cracking and crushing if appropriate. The first phase in this step is a pre-scanning process in which all the layers are checked to see if they have exceeded the allowable tensile or compressive stress tolerances by an excessive amount. If this occurs the basic load step is reduced and the problem of finding a converged displacement increment for the basic load step is repeated.

Once it has been determined that no stress criteria are exceeded by more than their tolerances any alteration in stiffness required by the cracking or crushing of a layer is made. The downward legs of the analytic stress-strain curves are used to convert strain increments into "fictitious stresses" which are used to unload layers which have been found to exceed cracking or crushing criteria. The "fictitious stresses" are used to compute nodal "fictitious forces" which hold the rest of the beam-column in equilibrium. This process produces a globally adequate but not locally exact redistribution of stresses. The global equilibrium problem corresponding to that set of "fictitious forces" is solved until convergence is attained. The layers are then rechecked to see if subsequent cracking or crushing has occurred. If so the cracking-crushing analysis is repeated. Execution of a given beam-column analysis is terminated in one of two ways: 1) the total stiffness matrix given by Eq.8 ceases to be positive-definite, or, 2) the process of cracking or crushing results in an inability to find a total solution for a given load step. The first mode of termination was most common in the examples presented here.

Alterations in the stiffness matrix arising from plastic flow like phenomena in reinforcing steels or in steel beam-columns are automatically accounted for by employing the appropriate Ramberg-Osgood curve.

NUMERICAL RESULTS

The rectangular, doubly reinforced section used here is shown in Fig.1. Beam-columns using the same cross-section have been analyzed using the CCC method (Ref.2). The section is 356mm deep, 305mm wide and has equal compressive and tensile areas of 21.68cm^2 each. The compressive strength of 17.58 MN/m^2 used in the CCC analysis was also used here. The yield strength of the steel was 310.27 MN/m^2. The 26 beam-columns which will be discussed herein are enumerated in the table below.

ANALYTIC REINFORCED CONCRETE BEAM COLUMNS

e = 0.0	L/t	10	10	10	10	10	20	20	20	20	20	30	30	30	30
	P/P_o	0.0	0.2	0.4	0.6	0.8	0.0	0.2	0.4	0.6	0.8	0.0	0.2	0.4	0.6
e = 0.3t	L/t	10	10	10	10	20	20	20	20	30	30	30	30		
	P/P_o	0.0	0.1	0.2	0.3	0.0	0.1	0.2	0.3	0.0	0.1	0.2	0.3		

The interaction curves produced by both the finite element and CCC methods for a concentric axial load are shown in Fig.2. It can be seen that the results of both analyses agree quite well for the curves with L/t=30 and L/t=20. The agreement with the CCC results for L/t=10 is not as good but is still within about 5% of the same Q/Q_o value for a given value of P/P_o.

The load-deflection curves produced using the current work for the case with L/t=20 is shown in Fig.3. The load-deflection curves do not appear to form a systematic pattern as was obtained when the same analysis was applied to a steel wide-flange beam-column (Ref.4). There are several reasons for this: 1) as seen in Fig.2, there are some values of P/P_o for which a reinforced concrete beam-column loaded in this manner can support a larger lateral load than is possible when $P/P_o = 0$. This was not true for the steel beam-columns, and 2) the effect of cracking is evident in these load-deflection curves as a relatively early change in slope. The amount of change is dependent on the extent of cracking along and through the beam-column.

Figure 4 is a comparison of interaction diagrams for an eccentrically loaded reinforced concrete beam-column. Good agreement with the corresponding CCC results is again noted. The finite element results do not extend as far along these interaction curves because of a limitation in the current iterative procedure. For the higher values of P/P_o in both the eccentric and concentric cases the axial load alone caused enough nonlinear behavior to result in a failure to converge to the first displacement increment. This is because the axial load is applied in one load step in the current algorithm while the subsequent lateral load is applied in small steps. The algorithm could be modified so as to apply the axial load in several steps. For the concentric load case it was relatively easy to circumvent this problem by using an initial stress field which satisfied equilibrium and strain compatibility.

Figure 5 is a set of load-deflection curves for the eccentric load case with L/t=20. The almost horizontal offset at the beginning of each curve represents the effect of the application of the total axial load and the first increment of lateral load.

This analysis technique has also been applied to steel wide-flange beam columns and the results were compared to those obtained using both the CCC and CDC methods. The corresponding interaction curves have been reported in Ref.4 and show even better agreement than indicated herein.

CONCLUSIONS

It can be concluded from this study that this incremental iteractive analysis technique using a simple layered beam-type finite element can provide solutions to inelastic beam-column problems. While there is already a large body of information in this area, this method does have several advantages which may prove useful in future beam-column studies: 1) a wide range of loadings can be handled. There is no intrinsic difference between one concentrated, several concentrated, uniform, symmetric or unsymmetric loads. 2) boundary conditions can also be handled easily. There is no change in the formulation for different boundary conditions. 3) There is no need for an a-priori moment-thrust-curvature curve. 4) There is nothing conceptually prohibitive about changing the order of loading or using simultaneous (but proportional) axial and lateral loads. 5) Previous work on prestressed concrete beams using basically the same simple model would indicate that prestressed concrete beam-columns could also be treated by this technique.

NOMENCLATURE

$\bar{A}$ = Generalized area
E = Initial modulus of elasticity
$\bar{I}$ = Generalized moment of inertia
J = Number of layers in an element
L = Beam-column length
M = Bending moment
N = Normal force
P = Axial load
Q = Lateral load
$\bar{S}$ = Generalized statical moment
e = Eccentricity of axial load

ℓ = Element length
U = Axial displacement
V = Lateral displacement
θ = Bending rotation
A_c = Concrete area
A_s = Steel area
P_o = $f''_c A_c + f_y A_s$
Q_o = Ultimate load of a concrete beam with no axial load
f''_c = $0.85f'_c$
f_y = Yield stress
$[K_E]$ = Stiffness matrix
$[K_G]$ = Geometric stiffness matrix
$\{\alpha\}$ = Constants in displacement polynomials

REFERENCES

1. Chen W.F., GENERAL SOLUTION OF INELASTIC BEAM-COLUMN PROBLEM, Journal of the Engineering Mechanics Division, ASCE, EM4, August 1970.

2. Chen, W. F. and A. C. T. Chen, STRENGTH OF LATERALLY LOADED REINFORCED CONCRETE COLUMNS, to be published in Symposium on Design and Safety of Reinforced Concrete Compression Members, IABSE Meeting, Quebec, 1974, Preliminary Report.

3. Kulicki, J.M. and C. N. Kostem, THE INELASTIC ANALYSIS OF REINFORCED AND PRESTRESSED CONCRETE BEAMS, Fritz Engineering Laboratory Report No. 378B.1, November 1972.

4. Kulicki, J. M. and C. N. Kostem, APPLICATIONS OF THE FINITE ELEMENT METHOD TO INELASTIC BEAM-COLUMN PROBLEMS, Fritz Engineering Laboratory Report No. 400.11, March 1973.

5. Lu, Le-Wu and H. Kamalvand, ULTIMATE STRENGTH OF LATERALLY LOADED COLUMNS, Journal of the Structural Division, ASCE, ST6, June 1968.

6. Tebedge, N., APPLICATIONS OF THE FINITE ELEMENT METHOD TO BEAM-COLUMN PROBLEMS, Ph.D. Dissertation submitted to Lehigh University, September 1972.

7. Zienkiewicz, O. C., THE FINITE ELEMENT METHOD IN ENGINEERING SCIENCE, McGraw-Hill, London, England, 1971.

SUMMARY

An efficient model has been developed which predicts the flexural load-deformation behaviour and stress history of inelastic reinforced concrete and steel beam-columns. The beam-column is discretized into an assemblage of layered beam type finite elements and is analyzed using an incremental, iterative, tangent stiffness approach, good agreement between interaction curves developed by this method and the column-curvature-curve method is demonstrated herein.

RESUME

On a développé un modèle efficace permettant de prévoir le comportement flexion-déformation et l'évolution des sollicitations de poutres-colonnes non élastiques en béton armé ou en acier. La poutre-colonne est traitée comme un assemblage d'éléments finis en forme de lamelles. Le calcul se base sur une approche progressive par itérations du module de rigidité tangentiel; on montre également une bonne concordance entre les courbes d'interaction obtenues par cette méthode et la méthode des courbes de courbure de colonne.

ZUSAMMENFASSUNG

Ein leistungsfähiges Modell wurde entwickelt, mit welchem die Vorhersage des Verformungsverhaltens und des Beanspruchungsverlaufs in unelastischen Balken - Stützen - Systemen aus Stahlbeton bzw. Stahl möglich ist. Das Balken - Stützen - System wird dabei aufgelöst in schichtförmige Finite Elemente und untersucht mittels eines stufenweisen iterativen Vorgehens, bei welchem die jeweilige Steifigkeit Verwendung findet. Die gute Uebereinstimmung der mittels der verliegenden Methode ermittelten Interaktions-Diagramme mit denjenigen aus einer Stützen - Krümmungs - Methode hergeleiteten wird aufgezeigt.

FIGURES

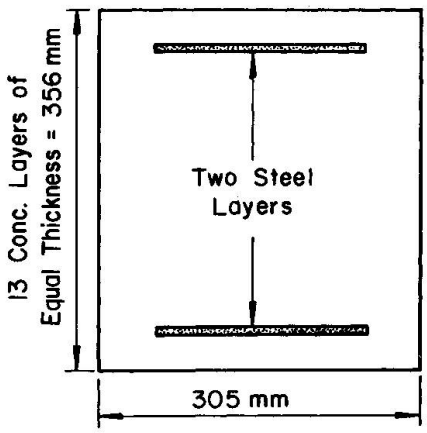

(a)

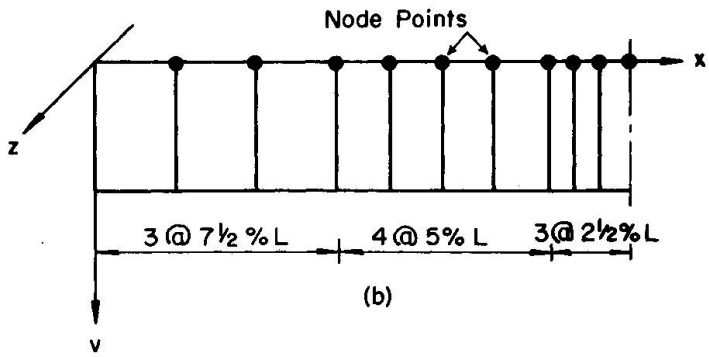

Fig.1 Discretization Models

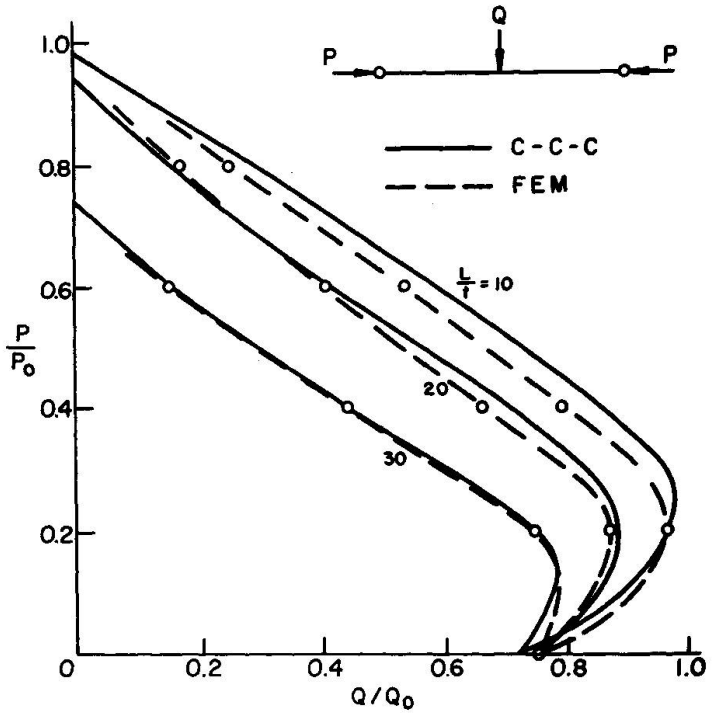

Fig.2 Interaction Curves, e/t=0

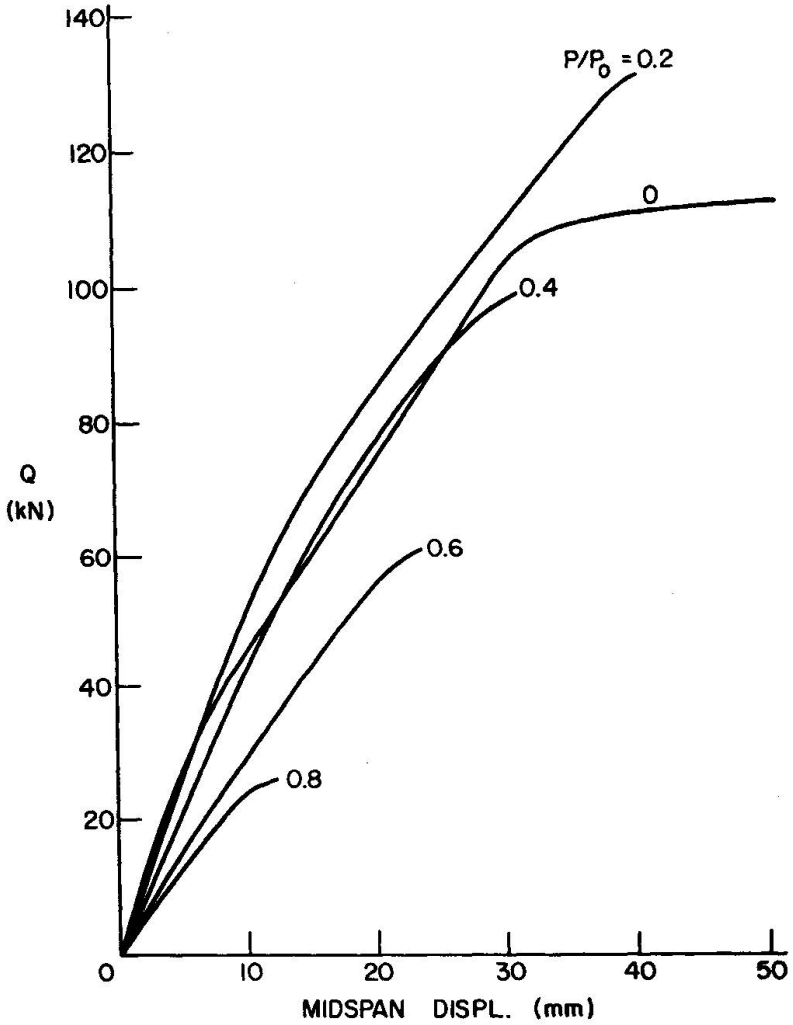

Fig.3 Load-Deflection Curves, e/t=0

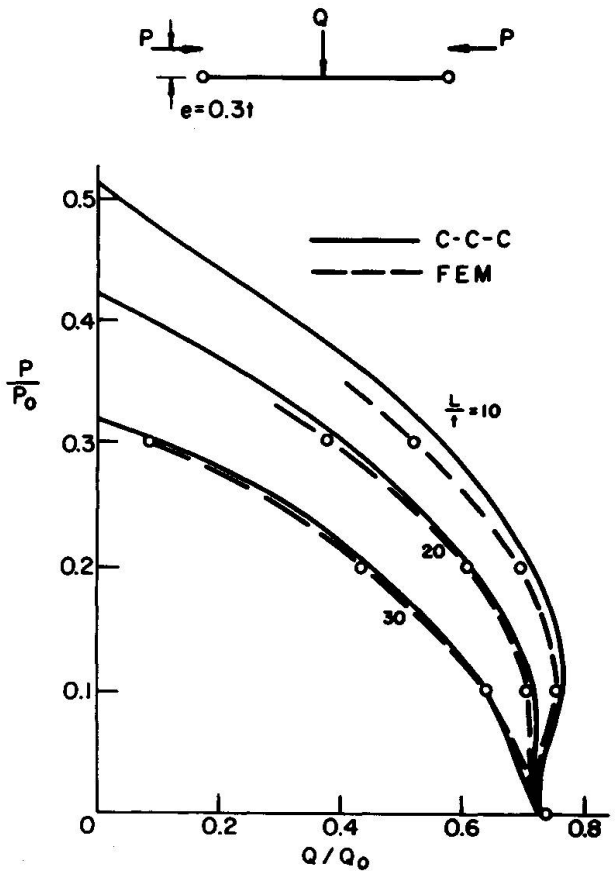

Fig.4 Interaction Curves, e/t=0.3

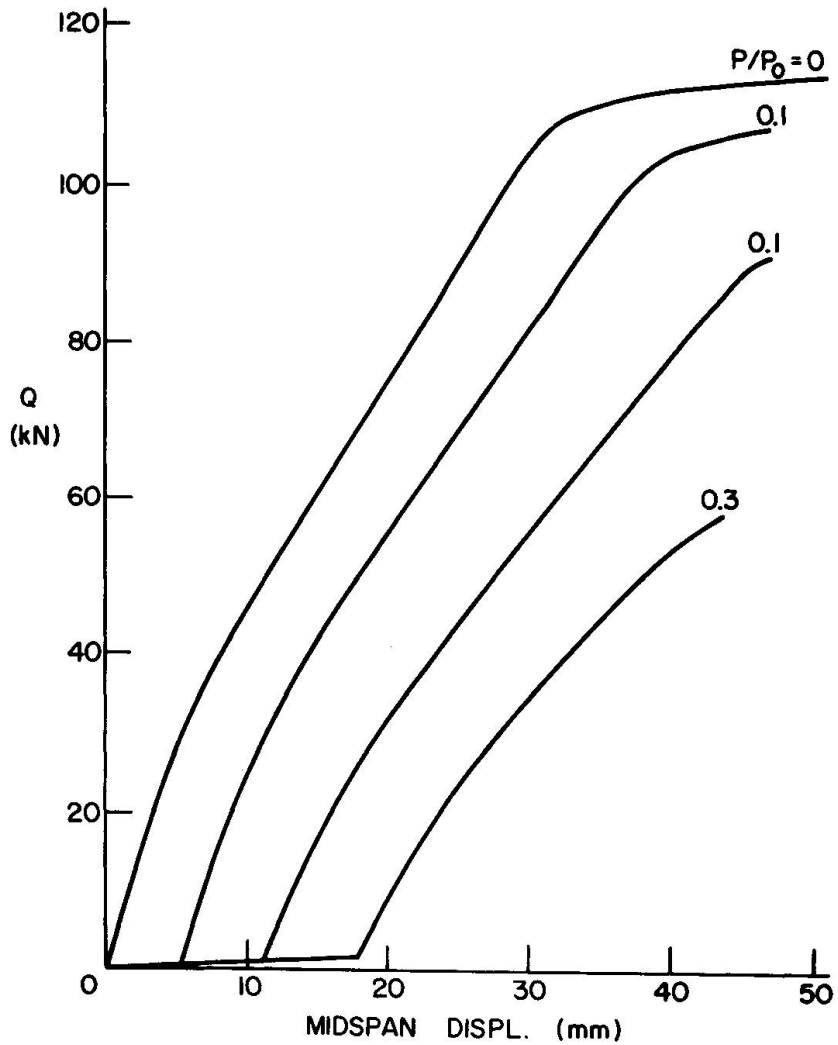

Fig.5 Load-Deflection Curves, e/t=0.3

Stabilität von Stahlbetonstützen und Stahlbetonrahmen

Stability of Reinforced Concrete Columns and Frames

Stabilité des colonnes et des cadres en béton armé

Wolfgang J. OBERNDORFER
Dipl.-Ing., Dr., M.S.
Firma Ing. Mayreder, Kraus & Co
Linz, Oesterreich

Dieter FISCHER
Koautor, Dipl.-Ing., Dr.
Linz, Oesterreich

1. Einleitung

Der Stabilitätsnachweis für außermittig gedrückte Stahlbetondruckglieder wird unter anderem nach den Vorschriften der einschlägigen Normen in den einzelnen Ländern geführt. In der Regel wird dabei das Verfahren der Ausweichzahlen ω_{kr} vorgeschrieben. Dieses Vefahren ist aber äußerst unbefriedigend, weil das tatsächliche Verhalten des Betondruckgliedes nicht in die Rechnung eingeht. Das Verformungsverhalten des Stahlbetons wird nicht richtig wiedergegeben. Der Anwendung des Hooke'schen Gesetzes für den Ausdruck für die Krümmung bei der Ableitung der Differentialgleichung steht bekanntlich entgegen:

- die beschränkte Zugfähigkeit des Betons
- die nichtlineare Arbeitslinie des Betons
- die elastoplastische Arbeitslinie des Bewehrungsstahles
- die Abhängigkeit der Krümmung vom Bewehrungsgehalt

Im folgenden Beitrag wird nun ein programmiertes Verfahren gebracht, das unter Berücksichtigung aller dieser Eigenarten von Stahlbetonquerschnitten den Nachweis der Stabilität von beliebig gelagerten und belasteten Stahlbetonstützen mit gleichzeitiger Ermittlung der erforderlichen Bewehrung ermöglicht.

2. Das Rechenverfahren und die getroffenen Annahmen

2.1. Grundsätzliches

Das nachstehend beschriebene Verfahren beruht auf der numerischen Lösung der Integraldarstellung der Gleichgewichtsbedingungen einer beliebig gelagerten und belasteten Stütze unter Verwendung einer wirklichkeitsnahen Momenten-Krümmungsbeziehung. Die Verformungen werden als klein angenommen, die Schubverformung wird nicht berück-

sichtigt und es wird drillfreie Biegung in einer Ebene vorausgesetzt. Die Steifigkeit der Stütze kann beliebig variieren (Abb. 1).

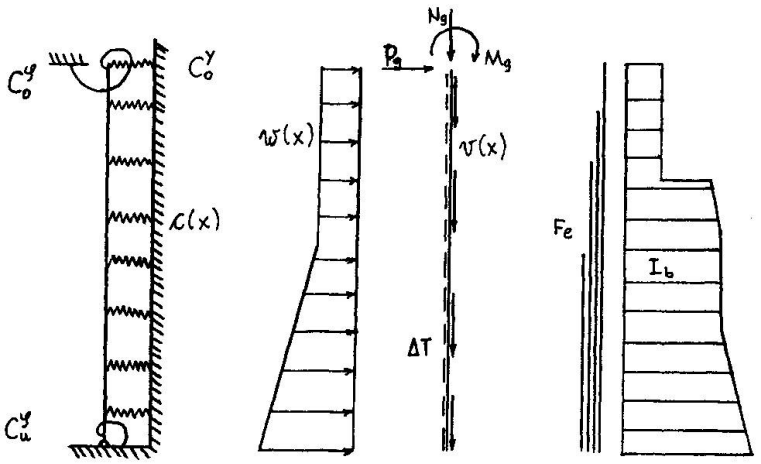

Abb.1: Art der Lagerung, Art der Belastung und Verteilung des Bewehrungsstahles und der Betonträgheitsmomente des Stabmodelles

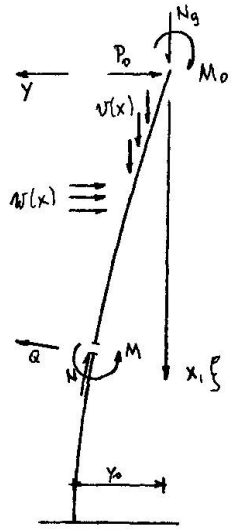

Abb.2: Schnittkräfte und Koordinationssystem

2.2. Ausgangsgleichungen und Lösungsverfahren

Es existieren die 2 Gleichgewichtsbedingungen (Abb.2):

$$N(x) = \int_0^x v(\xi)\,d\xi + N_g - y' \cdot \left\{ P_o + \int_0^x \left[w(\xi) - c(\xi) \cdot (y_o - y(\xi)) \right] d\xi \right\} \tag{1}$$

$$M(x) = M_o + P_o \cdot x + N_g \cdot y + \int_0^x (x-\xi) \cdot \left\{ w(\xi) - c(\xi) \cdot \left[y_o - y(\xi) \right] \right\} d\xi + \int_0^x v(\xi) \cdot \left[y(x) - y(\xi) \right] d\xi \tag{2}$$

und die allgemeine Momenten-Krümmungsbeziehung:

$$y'' = f\,(M(x), N(x)) = \psi\,(x) \tag{3}$$

Die Randbedingungen lauten:

$$x = 0: \quad y = 0 \qquad\qquad x = h: \quad M_u = C_u^\varphi \cdot y_u'$$

$$P_o = P_g - C_o^y \cdot y_o \tag{4}$$

$$M_o = M_g - C_o^\varphi \cdot y_o'$$

Über die Überführung dieser Gleichungen in ein Differenzenschema mit weitgehender Integraldarstellung wird auf [7] verwiesen.

2.3. Die Krümmungs-Momentenbeziehung

An Stelle der bekannten Beziehung

$$y'' \doteq \rho = -M/EI \tag{5}$$

bei Materialien mit linearem Elastizitätsgesetz tritt in diesem Falle die Funktion

$$y'' \doteq \rho = \varphi/d = f(M,N) \tag{6}$$

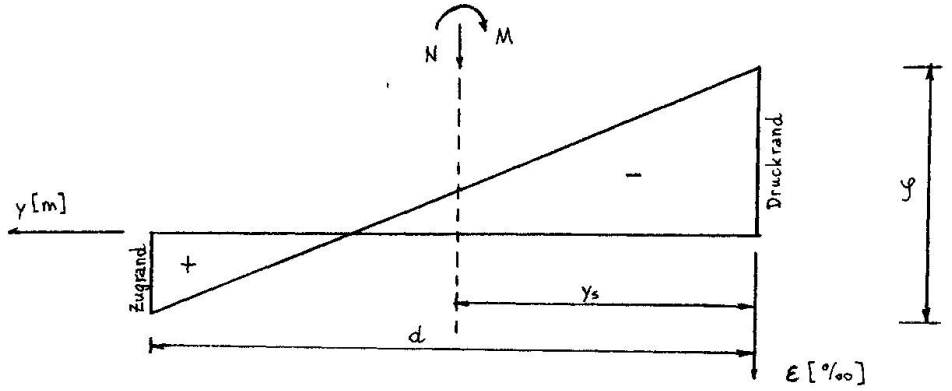

Abb.3: Schnittkräfte und Verteilung der Dehnung über dem Querschnitt

Das hier beschriebene Verfahren erfordert die Aufteilung der geometrischen Form in lauter Trapeze (Abb.4).

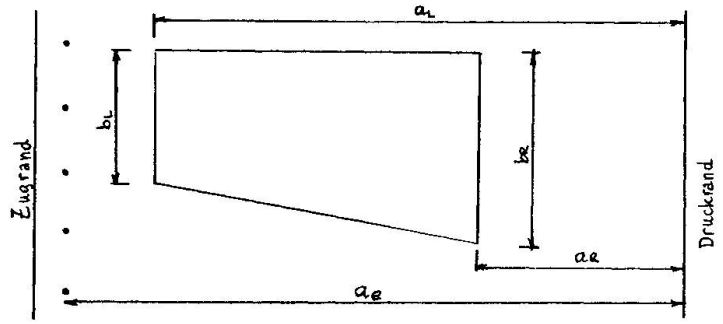

Abb.4: Örtliche Koordinaten eines Teiltrapezes

Für jedes Teiltrapez kann nun die Normalkraft und das Moment um den Druckrand wie folgt berechnet werden:

$$N_b = \int_{a_R}^{a_L} \sigma_b \cdot b(y)\,dy\,, \quad M_b = -\int_{a_R}^{a_L} \sigma_b \cdot b(y) \cdot y\,dy\,, \tag{7}$$

worin

$$b(y) = b_R + \frac{b_R - b_L}{a_R - a_L} \cdot (y - a_R) \quad \text{ist.} \tag{8}$$

Für die Betonarbeitslinie wird nun der Ansatz so gemacht, daß den CEB-Empfehlungen [4] entsprochen werden kann:

$$\sigma_b = \sigma_p \cdot \frac{\varepsilon}{\varepsilon_1} \cdot \left(2 - \frac{\varepsilon}{\varepsilon_1}\right) \quad \text{für} \quad 0 \geqslant \varepsilon \geqslant \varepsilon_1 \tag{9}$$

$$\sigma_b = \sigma_p \quad \text{für} \quad \varepsilon_1 \geqslant \varepsilon \geqslant \varepsilon_2\,. \tag{10}$$

Für $\varepsilon_1 = -2$ o/oo, $\varepsilon_2 = -3{,}5$ o/oo und $\sigma_p = 0{,}8$ x Rechenwert für die Betondruckfestigkeit folgt das Parabel-Rechteck-Diagramm; für $\varepsilon_1 = \varepsilon_2 = \varepsilon_{b\,max}$ und σ_p = Rechenwert für die Betondruckfestigkeit folgt das Parabel-Diagramm.
In ähnlicher Weise wird für den Bewehrungsstahl angesetzt:

$$N_e = F_e \cdot \sigma_e \;, \quad M_e = -F_e \cdot \sigma_e \cdot a_e \tag{11}$$

$$\text{mit} \quad \sigma_e = \alpha \cdot \varepsilon(y)^2 + \beta \cdot \varepsilon(y) + \gamma . \tag{12}$$

Durch geeignete Wahl von α, β und γ läßt sich abschnittsweise eine ausreichend genaue Anpassung an jede Stahlarbeitslinie finden. (Abb.5)

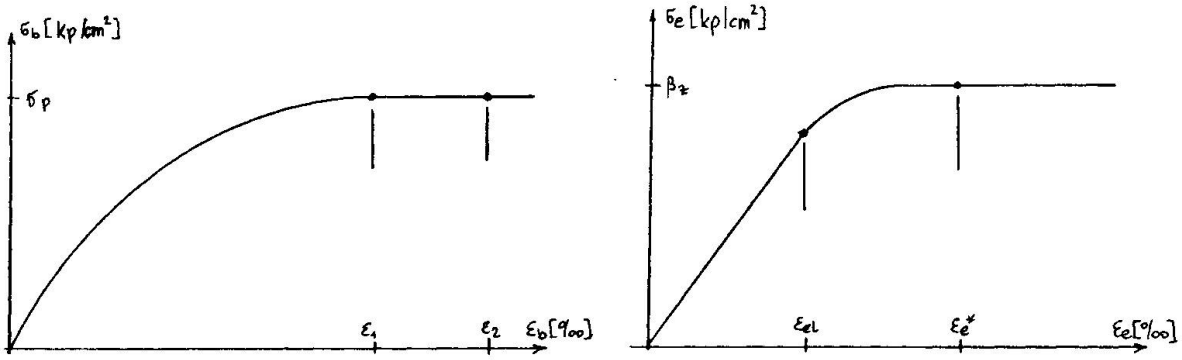

Abb.5: Arbeitslinien von Beton und Stahl

Nach Summierung der Normalkräfte und Momente über alle Teiltrapeze und Stahleinlagen und nach Gleichsetzung dieser Werte den äußeren Schnittkräften werden 2 quadratische Gleichungen mit den 2 Unbekannten φ und ε erhalten. Elimination von ε liefert eine Gleichung 4. Grades für φ von der Form:

$$f_0 \varphi^4 + f_1 \varphi^3 + f_2 \varphi^2 + f_3 \varphi + f_4 = 0 \tag{13}$$

Bei der Auswahl der maßgebenden Lösung aus den vier Ergebnissen wird wie folgt vorgegangen: bei gegebenem negativen Vorzeichen der Schnittkräfte M und N muß φ positiv sein (Abb.3). Die Lösungskurven können daher nur die in Abb. 6 gezeigten Formen annehmen.

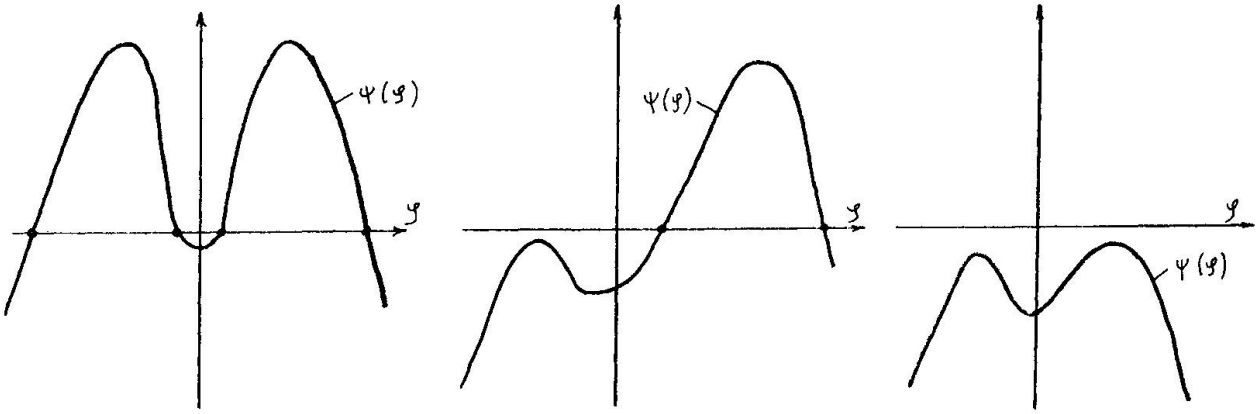

Abb.6: Varianten der Nullstellen von ψ (φ)

Wenn nur die zu stabilen inneren Spannungszuständen gehörigen Verdrehungen gesucht werden - wenn man daher in der Kurve, wie eine solche in Abb. 7 typisch dargestellt wurde,

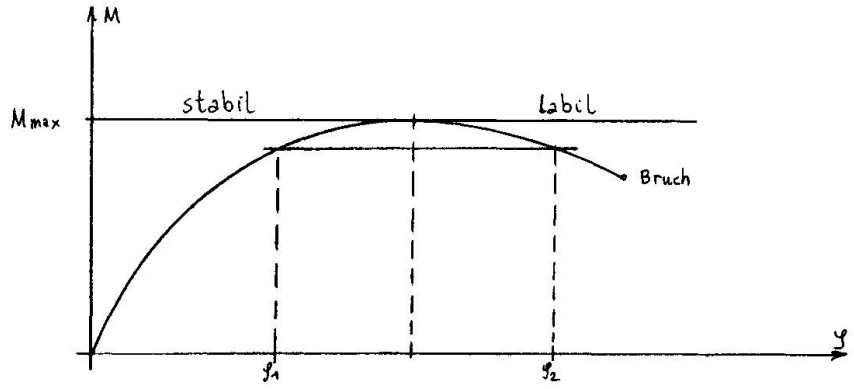

Abb.7: Typische M-φ-Kurve

nur den Bereich bis zum Maximum verfolgt -, ist die kleinere der beiden positiven Lösungen die gesuchte. Tritt einmal die in Abb. 8 ersichtliche dritte Variante der Lösung auf, so bedeutet dies, daß kein Gleichgewicht zwischen den äußeren Schnittkräften und dem Integral der inneren Spannungen mehr möglich ist. Das Verfahren wurde nun derart programmiert, daß die Bewehrungsflächen solange vergrößert werden, bis ein Gleichgewicht im Querschnitt möglich ist.

Das Vergrößern der Bewehrungsfläche wird mit einer eingegebenen Schrittweite η in Prozenten des Anfangswertes für die Bewehrung vorgenommen. Allgemein gilt, daß die erforderliche Stahlbewehrung umso genauer ermittelt wird, je kleiner die Schrittweite η gewählt wird. Andererseits sinkt mit der Vergrößerung der Schrittweite natürlich die Rechenzeit und man liegt außerdem auf der sicheren Seite (Abb.8).

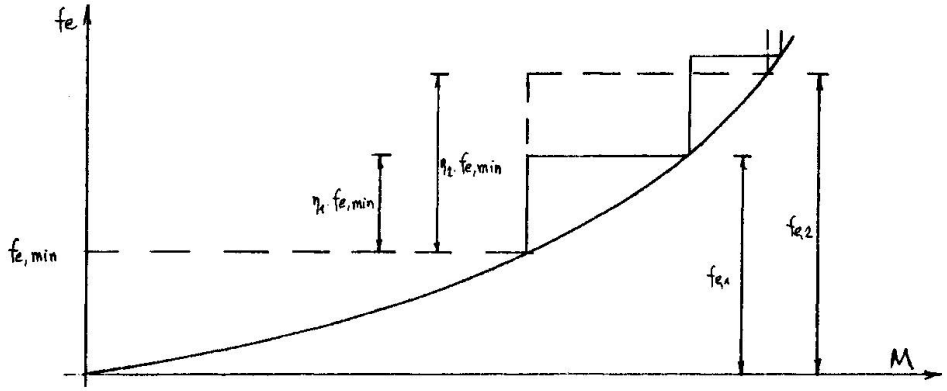

Abb.8: Zusammenhang Schrittweite - theoretisch erforderliche Bewehrung

3. EDV-Programm

Zur numerischen Durchrechnung einer Stahlbetonstütze

wurde ein Rechenprogramm in FORTRAN erstellt. Die Eingabe wurde so gestaltet, daß hinsichtlich der Sicherheitsphilosophie und hinsichtlich der Generierung von zusätzlichen Verformungen zufolge Kriechen, Fundamentschiefstellung und ungewollter Exzentrizität der Normalkraft voll der DIN [5] entsprochen werden kann.

In umfangreichen Vergleichsrechnungen wurden die Ergebnisse des Iterationsalgorithmus, der Bemessungsroutine und der endgültigen Verformungsberechnung mit in der Literatur bekannten Ergebnissen auf Übereinstimmung verglichen.

4. Stabilität von Stahlbetonrahmen

Das eben beschriebene Verfahren zur Untersuchung der Stabilität von Stahlbetonstützen läßt sich erweitern zur Untersuchung der Stabilität von eingeschossigen Rahmen. Die Vorgangsweise beruht darauf, daß für einen vorgegebenen Lastzustand

$$P = \sum \gamma_i P_i \tag{14}$$

(Summe aller mit den Sicherheitsfaktoren vervielfachten Lastfällen) die Kopfverschiebungen der Rahmenstützen kompatibel gemacht werden. Die Einspannung der Rahmenstützen in den Riegel wird durch eine linearelastische Drehfeder simuliert. Aus der Verträglichkeitsbedingung für die Stützenkopfverschiebungen ergeben sich Änderungsquerkräfte am Stützenkopf gegenüber der Berechnung nach der Theorie 1. Ordnung. Die Dehnungen, die diese Änderungskräfte im Riegel hervorrufen, werden vernachlässigt, was bedeutet, daß der Rahmenriegel unter den Änderungskräften inkompressibel ist.

Die gesamte Kopfverschiebung ist:

$$y = y_{el,1} + y_{el,2} + y_{\Delta,o}. \tag{15}$$

$y_{el,1}$ ist die Horizontalverschiebung im betrachteten Lastzustand nach der linear-elastischen Theorie 1. Ordnung:

$$y_{el,1} = y_{el,1}^{d} + y_{el,1}^{p+z} \tag{16}$$

$y_{el,1}^{d}$ = Verformung aus Dauerlasten

$y_{el,1}^{p+z}$ = Verformung aus Verkehrs- und Zusatzlasten

$y_{\Delta,o}$ ist die Horizontalverformung zufolge Abweichung der Stielachse von der lotrechten Wirkungslinie der Normalkraft

$$y_{\Delta,o} = y_{e,o} + y_{pl,o} + y_{f,o} \tag{17}$$

$y_{e,o}$ = Verformung zufolge ungewollter Exzentrizität der Normalkraft

$y_{pl,o}$ = plastische Verformung ($= \varphi_\infty \cdot y^{a}_{el,1}$)

$y_{f,o}$ = Verformung zufolge Fertigungsfehler der Stabachse

$y_{el,2}$ ist die zusätzliche Verschiebung zufolge Berücksichtigung des Gleichgewichtes am verformten Element und zufolge des nichtlinearen Werkstoffverhaltens

Besteht die Verbindung zwischen den Stützen und dem Rahmenriegel aus einem Gummilager, dann setzen sich die Verformungen $y^{d}_{el,1}$, $y^{p+z}_{el,1}$ und $y_{el,2}$ aus den Verformungen der Stütze und aus jener des Gummilagers

$$y^{Lager} = \frac{Q}{F \cdot G} \cdot h \tag{18}$$

(Q = Querkraft, F = Lagerfläche, G = Schubmodul, h = Lagerhöhe) zusammen.

Es werden nun die Stützenkopfquerkräfte der einzelnen Stiele betrachtet, die durch die genaue Rechnung eine Verteilungsänderung erfahren. Zur Verteilungsänderung dieser Kräfte tragen jene Verformungen nicht bei, die schon nach der Berechnung nach der linear-elastischen Theorie 1. Ordnung vorhanden waren ($(1+\varphi_\infty) y^{d}_{el,1} + y^{p+z}_{el,1}$). Die restlichen Verformungen berechnen sich mit:

$$\bar{y} = y - \left[(1+\varphi_\infty)\, y^{d}_{el,1} + y^{p+z}_{el,1} \right] = y_{e,o} + y_{f,o} + y_{el,2} \,. \tag{19}$$

Die Änderungskräfte werden mit H_i bezeichnet, n sei die Anzahl der Stützen. Die Verträglichkeitsbedingung lautet dann:

$$\bar{y}_i = \text{konst}; \quad i=1,\ldots n \tag{20}$$

und das Gleichungssystem für die Änderungskräfte:

$$f(H_i) = \bar{y}\,, \qquad i=1,\ldots n \tag{21}$$

$$\sum_{i=1}^{n} H_i = 0\,. \tag{22}$$

Dies sind n+1 Gleichungen für die n Unbekannten H_i und $\bar{y}$. Die Lösungen können nicht analytisch gefunden werden. Errechnet man für mehrere Werte von H_i die Verformungen $\bar{y}_i$ und trägt diese Kurven für jede Stütze in einem Diagramm ($H-\bar{y}$) auf, dann kann graphisch die lotrechte Schlußlinie so gezogen werden, daß $\sum H_i = 0$ wird. Die zur Schlußlinie gehörige Abszisse $\bar{y}$ ist die Lösung und liefert die Änderungskräfte H_i.

Beispiel

Gegeben ist ein statisches System gem. Abb. 9:

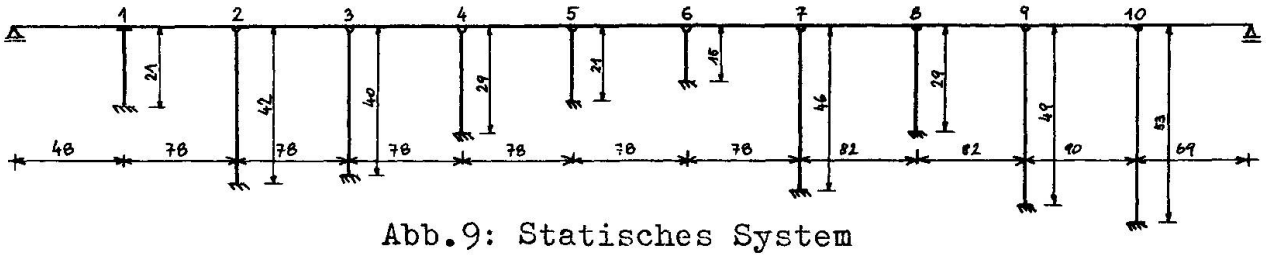

Abb.9: Statisches System

und die Baustoffe B 450 Tragwerk
B 300 Pfeiler
RT 50

mit dem Kriechbeiwert $\varphi_{\infty} = 1{,}8$.

Für den Pfeilerquerschnitt (Abb.10)

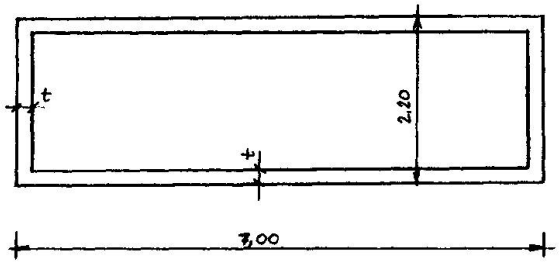

Pfeiler 1-8: t = 25 cm
Pfeiler 9,10: t = 35 cm

Abb.10: Pfeilerquerschnitt

wurde die Mindestbewehrung nach ÖNorm B 4200, 9. Teil vorgesehen (=1,4 o/oo). [6]
Gesucht ist der Nachweis der Tragsicherheit für folgende 5 Lastkombinationen:

I) Leere Brücke, voller Wind, kein Erdbeben zur Zeit $t = 0$ mit dem Sicherheitsfaktor $\gamma = 1{,}7$

II) Leere Brücke, voller Wind, mit Erdbeben zur Zeit $t = 0$ mit dem Sicherheitsfaktor $\gamma = 1{,}1$

III) Volle Brücke, halber Wind, ohne Erdbeben zur Zeit $t = \infty$ mit dem Sicherheitsfaktor $\gamma = 1{,}7$

IV) Stabilitätsnachweis für zentrische Belastung des Rahmensystems mit dem Sicherheitsfaktor $\gamma = 2{,}5$

V) wie Lastkombination I, sämtliche Horizontalkräfte wirken jedoch von der anderen Seite

Die Normal- und Querkräfte am Stützenkopf (die Momente sind identisch Null wegen der Gelenke am Pfeilerkopf) als Ergebnis der Rahmenrechnung nach der linearelastischen Theorie 1. Ordnung sind bekannt. Es wurde jede Lastkombination mit mehreren Ansätzen für die Änderungskräfte H_i mit dem EDV-Programm durchgerechnet. Die Kopfverschiebungen $\bar{y}$ wurden tabellarisch zusammengestellt und graphisch aufgetragen (Abb. 11 für Lastkombination II). Die Lösun-

gen wurden durch heuristisches Auffinden jener Kopfauslenkung $\bar{y}$ ermittelt, für die die Summe der positiven Änderungskräfte gleich der Summe der negativen Änderungskräfte ist.

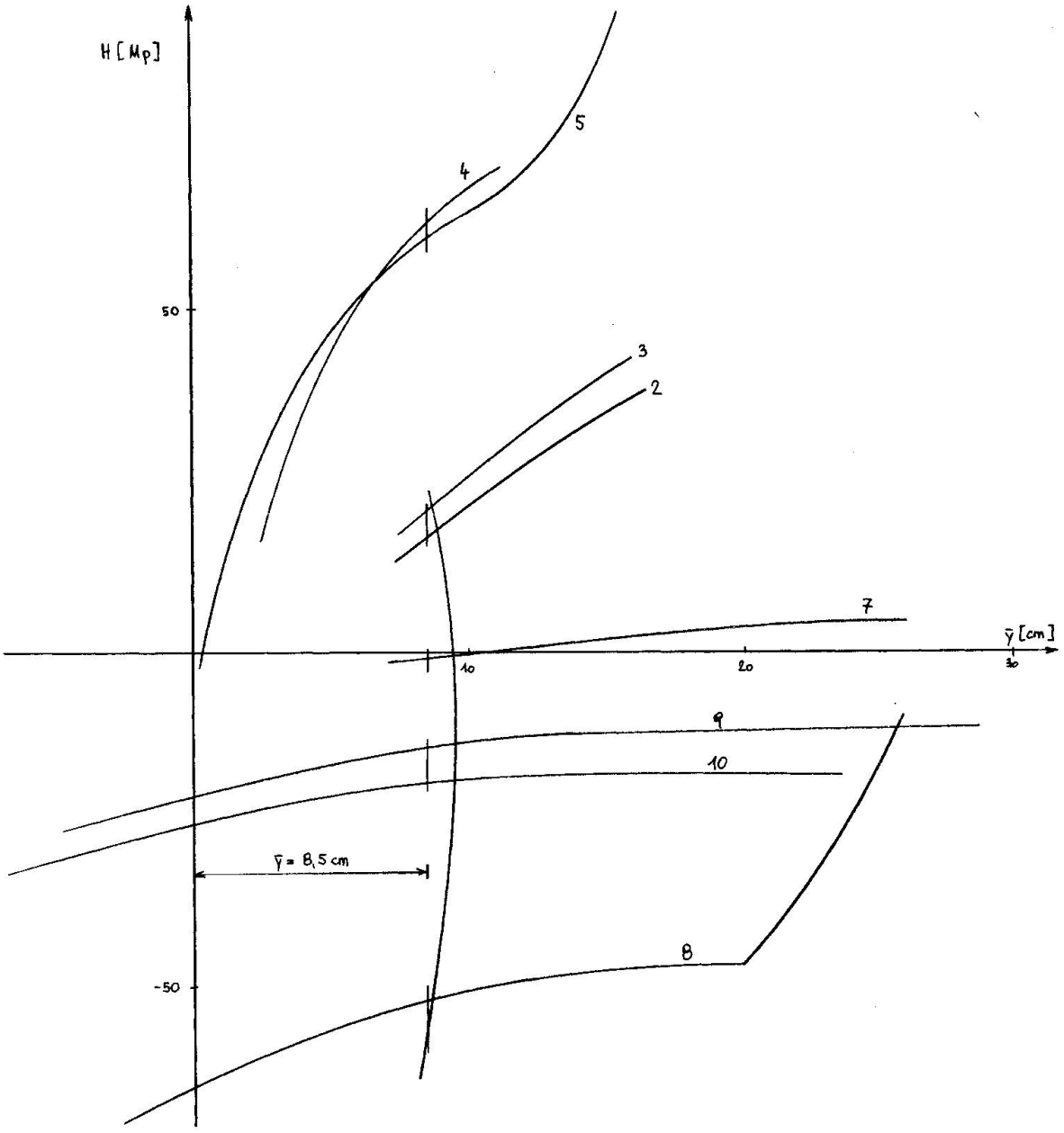

Abb.11: Pfeilercharakteristika Beispiel

Bemerkungen zu den Pfeilercharakteristiken:

Die Steigung der Kurven ist ein Maß für die Steifigkeit der Pfeiler. Aus den Abb. 11 sieht man deutlich, daß die Pfeiler 5 und 6 die steifsten und die Pfeiler 7,9 und 10 die weichsten sind.

Knickpunkte:

Sie können an 2 Stellen entstehen: dort, wo die Nullinie beginnt, in den Querschnitt hineinzuwandern, und dort, wo Gleichgewicht des Pfeilers nur mehr bei Vergrößerung der Bewehrungsfläche möglich ist (z.B. Pfeiler 5 und 8).

Asymptoten:

Sie treten dort auf, wo eine endlich kleine Vergrößerung der Horizontal(Änderungs)-Kraft eine unendlich große Verschiebung verursacht (z.B. Pfeiler 9 und 10). Bei dieser Art der Labilität hilft ein Vergrößern der Bewehrungsfläche nicht mehr (im Gegensatz zu Pfeiler 8, der sich durch Vergrößerung der Bewehrungsfläche noch retten läßt). Die Grenze für die Möglichkeit, einen Pfeiler durch Vergrößern der Bewehrungsfläche stabil zu machen, hängt einzig und allein von seiner Schlankheit und die in die Schlankheit eingehenden Materialkonstanten ab (Abb.12).

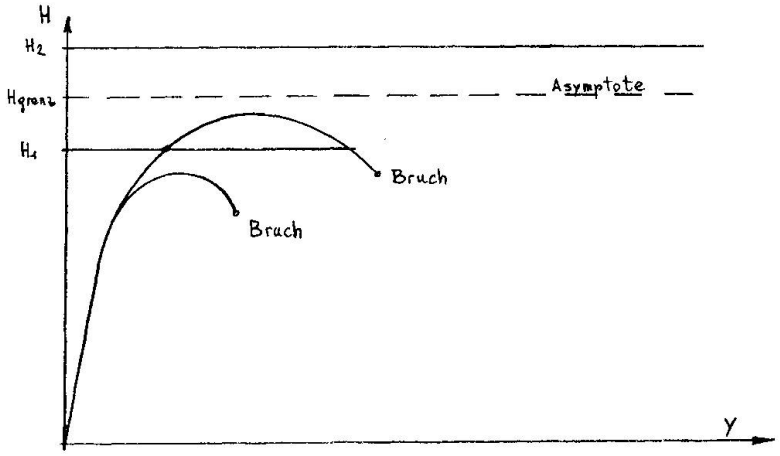

Abb.12: Verhalten einer Stahlbetonsäule unter seitlicher Horizontallast und Druck:

$H_1 < H_{grenz}$: Bewehrungsfläche vergrößern bewirkt Stabilität
$H_2 > H_{grenz}$: Keine Stabilität mehr möglich

Zick-Zack-Charakteristik:

Bei Pfeilern, deren Bewehrungsflächen sehr stark vergrößert werden bei den einzelnen Ansätzen für die Änderungskraft, kann das Auftragen der Ergebnispunkte zu einer wenig sinnvollen Zickzackkurve führen, wenn der Faktor der Eisenflächenvergrößerung groß gewählt wurde (z.B. η = 1,0). In diesem Fall muß dieser Pfeiler mit einem wesentlich kleineren η (z.B. 0,2) wiederholt werden, um eine möglichst glatte Kurve zu bekommen. In Abb. 13 wurde dieses Phänomen prinzipiell dargestellt.

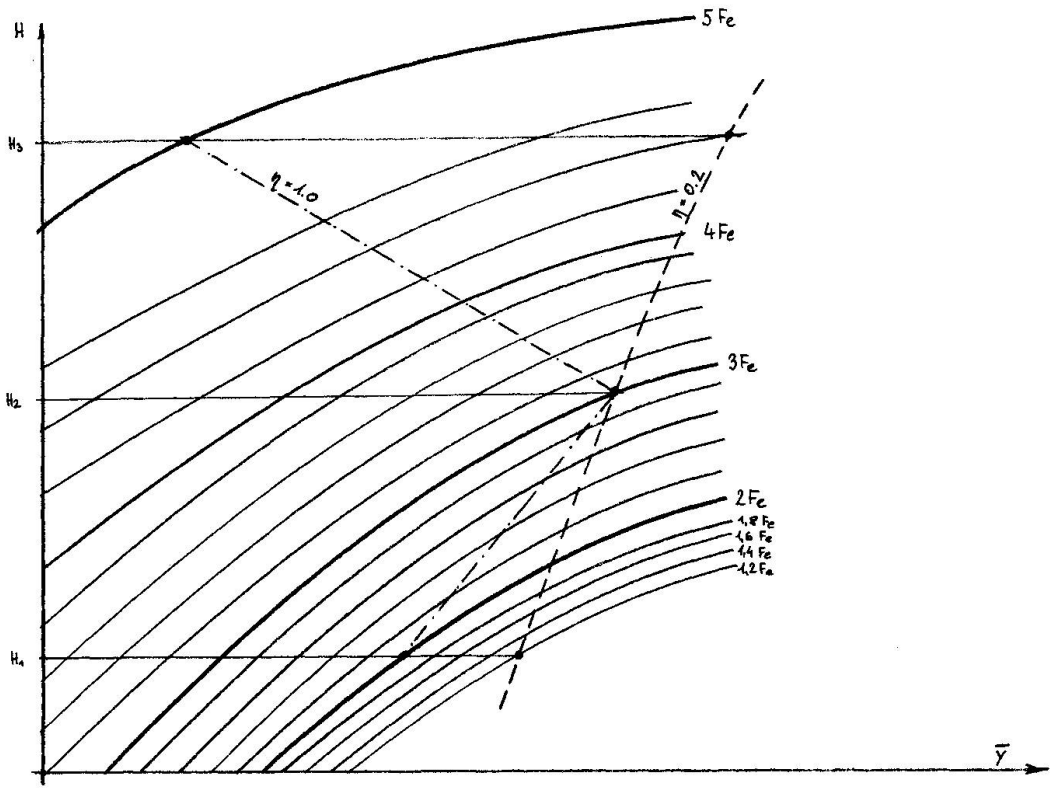

Abb. 13: Abhängigkeit der Charakteristik vom Faktor für die Bewehrungsflächenvergrößerung

Stabilitätsuntersuchung LK IV:

Für eine Stahlbetonstütze gibt es prinzipiell 2 Verhaltensarten: den Verzweigungsfall bei zentrischem Druck und den Traglastfall bei exzentrischem Druck.

Bei der Stabilitätsuntersuchung nach diesem Verfahren wird der Verzweigungsfall (der über die Ermittlung der Eigenwerte zu lösen wäre) auf den Traglastfall übergeführt dadurch, daß eine seitliche Störlast (ca. P/100) an dem Rahmentragwerk angebracht wird. Stellt sich unter der Störlast ein Gleichgewicht ein, so hat der Lastzustand noch nicht die kritische Last des Verzweigungszustandes erreicht. Im allgemeinen genügt wegen der Kleinheit der Verformungen unter der Störlast 1 Versuch und lineare Extra- und Interpolation.

Als Ergebnis konnte bei diesem Beispiel festgestellt werden, daß das Rahmentragwerk unter allen untersuchten Lastkombinationen stabil ist und daß mit der normenmäßigen Mindestbewehrung das Auslangen gefunden werden kann. Die nach diesem Verfahren ermittelten Änderungskräfte am Stützenkopf sind von der gleichen Größenordnung wie die Kopfquerkräfte aus der linear-elastischen Rechnung und haben daher ausschlaggebende Bedeutung für die Stabilität und Bemessung des Rahmentragwerkes.

Literaturverzeichnis:

[1] Luchner, H.: "Stabilitätsberechnung hoher Brückenpfeiler am Beispiel der Siegtalbrücke Eiserfeld", BETON- u. STAHLBETONBAU, Jg. 1967, Heft 2

[2] Ziegler, H.: "Principles of Structural Stability". Waltham: Blaisdell Publishing Company. 1968

[3] Zurmühl, R.: "Praktische Mathematik", 3. Auf., Springer: Berlin, 1961

[4] CEB: "Empfehlungen zur Berechnung und Ausführung von Stahlbetontragwerken", Deutscher Betonverein, Werner: Düsseldorf.

[5] DIN 1045, Ausgabe 1972 "Bemessung von Stahlbetontragwerken"

[6] ÖNORM 4200 "Bemessung von Stahlbetontragwerken", 9. Teil

[7] Fischer, D., Oberndorfer, W.: "Stabilität von Stahlbetonstützen", ÖST. INGENIEURZEITSCHRIFT, Jg. 1974, Heft 1

ZUSAMMENFASSUNG

Es wird ein Verfahren zur Untersuchung der Stabilität von Stahlbetonstützen und Stahlbetonrahmen beschrieben. Das Verformungsverhalten der Bauglieder wird von normgemässen Annahmen für die Arbeitslinien von Beton und Stahl abgeleitet. Bei Versagen der Stützen wird in einem Algorithmus untersucht, ob Vergrössern der Stahleinlagen stabiles Tragverhalten ergibt. Rahmentragwerke zeigen eine überraschend grosse Aenderung der Kopfquerkräfte gegenüber der Berechnung nach der linear-elastischen Theorie. Das Ergebnis ist eine Mobilisierung von Tragreserven. Die Berechnungen werden mit einem elektronischen Rechenprogramm durchgeführt.

SUMMARY

A method for the investigation of the stability of reinforced columns and frames is described. The load deformation behaviour of the structural members is derived from the standard assumptions for the stress-strain relations of steel and concrete. A special algorithm investigates whether stable structural behaviour can be reached by enlarging of the reinforcement if the columns fails. Reinforced concrete frameworks show an astonishing change in the shear forces at the top of the columns resulting in a mobilisation of unused structural capacities. The calculations are carried out with the aid of a computer program.

RESUME

On décrit un procédé pour l'étude de la stabilité des colonnes et des cadres en béton armé. Le comportement charge - déformation des éléments de construction est dérivé des hypothèses faites pour

les diagrammes tension - déformation du béton et de l'acier. On étudie un algorithme permettant, en cas de rupture des colonnes, de déterminer si le renforcement de l'armature conduit à un comportement stable. Les efforts tranchants au sommet des colonnes des cadres présentent des différences d'une ampleur étonnante par rapport à la théorie élastique linéaire, ce qui donne une "mobilisation" des capacités de charge, normalment négligées. Les calculs sont effectués à l'aide d'un programme d'ordinateur.

Leere Seite
Blank page
Page vide